2023

Right Treatment Wrong Time: Immunotherapy Administration Post-Radiotherapy Decreases Tumor Burden in a Preclinical Model of Brain Metastasis

Kathryn Elizabeth Blethen
West Virginia University, keblethen@mix.wvu.edu

Right Treatment Wrong Time: Immunotherapy Administration Post-Radiotherapy Decreases Tumor Burden in a Preclinical Model of Brain Metastasis

Kathryn E. Blethen, B.S.

Dissertation submitted
to the School of Pharmacy
at West Virginia University

in partial fulfillment of the requirements for the degree of

Doctor of Philosophy in
Pharmaceutical and Pharmacological Sciences

Paul R. Lockman, Ph.D., B.S.N., Chair
Marina Galvez-Peralta, Pharm.D., Ph.D.
Ahmad Hanif, Ph.D.
Salik Hussain, D.V.M., Ph.D.
Edwin Wan, Ph.D.

Department of Pharmaceutical and Pharmacological Sciences
Robert C. Byrd Health Sciences Center

Morgantown, West Virginia
2023

Keywords: Brain metastases, lung cancer, radiation therapy, blood-tumor barrier, immunotherapy, permeability

ABSTRACT

Right Treatment Wrong Time: Timed Immunotherapy Administration Post-Radiotherapy Decreases Tumor Burden in a Preclinical Model of Brain Metastasis

Kathryn E. Blethen

This dissertation (a) provided an in-depth literature review of methods to modulate the blood-brain and blood-tumor barriers to increase drug delivery and efficacy in brain metastases, (b) evaluated the effects of whole-brain radiation therapy on the blood-brain barrier in immunocompetent and immunocompromised mouse models and proposed a mechanism by which the immune response to radiation disrupts the blood-brain barrier, and (c) developed a syngeneic lung cancer brain metastasis model to determine the impact of coordinated immunotherapy administration with radiotherapy. The blood-brain barrier is an impediment to drug delivery to the brain. The inherent leakiness of the blood-tumor barrier does not allow cytotoxic concentrations of drugs to accumulate within the tumor bed. Methods to modulate the barrier are necessary to increase delivery and efficacy of therapeutics. Whole-brain radiation therapy increases blood-brain barrier permeability in a time- and size-dependent manner in immunocompetent, but not immunocompromised mice. Our findings indicate a window of time that may allow greater drug accumulation post-radiotherapy. Combining immunotherapy and radiotherapy has a synergistic effect. Our data demonstrate the impact immune response and treatment sequencing have on brain tumor burden.

DEDICATION

I dedicate this work to my fellow small-town students. Never let anyone tell you that you cannot achieve your dreams because of where you come from. Prove them wrong. You are more than capable. Not many people from Julian in Boone County, WV end up at WVU for an undergraduate degree, let alone a doctoral degree. I am so thankful for the teachers who recognized my love for learning and continued to encourage my curiosity.

ACKNOWLEDGEMENTS

This work would not exist without the continued support of my circle. Thank you all for graciously filling my cup when it felt empty, celebrating my accomplishments with me, and reminding me why I began research in the first place on the day's experiments were failing.

I am forever grateful to my mentor, Dr. Paul Lockman. Meeting you completely changed my research trajectory. From the moment I saw your presentation as a potential mentor, I was captivated and knew I had to do a rotation in the Lockman laboratory. I quickly fell in love with blood-brain barrier/brain metastasis research and everyone in the lab. You have cultivated an incredibly supportive, friendly lab environment, which is not easy to do. Thank you for accepting me into your lab, challenging me, providing continued support, and trusting me. There was never a moment I felt as though you were not in my corner, and I couldn't have asked for anything more. I aspire to be as successful and have as great of a work-life balance as you.

Thank you to my dissertation committee – Drs. Salik Hussain, Ahmad Hanif, Marina Galvez, and Edwin Wan. I appreciate your guidance and experimental design suggestions to support my project. You pushed me to be a better scientist. Dr. Marina Galvez, thank you for always checking in on me as my faculty advisor for AAPS. I could not have put together the Pharmaceutical Sciences Research Symposium without your help. You went above and beyond to make the symposium a success, and I cannot thank you enough.

To my compassionate, humble grandfather. You encouraged me to dream big for as long as I can remember. I may not have ended up a "dancing

dermatologist," but I know I still made you proud. Thank you for always pushing me to work hard and aspire for bigger and better things than our small town could offer. To my grandmother, I am proud to be your namesake. Thank you for teaching me to fight for what I want when circumstances are fighting against me. I love you both.

I would like to thank the most unwavering support system I have had throughout my life—my mother. I could not have made it here without you cheering me on from the sidelines. Thank you for consistently providing love, advice, strength, and friendship. I am lucky to have a mom as wonderful as you. I love you endlessly.

To my father, thank you for always being my go-to person to cheer me up. Your constant reminder that "tomorrow is another day" kept me going. You can finally brag about *officially* having a doctor in the family. I love you.

To my partner and best friend, Bryan, no one has witnessed the highs and lows of the past few years as closely as you have. Whenever I had to sacrifice time together to do (and redo) experiments, you were always understanding. You have been my greatest supporter- from buying me flowers when my grant was rejected to commissioning a personalized artistic frame for my first first-author publication. Life threw us some hectic moments in the middle of this academic endeavor and it only made us stronger. I could not have pushed through without your unconditional love. Thank you for being my personal chef, confidant, and roommate. I love you and can't wait for what our future holds!

I would not have considered I was capable of going to graduate school without the mentorship of Dr. Rosana Schafer, Dr. Jennifer Franko, and Dr. Christopher

Cuff. Dr. Schafer, you saw potential in me when I felt completely lost and uncertain of my future. I loved working in your lab and constantly learning immunology hands-on. Having you as a professor, academic advisor, and mentor was a pleasure. Thank you for all of your guidance. I hope you and Dr. Cuff are thoroughly enjoying retirement together. Dr. Franko, you have a special talent for explaining immunology and techniques in a way that makes it easy to comprehend and apply. I am glad I was able to spend many days in lab with you and Ande troubleshooting experiments and laughing. Thank you for supporting me from undergraduate research, working as a lab technician, and all the way through graduate school. Dr. Cuff, thank you for encouraging me to speak up and trust myself. As one of two undergraduates in an advanced immunology class full of graduate students, I had severe imposter syndrome. You noticed me quietly making connections between lectures, primary literature, and case studies then called on me to answer questions. “She doesn’t speak often, but when she does she is correct.” You helped build my confidence and guided me how to apply what I learned in real-world scenarios. I am grateful to you.

To the Immunology and Microbial Pathogenesis graduate students who inspired me to apply to the PhD program – Dr. Jesse Hall, Dr. Catherine Blackwood, Dr. Savannah Sims-Calandrelli, Dr. Kelly Monaghan, and Dr. Dudley McNitt. Thank you for sharing your knowledge and being admirable role models. You impacted me more than you realize. Keep inspiring the next generation of scientists!

To the mentors who made me a resilient scientist – Dr. John Barnett and Dr. Jamie McCall. Dr. Barnett, you made lab meetings fun with your quick-witted

jokes and stories. Thank you for taking a chance on hiring me as your lab technician post-graduation solely based on Dr. Schafer's recommendation. This experience prepared me for graduate school more than I anticipated. Congratulations on your retirement and success with ExesaLibero Pharma. Dr. McCall, I owe *so much* of my technical skills and knowledge to you. Thank you for being patient with me, answering numerous questions, double-checking my calculations, and allowing me to learn from my mistakes. Working alongside you made me a more rigorous scientist.

This project would not exist without the previous work of my former lab mate, Dr. Samuel Sprowls. You are one of the most hard-working and level-headed people I have met. Thank you for taking the time to properly train me and teach me everything about radiation therapy, pharmacokinetics, and blood-brain barrier physiology. I was unsure how I could ever learn our lab's challenging techniques once the COVID-19 pandemic shut down the lab for months, but you constantly reassured me that I wasn't behind. You deserve every bit of success you are receiving in your post-doctoral position. I am so proud of you and love watching you grow as a scientist! I have no doubt tenure is in your future. To the only other female graduate student during my time in the lab, Dr. Tasneem Arsiwala. Thank you for being a positive mentor and helpful resource. I am grateful you were there to lean on for support during some of my roughest moments in lab. I will always cherish our memories of attending the AAPS meeting in Philadelphia. Thank you for bringing Indian treats (especially the chai), teaching me Hindi, and always being down to chat about scary movies.

To my fellow Lockman Lab graduate students. Cullen, you stepped up and

took on responsibilities within your first year and a half and absolutely crushed it! I was constantly impressed by your work ethic and willingness to help. I love your excitement for research and insatiable desire to learn. You are a wonderful scientist and I have faith your work will make a difference. I'm so proud of you. Thank you for quite literally everything and keep up the great work. I have no doubt I'm leaving the lab in good hands and will miss our daily coffee breaks. Geoff, I'm glad you joined our lab. You are changing it for the better with your organizational skills, molecular techniques, and cancer biology expertise. I can't wait to see where you land with your project. Good luck guys!

To the Lockman lab volunteers/paid interns. Dr. Brooke Kielkowski, I think our generation of the lab will forever be singing your praises. Thank you for your positivity, hard work, and organizational skills. You were as much of a teacher to me as I was to you. There will never be another Brooke Kielkowski. Morgan Glass, I cannot thank you enough for all of your hard work on our (unpublished) western blots. You were our capillary isolation and western blot queen. Leah Dykstra, thank you for bringing positive energy, lighthearted jokes, and of course slicing countless mouse brains. I loved spending time with you all in the lab and I'm excited to see where the future takes each of you.

To the women who help run the lab behind the scenes, Dr. Lockman's administrative assistants— Mallory Zuercher and Teresa Lodge. Mallory, anytime we had issues with orders, travel, shipping, scheduling, etc. you were able to magically solve our problems. I am so thankful we had you to lean on. I hope you are enjoying your new job! Teresa, you have an upbeat personality and are always happy to help. Thank you for the logistical planning with my defense and

conference travels. I could not effectively do my job without the help of both of you.

To the Office of Research and Graduate Education (ORGE) faculty and staff. Thank you all so much for everything you do for us. To Dr. Julie Lockman, thank you for being such a positive light during students' journey through graduate school. You have brought so much good to the graduate program since you began your position as Assistant Vice President for Graduate Education. Keep inspiring others to use their strengths to reach their goals. Dr. Ed Pistilli, I admire how you carefully balance your work, personal life, and prioritize your lab. Thank you for thoughtfully taking on your new role as Director of Admissions. You have also made the office better. Connor Ferguson and Joe Andria, you are indispensable. Thank you for your help with student organizations and multiple form submissions required to progress through the program. Logan Miller, thank you for helping me with funding and event planning for the Pharmaceutical Sciences Research Symposium, CBTP T32 program events, and supporting me when my original experiential learning fell through.

Thank you to the faculty and staff of the imaging cores: Dr. Karen Martin, Sarah McLaughlin, Dr. Amanda Ammer, Dr. Neil Billington, and Dr. Amanda Stewart. Almost every figure in my papers required your facilities and expertise. Thank you for all of your help. To OLAR staff, especially Ethan Galand, thank you for taking care of our mice and being so understanding. You made large-scale animal studies less stressful.

To my fellow graduate school friends. Michael Winters, Ellie Aerts, Bailey Whitehead, Emily Rice, Carly Amato-Menker, and Serhii Bahdasariants— thank

you for being there throughout the ups and downs as we navigated graduate school in the middle of a pandemic together. No one truly understands what it feels like the way you do. Michael and Ellie, we have been a packaged deal since basically the first day of “boot camp.” I am eternally grateful for our w(h)ine nights, hiking adventures (we survived a **rattlesnake**?!), conversations, and friendship. Thank you for letting me cry on your shoulders during the lows and celebrating my wins during the highs. Dhruvi Panchal, thank you for encouraging me and helping with experiments when I needed you. Lauren Rentz, thank you for including me in Pistilli lab conversations and tier rankings, sharing your dad’s wacky freeze-dried snacks, indulging my obsession with dogs, sending me wet lab memes that you never fully understood, and most importantly – helping me format my dissertation. I’ll miss you all. Good luck!

To my close friends. Nathan Abia Lawer-Yolar. Full government name to express how mad I still am that you moved to the other side of the country. Thank you for being a voice of reason, providing tough love, and cheering me on no matter what. You are a true friend. Everyone deserves a Nate (*but not mine get your own*). Shelby Putnam, thank you for forcing me to step away from the stress of school to have some fun every now and then. Matthew Mills, thank you for standing by my side through many ups and downs in Morgantown. You were there when I needed you, whether that meant providing some laughs or pulling all-nighters studying together. Henna Bhatia, thank you for being my spontaneous travel partner, study buddy, fellow Dog Mom, and sushi connoisseur. Many of my favorite memories from undergrad and grad school include you. Thanks for always being there for me. Jared Bartee, Olivia Crum,

Dai'jah Diggs, Jaimie Blosser, and Elizabeth Young, thank you for continually checking in on me and offering support. I love you all and could not have done this without you!!

Last but not least, my emotional support pets. I adopted two kittens, Sol and Luna, at the beginning of the pandemic; they brought joy into one of the darkest periods of time. Then my partner and I adopted our shelter pup, Leo, once I started seeing the light at the end of my graduate school tunnel and it has been one of our best decisions. Thank you, Sol, Luna, and Leo, for keeping me (*slightly*) sane.

Everyone in the lab knew me as the girl who did experiments while exclusively listening to R&B, so naturally, I would like to end my acknowledgments with lyrics from one of my favorite artists.

"*All the times they thought that they could hold you back, but you've always known there was no chance of that. You're made too strong, and when you're going with your heart you can go further than you'd ever thought possible. Prove them all wrong*." – H.E.R.

TABLE OF CONTENTS

DEDICATION……iii

ACKNOWLEDGEMENTS..... iv

LIST OF FIGURES xv

LIST OF TABLES..... …xvii

LIST OF ABBREVIATIONS..... xviii

CHAPTER 1 1

INTRODUCTION 1

CHAPTER 2 4

Modulation of the blood-tumor barrier to enhance drug delivery and efficacy for brain metastases 4

2.1 Blood-Brain Barrier (BBB) and Blood-Tumor Barrier (BTB) 4

2.1.1 Brain Metastases vs Glioblastoma 4

2.1.2 Heterogeneity of Blood-Tumor Barrier in Brain Metastases..... 6

2.1.3 Drug Delivery for Brain Metastases 10

2.1.4 Immunotherapy for Brain Metastases..... 11

2.2 Modulation of BBB Permeability 15

2.2.1 Treatments to Increase BBB Permeability 17

2.2.2 Manipulation of BBB Receptors to Enter the Brain 21

2.3 Conclusion 24

2.4 References 26

CHAPTER 3 43

Effects of Whole-Brain Radiation Therapy on the Blood-Brain Barrier in Immunocompetent and Immunocompromised Mouse Models 43

3.1 Introduction **43**

3.2 Methods and Materials **45**

3.3 Results **49**

3.4 Discussion **52**

3.5 Conclusion **55**

3.6 References **57**

CHAPTER 4 ..... **77**

Timed administration of immunotherapy following whole-brain radiation therapy decreases tumor burden in a novel syngeneic lung cancer brain metastasis preclinical animal model. **77**

4.1 Introduction **77**

4.2 Methods and Materials **79**

4.3 Results **83**

4.4 Discussion **85**

4.5 Conclusion **87**

4.6 References **89**

CHAPTER 5 ..... **105**

Conclusion and Future Directions **105**

5.1 Conclusion **105**

5.2 Future Directions **107**

LIST OF FIGURES

Figure 2.1 Differences between the BBB and BTB 41

Figure 3.1. Disruption of BBB homeostasis following WBRT in immunocompetent mice 64

Figure 3.2. No significant changes in BBB homeostasis following WBRT in whole brains of immunocompromised mice..... 65

Figure 3.3. Increased BBB permeability following WBRT in immunocompetent mice is time and size-dependent..... 66

Figure 3.4. Increased proinflammatory mediators following WBRT in immunocompetent and immunocompromised mice..... 67

Figure 3.5. Proinflammatory cytokines significantly increased in brains of immunocompetent mice post-WBRT. 68

Figure 3.6. Proposed mechanism of T-cell dependent BBB disruption following WBRT.. 69

Supplemental Figure 3.1. Nude mice have significantly decreased efflux transporter function, but no differences in BBB integrity……70

Supplemental Figure 3.2. No changes in radiolabeled AIB permeability following WBRT in immunocompetent mice 3, 6, or 24 hours post-WBRT……...71

Supplemental Figure 3.3. No changes in TxRd dextran permeability following WBRT in immunocompetent mice 3, 6, or 24 hours post-WBRT..72

Supplemental Figure 3.4. No differences in proinflammatory cytokine concentrations in serum of immunocompetent mice post-WBRT……..73

Supplemental Figure 3.5. No changes in proinflammatory cytokine concentrations in serum of immunocompromised mice post-WBRT……74

Supplemental Figure 3.6. No differences in proinflammatory cytokine concentrations in brains of immunocompetent mice post-WBRT……..75

Supplemental Figure 3.7. No changes in proinflammatory cytokine concentrations in brain of immunocompromised mice post-WBRT……..76

Figure 4.1. Tumor burden in the brain increases with passages of LLC brain explants 94

Figure 4.2. LLC-Br has a higher migration rate but similar growth rate compared to LLC-P 95

Figure 4.3. Similar tumor burden and survival in WT and nude mice..... 96

Figure 4.4. No significant differences in tumor burden at day 22 in control immunocompetent groups. 97

Figure 4.5. Potential protective role of administering anti-CTLA-4 24 hours prior to whole-brain radiation therapy..... 98

Figure 4.6. Administering anti-CTLA-4 12 hours post-radiation decreases tumor burden…….. 99

Supplemental Figure 4.1. No significant differences in tumor burden or survival in control immunocompromised groups 100

Supplemental Figure 4.2. No changes in tumor burden or survival in irradiated immunocompromised groups…….101

Supplemental Figure 4.3. No significant differences in tumor burden or survival in immunotherapy groups of immunocompromised mice…….102

Supplemental Figure 4.4: Significant increase in percent survival of LLC-Br cells when treated with immunotherapy for 72 hours……..103

LIST OF TABLES

Table 2.1 Brain-to-plasma ratio of various P-gp and BCRP substrate chemotherapeutic agents for the treatment of brain metastases 42

LIST OF ABBREVIATIONS

ACT: adoptive cell therapy

AIB: α-aminoisobutyric acid

AQP: aquaporin

BBB: blood-brain barrier

BCRP: breast cancer resistance protein

BED: biologically effective dose

BLI: bioluminescent imaging

BTB: blood-tumor barrier

CAR: chimeric antigen receptors

CNS: central nervous system

CTLA-4: cytotoxic T-lymphocyte associated protein 4

CXCL1: C-X-C motif chemokine ligand 1

EGFR: epidermal growth factor receptor

GBM: glioblastoma multiforme

HIFU: high-intensity focused ultrasound

ICG: indocyanine green

IL: interleukin

LAT1: large amino acid transporter 1

LCBM: lung cancer brain metastasis

LDL: low-density lipoprotein

LIFU: low-intensity focused ultrasound

LITT: laser interstitial thermal therapy

LLC: Lewis lung carcinoma

LRP1: low-density lipoprotein receptor-related protein 1

MMP: matrix metalloproteinases

MRI: magnetic resonance imaging

MRP1: multidrug resistance protein 1

NSCLC: non-small cell lung cancer

NVU: neurovascular unit

PD-1: programmed cell death protein 1

PDGF: platelet-derived growth factor

P-gp: P-glycoprotein

Rh123: rhodamine 123

SRS: stereotactic radiosurgery

STAT3: signal transducer and activator of transcription 3

TKI: tyrosine kinase inhibitor

TNF-α: tumor necrosis factor-α

TxRd: Texas red

VEGF: vascular endothelial growth factor

WBRT: whole-brain radiation therapy

WT: wild-type

Chapter 1

Introduction

The blood-brain barrier (BBB) is the tightly regulated physiochemical barrier between the systemic circulation and the brain. The components of the BBB include endothelial cells, pericytes embedded in a basement membrane, and astrocytic end feet wrapped around the outer layer. In a healthy state, the primary functions of the BBB are neuroprotection and maintenance of homeostasis. However, the barrier becomes disrupted and dysfunctional with various disease pathologies, including Alzheimer's Disease, epilepsy, and brain tumors.

In the presence of brain metastases, the barrier is heterogeneously disrupted and referred to as the blood-tumor barrier (BTB). Although the BTB is leaky, it still restricts the distribution of therapeutics into brain lesions below cytotoxic concentrations. Drug delivery across the BTB remains a challenge to the curative treatment of patients with brain tumors.

The most common cancer types to metastasize to the brain are breast cancer, lung cancer, and melanoma. Approximately 50% of all cases of brain metastases are due to primary lung tumors. Unfortunately, lung cancer brain metastasis (LCBM) patients have poor prognosis, with most patients succumbing to the disease within 12 months of the development of CNS symptoms regardless of treatment strategy. Treatment options for brain tumors are scarce, including stereotactic radiosurgery (SRS), whole-brain radiation therapy (WBRT), surgical

resection, and/or systemic therapy (chemotherapy, targeted therapy). Currently, there is no available cure for brain tumors, only options to manage symptoms and prolong life by a few months.

In 2017, the American Society of Clinical Oncology (ASCO) and Friends of Cancer Research submitted recommendations to the U.S. Food and Drug Administration (FDA) to allow patients with brain metastases to participate in clinical trials. Before this, the majority of clinical trials excluded patients with brain metastases due to their poor outcomes regardless of treatment. Consequentially, brain metastasis falling under exclusion criteria has further delayed the development of potential treatment strategies for this vulnerable patient subset.

Alternative routes of drug administration, novel drug formulations, and techniques to disrupt the BBB have shown promising results in preclinical studies, but have yet to provide significant survival benefits in the clinic. In this dissertation, we investigate the use of combinatorial radiotherapy and immunotherapy to treat LCBM. First, we establish a window of time following WBRT where the immune response is activated, BBB is disrupted, and efflux transport is decreased. We then develop a novel syngeneic mouse model which is utilized to evaluate the efficacy of immunotherapy. Lastly, we demonstrate the importance of timed immunotherapy administration with radiotherapy.

Chapter 2 provides an in-depth review of the BTB, a comparison of the altered BTB of primary brain tumors and brain metastases, effects of therapeutics on the blood-tumor barrier, and mechanisms to increase drug delivery across the barrier. Preclinical and clinical data are discussed with recent advances to treat brain metastases.

Chapter 3 investigates the magnitude of BBB disruption following WBRT in immunocompetent and immunocompromised mice. Additionally, inflammatory markers were quantified in brains and serum post-radiation. A potential mechanism for T-cell specific BBB disruption in response to WBRT is provided.

Chapter 4 describes the development and characterization of a novel syngeneic lung cancer brain metastasis preclinical animal model. This model was used in immunocompetent and immunocompromised mice to evaluate the efficacy of WBRT and timed administration of immunotherapy. Total brain tumor burden, survival, and percent weight loss were carefully monitored and reported.

In summary, this dissertation contributes a comprehensive discussion of the blood-brain and blood-tumor barriers, describes the challenges of treating LCBM, and suggests an opportunity for immunotherapy and radiotherapy to improve survival outcomes. These data highlight the importance of further characterization of the effects of the immune response to various disruptive techniques on the blood-brain and blood-tumor barriers. Additionally, an LCBM preclinical model for use in immunotherapy studies was developed and utilized. The overall goal of this work was to understand the effects of the immune response to radiotherapy on blood-brain and blood-tumor barriers to help develop more effective treatment strategies for patients with LCBM.

Chapter 2

Modulation of the blood-tumor barrier to enhance drug delivery and efficacy for brain metastases.

2.1 Blood-Brain Barrier (BBB) and Blood-Tumor Barrier (BTB)

The BBB is comprised of a neurovascular unit (NVU) consisting of capillary endothelial cells, pericytes, astrocytes, and a basement membrane [1] The innermost layer of the BBB is formed by endothelial cells which establish a barrier between circulating blood and the brain parenchyma [2]. A basement membrane of extracellular matrix and pericytes envelops the endothelial cells to support structural integrity [3]. Astrocytic endfeet are located along the outermost layer of the NVU and play a significant role in regulatory processes such as K^+ buffering, brain pH, and other metabolic processes [4]. Interactions between these cells and their microenvironment are vital to maintain BBB integrity and brain homeostasis. However, when cancer cells displace endothelia from the other NVU cells the BBB breaks down and solute movement whether passive or actively transported is altered. It is important to note most of what is known about the BBB and BTB is due to preclinical work in mouse models.

2.1.1 Brain Metastases vs Glioblastoma

The BTB restricts chemotherapeutic efficacy and contributes to tumor progression in both primary and metastatic brain tumors. Glioblastoma (GBM) is

the most common, malignant primary brain tumor characterized often by a hypoxic necrotic center and invasive growth into normal brain tissue [5]. Disruption of the BBB by invasive GBM was long considered uniformly leaky but is now understood to have a nonuniform, heterogeneous microvasculature composition with increasing distance from the tumor core [6]. In early states, that is, low-grade glioma, the BBB remains nominally intact and little disruption is present as the tumor relies on the normal brain microvasculature [7]. However, this changes dramatically as the tumor grows and progresses into a higher grade glioma where tumor cells, through a variety of molecular signals, drive the separation of endothelial tight junctions, dissociation of astrocytic processes, and recruitment of differential pericyte populations [8] Malignant GBM cells are also highly migratory and remodel the extravascular basement membrane through release of several soluble factors and induction of a cascade of protumorigenic pathways [4, 9, 10]. These properties help promote both chemotherapeutic and radiation therapy resistance as the leading edge of the tumor continues to expand and co-opt existing brain capillaries [7].

In contrast to the development of GBM, metastatic brain tumors arise from a peripheral primary tumor location. The most common cancer types contributing to the formation of brain metastases are lung, breast, and melanoma [11]. Initial steps of lesion formation are similar to immune cell trans-endothelial migration, which include tethering, rolling, adhesion, and diapedesis [12]. Extravasating into the brain parenchyma beyond the endothelia level has been observed to take longer than in other organs ranging between 2 and 14 days depending upon primary tumor type [13, 14]. As the metastatic cells continue to grow beyond the

BBB, nutrient and oxygen demand increase leading to vascular co-option, a process by which tumor cells alter the existing brain microvasculature [15]. Simultaneously, angiogenesis occurs to provide cancer cells with nutrients to support proliferation and survival. The immature vessels formed during this process are fenestrated and lack endothelial tight junction protein complexes allowing increased vascular permeability [16]. These immature capillaries are “leaky” compared to normal BBB capillaries [17]. While the lesion continues to grow in size, the tumor becomes more hypoxic and secretes vascular endothelial growth factor (VEGF) to induce more angiogenesis [18]. This dynamic process contributes to BTB permeability. Interestingly, no correlation has been observed between lesion size and vascular permeability in preclinical brain metastasis models [17,19, 20]. Clinically, substantial intra- and inter-tumoral heterogeneity exists among brain metastases in the same brain [17, 21, 22]. Differences between the BBB and BTB are shown in **Fig 2.1**.

2.1.2 Heterogeneity of Blood-Tumor Barrier in Brain Metastases

There are relatively few studies comparing the vascular permeability of metastatic brain lesions (regardless of type) to a primary tumor. The data presented are often difficult to reconcile due to varying methods clinically available and disparities in how a given method is conducted. For example, in comparing data between CT perfusion studies for astrocytomas and GBM vs central metastatic lesions from lung, breast, and melanoma the permeability values (rPSmax) for primary tumors are largely 10 times the values of metastasis lesions in the brain. Though it should be noted astrocytoma values fell more in

line with metastatic lesions compared to the primary tumors [23, 24]. While these data generally agree with preclinical data using Ktrans, calculations obtained with MRI show metastases have approximately 2/3rd of primary tumor permeability measurements [25]. However, these data were a compilation of several lesion types, which could be the driving factor for this difference.

The BTB is anatomically different in brain metastases of breast cancer compared to a primary CNS tumor, which may help mechanistically explain variability and differences in permeability. The density of blood vessels in brain metastases of breast cancer lesions in mice is 40%-80% less than the vascular density of normal brain. Further, and more critical to this discussion the vascular density of the metastatic lesion is often only 12%-15% of a GBM [26]. Vascular density alone suggests permeability would be reduced in the lesion compared to the primary tumor. However, the defects in the respective BTB vasculature are also indicative. In preclinical glioma models, the size of the vascular defect (pore; cylindrical opening through the endothelial wall) is at a minimum of ~150 nm in size. This opening is large enough for antibodies to freely penetrate from the blood to the tumor. However, the pore size within metastases in the brain is roughly ~5-9 nm in diameter, though there is likely variability of actual pore sizes in the vasculature within and between the various lesions in the same brain [27]. The data suggest while the metastatic lesion will enhance with MRI, trastuzumab at an approximate size of 5.5-6 nm will be restricted from diffusing across vascular pores into the metastatic lesion to the degree it would have a clinical effect.

Our preclinical work generally agrees the BTB in metastatic lesions have

permeability values less than a primary tumor, but also have some degree of compromise regardless of the lesions size, location, and/or tumor type [20,27–34] Though, there is subtly in this assertion. The vascular permeability in brain metastases can range from 1.1- to 100-fold, depending on the polarity and size of the marker. For example, the small (104 Da) charged zwitterion amino-isobutyric acid (AIB) penetrates lesions from 1.1-fold to upwards of 35-fold higher compared to the normal brain vasculature. The marker AIB is a small water-soluble marker that should easily penetrate defects induced in the vasculature within a metastatic lesion. However, water-soluble molecules such as antibodies (~150 kDa) have significantly less permeability through the BTB defects (~1.01- to ~3-fold; compared to normal brain).

Clinically, there are reports of a subset of breast cancer brain metastases that poorly or do not enhance with MRI, yet a large majority do. For the lesions that enhance, it may not be uniform throughout the lesion, leaving detection of total tumor mass difficult at times [35]. Our preclinical data strongly agree with the heterogeneity of permeability seen within a lesion and between lesions in the same brain. When evaluating the distribution of lesion permeability of a small molecular weight marker the majority of lesions (~80%) had permeability increases of 1.5- to 3-fold and only 10% of lesions had permeation increases of greater than 10 compared to normal brain [17]. A very similar pattern of variability is seen when looking at permeability within a single lesion. We have observed permeability variances can range as much as 1.1- to 25-fold [17].

There have been reports in the literature regarding the positive correlation between increasing size [36] and nuclear compactness [37] with permeability

increases. However, we have evaluated thousands of lesions across multiple sized markers, and different preclinical brain metastases models and 80% of the lesions fail to significantly associate size and increases in permeability [17], which agrees with other data obtained with MRI [35]. We have observed quantifiable permeability increases, albeit sometimes subtle, in nearly every metastatic brain lesion. It should be noted for us to quantify the slight permeability increases, we use quantitative multimodal fluorescent and laser phosphorescent autoradiography to detect spatial permeability changes at a 1-micron resolution and drug tissue concentrations of 1 femtogram [38]. This technique was adapted from prior double or triple autoradiography techniques [39] and is well suited to study preclinical metastases since it has <1-μm resolution and with ^{14}C-phosphorescence, tracer distribution can be mapped in 10-μm pixels at levels (~0.3 nCi/g). The variability in permeability has significant implications for the effective delivery of chemotherapeutics within and between lesions in the same brain.

Despite the breakdown of the BBB in brain metastases of breast cancer, it still significantly restricts drug delivery and inhibits cytotoxicity in ~90% of CNS metastases [20, 27, 34]. The poor delivery of chemotherapy within the brain lesion provides a sanctuary for the lesion to progress, in the presence of sub-therapeutic chemotherapy concentrations, within the brain microenvironment. Many chemotherapeutics exhibit restricted distribution because permeability increases are inadequate and or they are removed by efflux transporters that remain highly active despite the breakdown of the vasculature [22, 28]. This phenomenon we have observed for paclitaxel and doxorubicin [40, 41] as well as

trastuzumab, lapatinib, and vorinostat [38, 42, 43].

2.1.3 Drug Delivery for Brain Metastases

Although many successful compounds have shown effectiveness in treating peripheral tumors with targeted agents, the same cannot be said for treating brain tumors. This lack of success may be due to inadequate delivery of otherwise effective compounds. Many factors affect how these drugs are delivered to the brain, but one major challenge is a heterogeneously leaky BTB. Future success of brain cancer therapeutics depends on the delivery of active drugs to the target at efficacious concentrations, which may include combinations of targeted drugs tailored to each patient's tumor type [44].

Traditional cytotoxic therapeutics have played a limited role in the treatment of brain metastases. The distribution of systemically administered chemotherapies is hampered by the BTB, which is frequently disrupted in patients with brain metastases [45, 46]. We analyzed over 2000 brain metastases in different preclinical models of metastatic breast cancer (human 231-BR-HER2 and murine 4T1-BR5) and found in over 89% of lesions, there was a partial compromise in BTB permeability. Nevertheless, the concentration of drugs only reached lethal levels in a small fraction (10%) of the most permeable metastases [17]. Several trials evaluating the use of systemic drugs in patients with brain metastases have failed to demonstrate notable response rates, including cisplatin and pemetrexed [47, 48], cisplatin and vinorelbine [49], paclitaxel and cisplatin [50] and temozolomide [51, 52].

Targeted therapies utilized to treat brain metastases have minimal brain

distribution. Only 5% administered dose of Trastuzumab, which targets HER2+ breast cancer, is found in brain lesions in preclinical mouse models [34]. Clinically, the ratio of trastuzumab in serum to cerebrospinal fluid is 420:1 [53]. Often a factor limiting drug delivery to brain metastases is the high degree of expression of ABC efflux transporters at the BBB and BTB. In preclinical studies, there is strong evidence for the interaction of vemurafenib, dabrafenib, trametinib, palbociclib, cobimetinib, doxorubicin, and paclitaxel being effluxed by P-gp (P-glycoprotein) and BCRP (breast cancer resistance protein). The brain concentrations achieved by most of these drugs are less than 10% of their plasma concentrations (**Table 2.1**). Moreover, the multidrug resistance protein 1 (MRP1) receptor acts by promoting drug resistance [54] along with active efflux of drugs. This provides an additional challenge to achieving optimal drug concentrations across the BTB [55]

2.1.4 Immunotherapy for Brain Metastases

Although the CNS was once considered immune privileged, studies have shown immune cells, specifically T cells, cross the BBB to perform immune surveillance [56]. Brain metastases are now being researched as possible targets for a variety of immunotherapies, such as checkpoint inhibitors and adoptive cell therapy (ACT). However, the microenvironment of solid tumors can evade immune responses by impeding the infiltration of immune cells into the tumor, contributing to the variability in responses seen among patients [57].

Checkpoint protein receptors, such as CTLA-4 (cytotoxic T-lymphocyte-associated antigen 4) and PD-1 (programmed death 1), are expressed on T

cells. These checkpoints block immune responses and allow the tumor cells to evade the immune system. When checkpoints are inhibited, T cells are activated by the primary tumor and then kill the cancer cells. Examples of immune checkpoint inhibitors are ipilimumab, which blocks CTLA-4, and pembrolizumab and nivolumab, which block the ligand PD-L1. Checkpoint immunotherapy is in clinical trials for patients with brain tumors, including advanced metastases and GBM. A 2010 study of individuals initially treated for metastatic melanoma which allowed enrollment of patients with treated CNS metastases was the first study to establish ipilimumab treatment improved survival [58]. In addition, pembrolizumab and nivolumab have been clinically assessed for efficacy in patients with melanoma and lung cancer brain metastasis [59]. Increased PD-L1 and CTLA-4 expression are indicative of therapeutic efficacy. In a study of patients with melanoma brain metastases, patients with tumor PD-L1 expression of 5% or more had a higher chance of benefiting from combination therapy (nivolumab and ipilimumab) than those with <5% tumor PD-L1 expression [60].

Some issues have arisen as a result of the increased use of checkpoint inhibitors. Tumor inflammation and pseudoprogression, which are often seen on imaging, may cause additional symptoms and make tumor growth assessment difficult [61]. The ability to successfully target brain metastases only among certain patients, such as those expressing high levels of PD-L1, may be a potential limitation of checkpoint inhibitors [62]. These limitations are significant in some patients to the degree that they may have little to no benefit from the currently available checkpoint inhibition therapies. The efficacy of immune checkpoint inhibitors on brain metastases is dependent on the ability of T cells to

become activated by the primary tumor, cross the BBB and/or BTB, and attack tumor cells in the brain [63]. Most of the data reported for checkpoint inhibitors in brain metastases have combinatorial therapy with other immunotherapeutic agents, radiation, chemotherapeutic agents, or neurosurgery. Additional studies are necessary to explore these challenges and determine how to successfully target tumor cells in the brain.

ACT is a procedure that involves the transfer of autologous immune cells to a recipient to induce an antineoplastic effect [64]. Cells from the primary tumor site or peripheral metastases are cultured in vitro with cytokines and lymphocytes. The immune cells are expanded and re-infused to the patient. One of the most common ACT to treat brain metastases is chimeric antigen receptor T-cell (CAR T-cell) therapy. Chimeric antigen receptors (CARs) are synthetic immune receptors instructing T cells to kill tumors by recognizing unique surface proteins on tumor cells [65]. The initial CD19 CAR T-cell ACT for metastatic melanoma raised hope for this treatment strategy against brain metastases. A study from 2000 to 2010 identified a subgroup of patients (9.85% of 264 patients) with melanoma brain metastases and treated them with ACT using either autologous tumor-infiltrating lymphocytes or lymphocytes designed to express a T-cell receptor to recognize melanocyte differentiation antigens. Nine of the patients achieved a complete response in the brain and 7 patients reached an overall partial response [66].

Although ACT for brain tumors is still in the early stages of development and clinical responses are often unsuccessful, these results demonstrate T-cell therapy has potential clinical benefit for patients with brain metastases. Tumor

heterogeneity has rendered CAR T-cell treatment for brain and other solid cancers challenging. In fact, this treatment has yet to be proven efficacious in solid tumors. The performance of CD19 CAR T cells emphasizes the importance of a CAR target commonly distributed across tumors. Discovering unique antigens in brain tumors has proven difficult because they express many markers found in normal brain regions (eg, CD133, CD44, Nestin, GFAP) and nonspecific cytotoxic effects in the CNS are much less tolerable than in most other areas of the human body [65]. Clinical CAR T-cell studies have also reported points of restraint for neurotoxicity and lethal cerebral edema, highlighting the life-threatening risks of immune-inflammatory responses in the CNS [67]. Almost 12%-32% of patients treated with CAR T cells suffer from extreme neurotoxicity which includes symptoms of confusion, delirium, and seizures. The extent of these neurologic toxicities is referred to as CAR T-related encephalopathy syndrome (CRES). A study by Gust et al reported patients with severe neurotoxicity may have endothelial cell activation which includes intravascular coagulation, capillary leakage, and increased BBB permeability. The cerebrospinal fluid contained high concentrations of inflammatory cytokines leading to pericyte stress, activation of endothelial cells, and further damage to BBB integrity [67].

Immunotherapy for brain metastases has come a long way since its establishment. The interplay between activating the immune system against tumors while limiting neurotoxic effects is a complex balance. T cells naturally cross the BBB, but the main hurdle with this treatment is determining the proper antigen to activate the cytotoxic T cells. More research is necessary to solidify

this as an effective therapy for patients with brain metastases.

2.2 Modulation of BBB Permeability

Bevacizumab is a recombinant humanized monoclonal immunoglobulin G1 antibody that binds to VEGF to decrease endothelial proliferation and formation of new blood vessels [68]. Bevacizumab in primary brain cancer, such as GBM, is well known to improve progression-free survival when used alone and/or in combination with chemotherapeutic agents [69]. The objective of bevacizumab is to normalize the vasculature of the tumor and improve oxygenation to aid in delivery of anti-cancer drugs. Bevacizumab also contributes to normalization of the blood vessels in the tumor with low permeability, hence leading to decreased penetration of drugs. Additionally, these tumors would become more invasive by co-opting normal blood vessels [70]. Preclinical studies suggest long-term use of bevacizumab leads to decrease in BBB permeability [71].

Recently, bevacizumab has been studied in combination with radiation therapy. The REBECA trial was the first clinical trial to study the effects of bevacizumab and whole-brain radiation therapy in patients with brain metastases. Results demonstrated a synergistic effect between the two treatment modalities [72]. One study combining bevacizumab with stereotactic radiosurgery improved treatment efficacy and reduced edema in a study of patients with lung cancer brain metastases [73]. Clinical studies in GBM patients show increased progression-free survival in phase II and III trials, but little to no change in overall survival [74, 75]. Bevacizumab is more efficacious as a preventative treatment for brain tissue necrosis than as a tumor treatment with

radiotherapy [76].

Matrix metalloproteinases (MMPs) are zinc-dependent endopeptidases with the primary function to degrade extracellular matrix. These MMPs have role in breast cancer initiation, growth, angiogenesis as well as activation of growth factors. Currently, MMP inhibitors are being studied to evaluate their efficacy in breast cancer. While the use of MMP inhibitors in several brain diseases such as intracerebral hemorrhage, cerebral ischemia, and cold injury has shown to decrease the BBB permeability, there is no concrete evidence to support its efficacy with brain tumors. Studies show MMPs contribute to tumor cells entering and exiting the vasculature to seed in metastatic sites throughout the body. Although results are inconclusive if MMP inhibitors can treat brain metastases, they could potentially prevent metastatic malignant cells invasion [77]. The role of MMP and its inhibitors may be investigated further in brain metastases [78].

Aquaporins (AQPs) regulate intra-/extracellular water balance by transportation of fluid across the plasma membranes. Among 13 subtypes of AQP, AQP4 is most abundantly present in the brain and is responsible for cytotoxic edema. Since AQP inhibitors including cryoablation have been in use for the clinical management of breast cancer, inhibition of AQP may be used as an adjunct treatment to lower the BBB permeability [79].

Dexamethasone is a corticosteroid with anti-inflammatory effects and low mineralocorticoid activity. Among several roles in cancer management, dexamethasone is widely used in controlling pain, nausea, and fatigue. Clinical and preclinical reports suggest dexamethasone can dramatically decrease the BBB/BTB permeability as well as regional vascular tight junction structure [80].

2.2.1 Treatments to Increase BBB Permeability

Lack of BBB permeation of therapeutics has fueled research into techniques to increase BBB permeability to increase distribution of drugs into brain and tumor lesions. MRI-guided focused ultrasound is a relatively newer technique for BBB/BTB disruption. The delivery of focused ultrasound at higher energies is able to ablate a tumor mass within the brain (high-intensity focused ultrasound [HIFU]). However, at lower energies in the presence of vascular gas-filled microbubbles (low-intensity focused ultrasound [LIFU]) the LIFU causes a BBB opening.

The LIFU-mediated increase in BBB permeability occurs by a combination of physical effects on the NVU and secondary inflammatory responses [81]. Under the exposure of focused ultrasound, microbubbles undergo oscillations within the vasculature impacting the endothelial cell membrane. The exerted pressure of the microbubble against spaces between endothelia transiently increases the aqueous diffusion of drugs into the brain. The secondary effect of acoustic cavitations includes sterile inflammation. After LIFU, there is a release and elevation of heat-shock protein 70, IL-8, TNF-α, and damage-associated molecular patterns in the parenchyma [82]. Aravantis et al examined the effect of focused ultrasound with the uptake of two relevant chemotherapies, doxorubicin and ado-trastuzumab emtansine83 in a HER2 amplified estrogen-dependent model of breast cancer brain metastasis. They observed a 7-fold increase in doxorubicin brain uptake and 2-fold increase in the antibody-drug conjugate. Similarly, trastuzumab plus LIFU increased median survival and reduced tumor

volume as compared to non-treated group in a Her2 and neu positive model of brain metastasis of breast cancer [84]. Despite evidence of preclinical success, LIFU parameters such as including power, cavitation dose, and duration of sonication needs to be elucidated to achieve consistent and reliable BBB/BTB opening in clinical studies.

While radiation remains the standard of care treatment therapy for most brain malignancies, it has been shown that low doses of radiotherapy may enhance BTB permeability to chemotherapy. For example, early work demonstrated that CNS irradiation of 60Gy caused BBB and BTB leakage of horseradish peroxidase, loss of capillary networks, white matter necrosis, and cortical atrophy. These effects were ameliorated 6- to 12-week post-radiation injury [85]. Later work demonstrated effects were dose-dependent and fractionated doses up to 20-30 Gy increased BBB permeability without producing acute or chronic side effects.

Increased permeability following radiotherapy occurs by a primary physiological effect on the brain endothelium followed by a secondary neuroinflammatory response. The inflammatory response may be through an extracranial abscopal effect where radiation damage at the endothelia causes a release of tumor-associated antigens. Direct effects of radiation include a decrease in tight junction protein expression, decreased endothelial cell density, endothelial apoptosis, and higher transcellular transport. Acute effects post-radiotherapy are initiated by inflammatory mediators like activated astrocytes and microglia, TNFα, IL-6, ICAM-1, and IL-1β.

Reports regarding the extent and time course of radiation-mediated BBB/BTB

opening are not consistent. A study by Yuan and colleagues evaluating the effects of fractionated radiotherapy (2Gy, 5 days a week) on brain microvasculature showed BBB permeability did not increase until 90-day post-irradiation [86]. They found higher vesicular activity, lower tight junction density, and increased number of astrocytes in the brain between 90- and 180-day post-irradiation. However, a separate study found acute increase in BBB permeability 24-48 hours post-radiation after a 20Gy radiation dose [87]. Interestingly, the radiation-induced increase in microvascular network could be rescued by anti-TNF treatment. A 2016 preclinical study investigated the effects of radiotherapy on tumor burden and permeability in a breast cancer brain metastasis model. The study demonstrated clinically relevant doses of whole-brain radiation of 20Gy fractions reduced tumor volumes of enhancing tumors but not non-enhancing impermeable tumors [88].

Physical disruption of the BBB can also be carried out by the infusion of a hyperosmotic solution of mannitol (25% w/v) or arabinose into the internal carotid artery. Change in osmolarity of the cerebrovascular endothelial cells causes dilation and shrinkage of the vasculature, leading to an increase in the inter-endothelial space. Widening between the tight junctions (approx. 200 Å) and contraction of endothelial cytoskeleton by calcium causes increase in the BBB permeability, which is highly transient and can last from a few minutes to a few hours [89]. In addition to higher bulk flow rates, there may also be secondary neuroinflammatory responses with osmotic opening. Higher brain levels of cytokines, tropic factors, damage-associated molecular patterns, and cell adhesion molecules have been observed to occur 5-minute post-infusion.

Moreover, sterile inflammatory responses were also observed in the contralateral hemispheres. Neuroinflammatory processes returned back to baseline 96-hour post-osmotic disruption.

While this technique has been extensively explored in primary brain malignancies, its effect on brain metastasis remains unknown. The ability of osmotic disruption to improve delivery of temozolomide was tested in an MGMT negative lung cancer brain metastasis model. The study revealed BTB disruption enhanced temozolomide delivery within tumors by approximately 3-fold as compared to healthy brain. However, it is important to note BBB disruption with temozolomide was highly toxic and the study group was terminated.

An alternate approach to increase BBB permeability is exploiting the activation of endothelial receptors through natural ligands or their analogs. Biochemical activation of receptors like the adenosine 2A, bradykinin type 2 (B2), calcium-activated potassium channels, or ATP-sensitive potassium channels can increase endocytosis as well as downstream signaling to increase BBB permeation. The effect of bradykinin-induced BBB permeability is dose-dependent, transient, and reversible [90]. A proposed mechanism for bradykinin-induced BBB breakdown involves increase in trans-endothelial transport by pinocytic vesicles, as animals that were pretreated with imidazole, trifluoperazine or indomethacin had a decreased effect. Endogenous peptides, like bradykinin, increase intracellular cytoplasmic Ca2+ levels mediated by endothelial connexin hemichannels. Alternate downstream events include release of free radical oxygen species and arachidonic acid, activation of phospholipase A2, and higher production of IL-1β [91].

While preclinical studies have promising data, clinical translation has been difficult. First, biochemical modulation of the BBB with bradykinin requires administration of high concentrations of the endogenous ligand, which can cause severe damage to the brain microvasculature. Secondly, bradykinin has a short half-life and very potent metabolites with vasoactive action. This limits the ability of widespread use of bradykinin in the clinic. While selective B2 agonists like labradimil can potentially reduce some the nonspecific side effects, it is yet to be effectively used within the clinic.

In the past decade, laser interstitial thermal therapy (LITT) was developed for treatment of gliomas. Recent evidence suggests this procedure disrupts the BBB [92]. LITT is a minimally invasive ablative technique that induces cell death of cancerous cells while simultaneously disrupting the BBB for several weeks [93, 94]. The mechanism behind the novel technique is based on the principle cancer cells are more sensitive to thermal damage than healthy cells. The therapeutic window of LITT, however, is small because tumor cells are damaged at 42°C while normal neurons are damaged at 43°C [92].

2.2.2. Manipulation of BBB Receptors to Enter the Brain

Drugs or drug delivery systems can be designed to take advantage of the unique BTB in brain metastases. For example, the “trojan horse” method transports drugs across the BBB by attaching an antibody or peptide to a drug/nanoparticle to target receptors along the BBB which facilitate receptor transcytosis. Some of the most common receptors used for this purpose in different brain pathologies are transferrin receptor (TfR), insulin receptor (InsR),

and LDLrelated protein type 1 (LRP1) [95].

Transferrin receptors are expressed on the luminal side of the BBB. The TfR uses receptor-mediated transcytosis to bind transferrin, an iron sequestering peptide, and shuttle iron into the brain. Using this approach, docetaxel-loaded micelles conjugated to transferrin had a 20.8-fold increase in comparison to free docetaxel [96]. A few in vivo studies have been performed targeting TfR with brain metastasis animal models and show positive results of increased drug uptake in the brain [97, 98]. A study by Wyatt et al assessed the permeability of transferrin-targeted nanoparticles in three different models of brain tumors: intracranial, intracardiac, and intravenous (tail vein). They observed different levels of uptake in the models. The intravenous model was the least permeable to their nanoparticles, followed by the intracranial model, with the intracardiac model being the most permeable [99]. These data highlight the importance of utilizing translationally relevant animal models when evaluating drug delivery to the brain.

A lipid transporter (LRP1 [low-density lipoprotein receptor-related protein 1]) at the BBB binds to LDL and allows lipoproteins to be transcytosed across endothelial cells [100]. One study utilizing an in vivo model of brain metastases showed upregulation of LRP1 increased transcytosis of nanoparticles loaded with doxorubicin and increased survival of mice bearing brain metastases [101]. Whereas a preclinical glioma model demonstrated increased brain uptake and survival with angiopep-2 peptide (ligand for LRP1) conjugated to paclitaxel [102]. More studies are necessary to determine if LRP1 targeted drugs could be efficacious in clinical trials.

Large amino acid transporter 1 (LAT1) transports neutral L-amino acids across the BBB. It is overexpressed in GBM and studies using LAT1 targeting liposomes showed increased brain uptake in glioma models [103]. One study observed a 60% increase in survival with LAT1 liposomes loaded with a STAT3 inhibitor, WP1066 [104]. The other study noted their LAT1 liposomes loaded with docetaxel were more cytotoxic in the gliomas of their animal model than docetaxel alone [103].

Another mechanism of manipulating the BBB to deliver drugs to the brain is by inhibition of efflux transporters, which in theory should allow more influx of chemotherapeutic drugs across the BBB and/or BTB. A study in 2019 measured the uptake of radiolabeled erlotinib in the brains of mice after administration of other P-gp/BCRP substrates. There were significant increases in brain uptake of erlotinib, despite complete inhibition of P-gp and BCRP not being achieved. The most promising inhibitor, tariquidar, increased uptake of erlotinib by 69% [105]. Similarly, animals pretreated with valspodar, a P-gp inhibitor, had increased uptake of paclitaxel by almost 10-fold into the brain and resulted in decreased tumor burden [106]. Sorafenib, a tyrosine kinase inhibitor, in the presence of elacridar, predominantly a BCRP inhibitor, increased the brain-to-plasma ratio by 5-fold [107]. Although these inhibitors were effective increasing drug concentrations delivered to the brain, none have significantly increased patient survival in clinical trials [108].

A clinical study with healthy male patients observed enhanced brain uptake of radiolabeled erlotinib when an oral dose of erlotinib was administered first. The study also investigated the effects of tariquidar administration on erlotinib brain

uptake. Tariquidar was not as effective in increasing radiolabeled erlotinib brain concentrations as pre-administration of erlotinib. This is hypothesized to occur due to saturation of the P-gp and BCRP efflux transporters. Although it is important to note the dosage of erlotinib used was much higher than traditionally recommended and has potentially toxic side effects [109].

2.3 Conclusion

The BTB remains a hurdle in the treatment of CNS tumors. This is notably observed when therapeutics are effective in treating peripheral disease, yet treatment of CNS lesions is largely unsuccessful with the same therapy, presumably because of limited drug penetrance in the central lesion. Currently, in the clinic, mechanisms to alter the BTB of brain metastases specifically and increase drug uptake are unavailable. The typical regimen is to use therapeutics already designed to penetrate the BTB with 60%-80% bioavailability along with use of radiotherapy. Many techniques have been developed to improve drug delivery to the brain. LiFU shows efficacy in increasing BBB permeability and delivering drug, but more studies are needed to determine optimal treatment strategies. Exploitation of transporters at the BBB for drug delivery are promising techniques to increase brain uptake; however, this methodology remains nascent in the clinic.

In the future, it may be beneficial to use BTB molecular differences to target treatment of brain metastases. Ongoing studies of molecular markers of the BTB show differences in pericyte populations, basement membrane formation, and astrocyte attachment to the vessels. One study evaluated vasculature growth

patterns of lung, colon, and breast cancer brain metastases from patients. Lung and colon brain metastases had fewer vessels and collagen accumulation in the brain parenchyma, while breast cancer brain metastases had more vessels with collagen accumulation in the tumor core. The vessels also had increased collagen along the walls, increased density and diameter of vessels, added layers of PDGF-β + pericytes, and detachment of astrocytes [110]. A preclinical study observed dilated capillaries with increased CD31 expression and desmin+ pericytes in a lung cancer brain metastasis model. The study noted a 12-fold decrease in AQP4 along the BTB, which correlates with patient samples [111]. Additional research is necessary to determine molecular disparities between the BBB and BTB for this to be an effective therapeutic target.

Most preclinical works focused on modulation of the BBB to enhance drug delivery have been done in GBM models. It is important to consider the differences in the permeability of the BTB between GBM and brain metastases when developing treatment strategies. While not perfect, numerous intracranial tumor implantation models can mimic the BTB of central tumors, similarly, intracardiac mouse models produce a BTB that has similar heterogeneity of breakdown as clinical brain metastases. Although some preclinical studies show increased penetrance of drugs, this does not always correlate to decreased tumor burden and increased survival, since concentrations generally are sub-therapeutic. Penetrance, accumulation, and final central lesion concentration of chemotherapeutics are critical for successful clinical trials.

2.4 References

1. Sharif Y, Jumah F, Coplan L, Krosser A, Sharif K, Tubbs RS. Blood brain barrier: a review of its anatomy and physiology in health and disease. Clin Anat. 2018;31(6):812–823.
2. Abbott NJ, Patabendige AA, Dolman DE, Yusof SR, Begley DJ. Structure and function of the blood-brain barrier. Neurobiol Dis. 2010;37(1):13–25.
3. Thomsen MS, Routhe LJ, Moos T. The vascular basement membrane in the healthy and pathological brain. J Cereb Blood Flow Metab. 2017;37(10):3300–3317.
4. Cabezas R, Avila M, Gonzalez J, et al. Astrocytic modulation of blood brain barrier: perspectives on Parkinson's disease. Front Cell Neurosci. 2014;8:211.
5. Grossman SA, Ye X, Piantadosi S, et al.; NABTT CNS Consortium. Survival of patients with newly diagnosed glioblastoma treated with radiation and temozolomide in research studies in the United States. Clin Cancer Res. 2010;16(8):2443–2449.
6. Griffith JI, Rathi S, Zhang W, et al. Addressing BBB heterogeneity: a new paradigm for drug delivery to brain tumors. Pharmaceutics. 2020;12(12):1205.
7. Kane JR. The role of brain vasculature in glioblastoma. Mol Neurobiol. 2019;56(9):6645–6653.
8. Watkins S, Robel S, Kimbrough IF, Robert SM, Ellis-Davies G, Sontheimer H. Disruption of astrocyte-vascular coupling and the bloodbrain barrier by invading glioma cells. Nat Commun. 2014;5:4196.
9. Infanger DW, Cho Y, Lopez BS, et al. Glioblastoma stem cells are regulated by interleukin-8 signaling in a tumoral perivascular niche. Cancer Res.

2013;73(23):7079–7089.

10. Pietras A, Katz AM, Ekström EJ, et al. Osteopontin-CD44 signaling in the glioma perivascular niche enhances cancer stem cell phenotypes and promotes aggressive tumor growth. Cell Stem Cell. 2014;14(3):357–369.

11. Nayak L, Lee EQ, Wen PY. Epidemiology of brain metastases. Curr Oncol Rep. 2012;14(1):48–54.

12. Zavyalova MV, Denisov EV, Tashireva LA, et al. Intravasation as a key step in cancer metastasis. Biochemistry (Mosc). 2019;84(7):762–772.

13. Paku S, Döme B, Tóth R, Timár J. Organ-specificity of the extravasation process: an ultrastructural study. Clin Exp Metastasis. 2000;18(6):481–492.

14. Lorger M, Felding-Habermann B. Capturing changes in the brain microenvironment during initial steps of breast cancer brain metastasis. Am J Pathol. 2010;176(6):2958–2971.

15. Kuczynski EA, Vermeulen PB, Pezzella F, Kerbel RS, Reynolds AR. Vessel co-option in cancer. Nat Rev Clin Oncol. 2019;16(8):469–493.

16. Blasberg RG, Gazendam J, Patlak CS, Shapiro WS, Fenstermacher JD. Changes in blood-brain transfer parameters induced by hyperosmolar intracarotid infusion and by metastatic tumor growth. Adv Exp Med Biol. 1980;131:307–319.

17. Lockman PR, Mittapalli RK, Taskar KS, et al. Heterogeneous blood-tumor barrier permeability determines drug efficacy in experimental brain metastases of breast cancer. Clin Cancer Res. 2010;16(23):5664–5678.

18. Folkman J. Tumor angiogenesis: therapeutic implications. N Engl J Med. 1971;285(21):1182–1186.

19. Shah N, Liu Z, Tallman RM, et al. Drug resistance occurred in a newly characterized preclinical model of lung cancer brain metastasis. BMC Cancer. 2020;20(1):292.

20. Adkins CE, Mohammad AS, Terrell-Hall TB, et al. Characterization of passive permeability at the blood-tumor barrier in five preclinical models of brain metastases of breast cancer. Clin Exp Metastasis. 2016;33(4):373–383.

21. Mohammad AS, Adkins CE, Shah N, et al. Permeability changes and effect of chemotherapy in brain adjacent to tumor in an experimental model of metastatic brain tumor from breast cancer. BMC Cancer. 2018;18(1):1225.

22. Mittapalli RK, Adkins CE, Bohn KA, Mohammad AS, Lockman JA, Lockman PR. Quantitative fluorescence microscopy measures vascular pore size in primary and metastatic brain tumors. Cancer Res. 2017;77(2):238–246.

23. Millar BA, Purdie TG, Yeung I, et al. Assessing perfusion changes during whole brain irradiation for patients with cerebral metastases. J Neurooncol. 2005;71(3):281–286.

24. Ding B, Ling HW, Chen KM, Jiang H, Zhu YB. Comparison of cerebral blood volume and permeability in preoperative grading of intracranial glioma using CT perfusion imaging. Neuroradiology. 2006;48(10):773–781.

25. Nakagawa H, Groothuis DR, Owens ES, Patlak CS, Pettigrew KD, Glasberg RR. Dexamethasone effects on vascular volume and tissue hematocrit in experimental RG-2 gliomas and adjacent brain. J Neurooncol. 1988;6(2):157–168.

26. Yano S, Shinohara H, Herbst RS, et al. Expression of vascular endothelial growth factor is necessary but not sufficient for production and growth of brain

metastasis. Cancer Res. 2000;60(17):4959–4967.

27. Mittapalli RK, Manda VK, Bohn KA, Adkins CE, Lockman PR. Quantitative fluorescence microscopy provides high resolution imaging of passive diffusion and P-gp mediated efflux at the in vivo blood-brain barrier. J Neurosci Methods. 2013;219(1):188–195.

28. Adkins CE, Mittapalli RK, Manda VK, et al. P-glycoprotein mediated efflux limits substrate and drug uptake in a preclinical brain metastases of breast cancer model. Front Pharmacol. 2013;4:136.

29. Adkins CE, Nounou MI, Hye T, et al. NKTR-102 efficacy versus irinotecan in a mouse model of brain metastases of breast cancer. BMC Cancer. 2015;15:685.

30. Bohn KA, Adkins CE, Nounou MI, Lockman PR. Inhibition of VEGF and angiopoietin-2 to reduce brain metastases of breast cancer burden. Front Pharmacol. 2017;8:193.

31. Mohammad AS, Griffith JI, Adkins CE, et al. Liposomal irinotecan accumulates in metastatic lesions, crosses the blood-tumor barrier (BTB), and prolongs survival in an experimental model of brain metastases of triple negative breast cancer. Pharm Res. 2018;35(2):31.

32. Nounou MI, Adkins CE, Rubinchik E, et al. Anti-cancer antibody trastuzumab-melanotransferrin conjugate (BT2111) for the treatment of metastatic HER2+ breast cancer tumors in the brain: an in-vivo study. Pharm Res. 2016;33(12):2930–2942.

33. Shah N, Mohammad AS, Saralkar P, et al. Investigational chemotherapy and novel pharmacokinetic mechanisms for the treatment of breast cancer brain metastases. Pharmacol Res. 2018;132:47–68.

34. Terrell-Hall TB, Nounou MI, El-Amrawy F, Griffith JIG, Lockman PR. Trastuzumab distribution in an in-vivo and in-vitro model of brain metastases of breast cancer. Oncotarget. 2017;8(48):83734–83744.

35. Percy DB, Ribot EJ, Chen Y, et al. In vivo characterization of changing blood-tumor barrier permeability in a mouse model of breast cancer metastasis: a complementary magnetic resonance imaging approach. Invest Radiol. 2011;46(11):718–725.

36. Budde MD, Gold E, Jordan EK, Smith-Brown M, Frank JA. Phase contrast MRI is an early marker of micrometastatic breast cancer development in the rat brain. Nmr Biomed. 2012;25(5):726–736.

37. Zhang RD, Price JE, Fujimaki T, Bucana CD, Fidler IJ. Differential permeability of the blood-brain barrier in experimental brain metastases produced by human neoplasms implanted into nude mice. Am J Pathol. 1992;141(5):1115–1124.

38. Palmieri D, Lockman PR, Thomas FC, et al. Vorinostat inhibits brain metastatic colonization in a model of triple-negative breast cancer and induces DNA double-strand breaks. Clin Cancer Res. 2009;15(19):6148–6157.

39. Uehara H, Miyagawa T, Tjuvajev J, et al. Imaging experimental brain tumors with 1-aminocyclopentane carboxylic acid and alpha-aminoisobutyric acid: comparison to fluorodeoxyglucose and diethylenetriaminepentaacetic acid in morphologically defined tumor regions. J Cereb Blood Flow Metab. 1997;17(11):1239–1253.

40. Colombo T, Zucchetti M, D'Incalci M. Cyclosporin A markedly changes the distribution of doxorubicin in mice and rats. J Pharmacol Exp Ther. 1994;269(1):22–27.

41. Kemper EM, van Zandbergen AE, Cleypool C, et al. Increased penetration of paclitaxel into the brain by inhibition of P-glycoprotein. Clin Cancer Res. 2003;9(7):2849–2855.

42. Thomas FC, Taskar K, Rudraraju V, et al. Uptake of ANG1005, a novel paclitaxel derivative, through the blood-brain barrier into brain and experimental brain metastases of breast cancer. Pharm Res. 2009;26(11):2486–2494.

43. Taskar KS, Rudraraju V, Mittapalli RK, et al. Lapatinib distribution in HER2 overexpressing experimental brain metastases of breast cancer. Pharm Res. 2012;29(3):770–781.

44. Kim M, Kizilbash SH, Laramy JK, et al. Barriers to effective drug treatment for brain metastases: a multifactorial problem in the delivery of precision medicine. Pharm Res. 2018;35(9):177.

45. Suh JH, Kotecha R, Chao ST, Ahluwalia MS, Sahgal A, Chang EL. Current approaches to the management of brain metastases. Nat Rev Clin Oncol. 2020;17(5):279–299.

46. Fidler IJ, Yano S, Zhang RD, Fujimaki T, Bucana CD. The seed and soil hypothesis: vascularisation and brain metastases. Lancet Oncol. 2002;3(1):53–57.

47. Barlesi F, Gervais R, Lena H, et al. Pemetrexed and cisplatin as first-line chemotherapy for advanced non-small-cell lung cancer (NSCLC) with asymptomatic inoperable brain metastases: a multicenter phase II trial (GFPC 07-01). Ann Oncol. 2011;22(11):2466–2470.

48. Dinglin XX, Huang Y, Liu H, Zeng YD, Hou X, Chen LK. Pemetrexed and cisplatin combination with concurrent whole brain radiotherapy in patients with

brain metastases of lung adenocarcinoma: a single-arm phase II clinical trial. J Neurooncol. 2013;112(3):461–466.

49. Robinet G, Thomas P, Breton JL, et al. Results of a phase III study of early versus delayed whole brain radiotherapy with concurrent cisplatin and vinorelbine combination in inoperable brain metastasis of non-small-cell lung cancer: Groupe Français de Pneumo-Cancérologie (GFPC) Protocol 95-1. Ann Oncol. 2001;12(1):59–67.

50. Cortes J, Rodriguez J, Aramendia JM, et al. Front-line paclitaxel/cisplatin-based chemotherapy in brain metastases from non-small-cell lung cancer. Oncology. 2003;64(1):28–35.

51. Antonadou D, Paraskevaidis M, Sarris G, et al. Phase II randomized trial of temozolomide and concurrent radiotherapy in patients with brain metastases. J Clin Oncol. 2002;20(17):3644–3650.

52. Verger E, Gil M, Yaya R, et al. Temozolomide and concomitant whole brain radiotherapy in patients with brain metastases: a phase II randomized trial. Int J Radiat Oncol Biol Phys. 2005;61(1):185–191.

53. Stemmler HJ, Schmitt M, Willems A, Bernhard H, Harbeck N, Heinemann V. Ratio of trastuzumab levels in serum and cerebrospinal fluid is altered in HER2-positive breast cancer patients with brain metastases and impairment of blood-brain barrier. Anticancer Drugs. 2007;18(1):23–28.

54. Zhang YK, Wang YJ, Gupta P, Chen ZS. Multidrug resistance proteins (MRPs) and cancer therapy. AAPS J. 2015;17(4):802–812.

55. Mansoori B, Mohammadi A, Davudian S, Shirjang S, Baradaran B. The different mechanisms of cancer drug resistance: a brief review. Adv Pharm Bull.

2017;7(3):339–348.

56. Mundt S, Greter M, Flügel A, Becher B. The CNS immune landscape from the viewpoint of a T cell. Trends Neurosci. 2019;42(10):667–679.

57. Restifo NP, Smyth MJ, Snyder A. Acquired resistance to immunotherapy and future challenges. Nat Rev Cancer. 2016;16(2):121–126.

58. Hodi FS, O'Day SJ, McDermott DF, et al. Improved survival with ipilimumab in patients with metastatic melanoma. N Engl J Med. 2010;363(8):711–723.

59. Goldberg SB, Schalper KA, Gettinger SN, et al. Pembrolizumab for management of patients with NSCLC and brain metastases: long-term results and biomarker analysis from a non- randomised, open-label, phase 2 trial. Lancet Oncol. 2020;21(5):655–663.

60. Tawbi HA, Forsyth PA, Algazi A, et al. Combined nivolumab and ipilimumab in melanoma metastatic to the brain. N Engl J Med. 2018;379(8):722–730.

61. Postow MA, Sidlow R, Hellmann MD. Immune-related adverse events associated with immune checkpoint blockade. N Engl J Med. 2018;378(2):158–168.

62. Havel JJ, Chowell D, Chan TA. The evolving landscape of biomarkers for checkpoint inhibitor immunotherapy. Nat Rev Cancer. 2019;19(3):133–150.

63. Zhou S, Xie J, Huang Z, et al. Anti-PD-(L)1 immunotherapy for brain metastases in non-small cell lung cancer: mechanisms, advances, and challenges. Cancer Lett. 2021;502:166–179.

64. Cohen JE, Merims S, Frank S, Engelstein R, Peretz T, Lotem M. Adoptive cell therapy: past, present and future. Immunotherapy. 2017;9(2):183–196.

65. Akhavan D, Alizadeh D, Wang D, Weist MR, Shepphird JK, Brown CE. CAR T

cells for brain tumors: lessons learned and road ahead. Immunol Rev. 2019;290(1):60–84.

66. Hong JJ, Rosenberg SA, Dudley ME, et al. Successful treatment of melanoma brain metastases with adoptive cell therapy. Clin Cancer Res. 2010;16(19):4892–4898.

67. Gust J, Hay KA, Hanafi LA, et al. Endothelial activation and blood-brain barrier disruption in neurotoxicity after adoptive immunotherapy with CD19 CAR-T cells. Cancer Discov. 2017;7(12):1404–1419.

68. Ribatti D, Vacca A. Overview of angiogenesis during tumor growth. In: Figg WD, Folkman J, eds. Angiogenesis: An Integrative Approach from Science to Medicine. Boston, MA: Springer US; 2008:161–168.

69. Lai A, Filka E, McGibbon B, et al. Phase II pilot study of bevacizumab in combination with temozolomide and regional radiation therapy for up-front treatment of patients with newly diagnosed glioblastoma multiforme: interim analysis of safety and tolerability. Int J Radiat Oncol Biol Phys. 2008;71(5):1372–1380.

70. de Groot JF, Fuller G, Kumar AJ, et al. Tumor invasion after treatment of glioblastoma with bevacizumab: radiographic and pathologic correlation in humans and mice. Neuro Oncol. 2010;12(3):233–242.

71. Stegmayr C, Oliveira D, Niemietz N, et al. Influence of bevacizumab on blood-brain barrier permeability and O-(2-18F-fluoroethyl)-l-tyrosine uptake in rat gliomas. J Nucl Med. 2017;58(5):700–705.

72. Lévy C, Allouache D, Lacroix J, et al. REBECA: a phase I study of bevacizumab and whole-brain radiation therapy for the treatment of brain metastasis from

solid tumours. Ann Oncol. 2014;25(12):2351–2356.

73. Li L, Feng M, Xu P, et al. Stereotactic radiosurgery with whole brain radiotherapy combined with bevacizumab in the treatment of brain metastases from NSCLC. Int J Neurosci. 2021:1–12. Online ahead of print.

74. Chinot OL, Wick W, Mason W, et al. Bevacizumab plus radiotherapy temozolomide for newly diagnosed glioblastoma. N Engl J Med. 2014;370(8):709–722.

75. Gilbert MR, Dignam JJ, Armstrong TS, et al. A randomized trial of bevacizumab for newly diagnosed glioblastoma. N Engl J Med. 2014;370(8):699–708.

76. Levin VA, Bidaut L, Hou P, et al. Randomized double-blind placebo controlled trial of bevacizumab therapy for radiation necrosis of the central nervous system. Int J Radiat Oncol Biol Phys. 2011;79(5):1487–1495.

77. Artacho-Cordón F, Ríos-Arrabal S, Lara PC, Artacho-Cordón A, Calvente I, Núñez MI. Matrix metalloproteinases: potential therapy to prevent the development of second malignancies after breast radiotherapy. Surg Oncol. 2012;21(3):e143–e151.

78. Sood RR, Taheri S, Candelario-Jalil E, Estrada EY, Rosenberg GA. Early beneficial effect of matrix metalloproteinase inhibition on blood-brain barrier permeability as measured by magnetic resonance imaging countered by impaired long-term recovery after stroke in rat brain. J Cereb Blood Flow Metab. 2008;28(2):431–438.

79. Igarashi H, Huber VJ, Tsujita M, Nakada T. Pretreatment with a novel aquaporin 4 inhibitor, TGN-020, significantly reduces ischemic cerebral edema. Neurol Sci. 2011;32(1):113–116.

80. Ostergaard L, Hochberg FH, Rabinov JD, et al. Early changes measured by magnetic resonance imaging in cerebral blood flow, blood volume, and blood-brain barrier permeability following dexamethasone treatment in patients with brain tumors. J Neurosurg. 1999;90(2):300–305.

81. Arsiwala TA, Sprowls SA, Blethen KE, et al. Ultrasound-mediated disruption of the blood tumor barrier for improved therapeutic delivery. Neoplasia. 2021;23(7):676–691.

82. Kovacs ZI, Kim S, Jikaria N, et al. Disrupting the blood-brain barrier by focused ultrasound induces sterile inflammation. Proc Natl Acad Sci USA. 2017;114(1):E75–E84.

83. Arvanitis CD, Askoxylakis V, Guo Y, et al. Mechanisms of enhanced drug delivery in brain metastases with focused ultrasound induced blood-tumor barrier disruption. Proc Natl Acad Sci USA. 2018;115(37):E8717–E8726.

84. Park EJ, Zhang YZ, Vykhodtseva N, McDannold N. Ultrasound-mediated blood-brain/blood-tumor barrier disruption improves outcomes with trastuzumab in a breast cancer brain metastasis model. J Control Release. 2012;163(3):277–284.

85. Rubin P, Gash DM, Hansen JT, Nelson DF, Williams JP. Disruption of the blood-brain barrier as the primary effect of CNS irradiation. Radiother Oncol. 1994;31(1):51–60.

86. Yuan H, Gaber MW, Boyd K, Wilson CM, Kiani MF, Merchant TE. Effects of fractionated radiation on the brain vasculature in a murine model: blood-brain barrier permeability, astrocyte proliferation, and ultrastructural changes. Int J Radiat Oncol Biol Phys. 2006;66(3):860–866.

87. Wilson CM, Gaber MW, Sabek OM, Zawaski JA, Merchant TE. Radiation-induced astrogliosis and blood-brain barrier damage can be abrogated using anti-TNF treatment. Int J Radiat Oncol Biol Phys. 2009;74(3):934–941.

88. Murrell DH, Zarghami N, Jensen MD, Chambers AF, Wong E, Foster PJ. Evaluating changes to blood-brain barrier integrity in brain metastasis over time and after radiation treatment. Transl Oncol. 2016;9(3):219–227.

89. Rapoport SI. Osmotic opening of the blood-brain barrier: principles, mechanism, and therapeutic applications. Cell Mol Neurobiol. 2000;20(2):217–230.

90. Sarker MH, Hu DE, Fraser PA. Acute effects of bradykinin on cerebral microvascular permeability in the anaesthetized rat. J Physiol. 2000;528(Pt 1):177–187.

91. Abbott NJ. Inflammatory mediators and modulation of blood-brain barrier permeability. Cell Mol Neurobiol. 2000;20(2):131–147.

92. Patel B, Yang PH, Kim AH. The effect of thermal therapy on the blood-brain barrier and blood-tumor barrier. Int J Hyperthermia. 2020;37(2):35–43.

93. Salehi A, Paturu MR, Patel B, et al. Therapeutic enhancement of blood-brain and blood-tumor barriers permeability by laser interstitial thermal therapy. Neurooncol Adv. 2020;2(1):vdaa071.

94. Leuthardt EC, Duan C, Kim MJ, et al. Hyperthermic laser ablation of recurrent glioblastoma leads to temporary disruption of the peritumoral blood brain barrier. PLoS One. 2016;11(2):e0148613.

95. Pardridge WM. Drug transport across the blood-brain barrier. J Cereb Blood Flow Metab. 2012;32(11):1959–1972.

96. Sonali, Agrawal P, Singh RP, et al. Transferrin receptor-targeted vitamin E

TPGS micelles for brain cancer therapy: preparation, characterization and brain distribution in rats. Drug Deliv. 2016;23(5):1788–1798.

97. Yin W, Zhao Y, Kang X, et al. BBB-penetrating codelivery liposomes treat brain metastasis of non-small cell lung cancer with EGFRT790M mutation. Theranostics. 2020;10(14):6122–6135.

98. Wang X, Mao W, Wang Z, et al. Enhanced anti-brain metastasis from non-small cell lung cancer of osimertinib and doxorubicin co-delivery targeted nanocarrier. Int J Nanomedicine. 2020;15:5491–5501.

99. Wyatt EA, Davis ME. Method of establishing breast cancer brain metastases affects brain uptake and efficacy of targeted, therapeutic nanoparticles. Bioeng Transl Med. 2019;4(1):30–37.

100. Dehouck B, Fenart L, Dehouck MP, Pierce A, Torpier G, Cecchelli R. A new function for the LDL receptor: transcytosis of LDL across the blood-brain barrier. J Cell Biol. 1997;138(4):877–889.

101. Guo Q, Zhu Q, Miao T, et al. LRP1-upregulated nanoparticles for efficiently conquering the blood-brain barrier and targetedly suppressing multifocal and infiltrative brain metastases. J Control Release. 2019;303:117–129.

102. Li Y, Zheng X, Gong M, Zhang J. Delivery of a peptide-drug conjugate targeting the blood-brain barrier improved the efficacy of paclitaxel against glioma. Oncotarget. 2016;7(48):79401–79407.

103. Li L, Di X, Zhang S, et al. Large amino acid transporter 1 mediated glutamate modified docetaxel-loaded liposomes for glioma targeting. Colloids Surf B Biointerfaces. 2016;141:260–267.

104. Bhunia S, Vangala V, Bhattacharya D, et al. Large amino acid transporter 1

selective liposomes of l-DOPA functionalized amphiphile for combating glioblastoma. Mol Pharm. 2017;14(11):3834–3847.

105. Traxl A, Mairinger S, Filip T, et al. Inhibition of ABCB1 and ABCG2 at the mouse blood-brain barrier with marketed drugs to improve brain delivery of the model ABCB1/ABCG2 substrate [11C]erlotinib. Mol Pharm. 2019;16(3):1282–1293.

106. Fellner S, Bauer B, Miller DS, et al. Transport of paclitaxel (Taxol) across the blood-brain barrier in vitro and in vivo. J Clin Invest. 2002;110(9):1309–1318.

107. Agarwal S, Sane R, Ohlfest JR, Elmquist WF. The role of the breast cancer resistance protein (ABCG2) in the distribution of sorafenib to the brain. J Pharmacol Exp Ther. 2011;336(1):223–233.

108. Bhowmik A, Khan R, Ghosh MK. Blood brain barrier: a challenge for effectual therapy of brain tumors. Biomed Res Int. 2015;2015:320941.

109. Bauer M, Karch R, Wulkersdorfer B, et al. A proof-of-concept study to inhibit ABCG2- and ABCB1-mediated efflux transport at the human blood-brain barrier. J Nucl Med. 2019;60(4):486–491.

110. Téglási V, Csűry DT, Dezső K, et al. Origin and distribution of connective tissue and pericytes impacting vascularization in brain metastases with different growth patterns. J Neuropathol Exp Neurol. 2019;78(4):326–339.

111. Uzunalli G, Dieterly AM, Kemet CM, et al. Dynamic transition of the blood-brain barrier in the development of non-small cell lung cancer brain metastases. Oncotarget. 2019;10(59):6334–6348.

112. Darmus S, Sparidans RW, Wagenaar E, Beijnen JH, Schinkel AH. Oral availability and brain penetration of the B-RAFV600E inhibitor vemurafenib can be enhanced by the P-GLYCOprotein (ABCB1) and breast cancer resistance

protein (ABCG2) inhibitor elacridar. Mol Pharm. 2012;9(11):3236–3245.

113. Mittapalli RK, Vaidhyanathan S, Sane R, Elmquist WF. Impact of P-glycoprotein (ABCB1) and breast cancer resistance protein (ABCG2) on the brain distribution of a novel BRAF inhibitor: vemurafenib (PLX4032). J Pharmacol Exp Ther. 2012;342(1):33–40.

114. Mittapalli RK, Vaidhyanathan S, Dudek AZ, Elmquist WF. Mechanisms limiting distribution of the threonine-protein kinase B-RaF(V600E) inhibitor dabrafenib to the brain: implications for the treatment of melanoma brain metastases. J Pharmacol Exp Ther. 2013;344(3):655–664.

115. Vaidhyanathan S, Mittapalli RK, Sarkaria JN, Elmquist WF. Factors influencing the CNS distribution of a novel MEK-1/2 inhibitor: implications for combination therapy for melanoma brain metastases. Drug Metab Dispos. 2014;42(8):1292–1300.

116. Choo EF, Ly J, Chan J, et al. Role of P-glycoprotein on the brain penetration and brain pharmacodynamic activity of the MEK inhibitor cobimetinib. Mol Pharm. 2014;11(11):4199–4207.

117. Parrish KE, Pokorny J, Mittapalli RK, Bakken K, Sarkaria JN, Elmquist WF. Efflux transporters at the blood-brain barrier limit delivery and efficacy of cyclin-dependent kinase 4/6 inhibitor palbociclib (PD- 0332991) in an orthotopic brain tumor model. J Pharmacol Exp Ther. 2015;355(2):264–271.

118. Gaillard PJ, Appeldoorn CC, Dorland R, et al. Pharmacokinetics, brain delivery, and efficacy in brain tumor-bearing mice of glutathione pegylated liposomal doxorubicin (2B3-101). PLoS One. 2014;9(1):e82331.

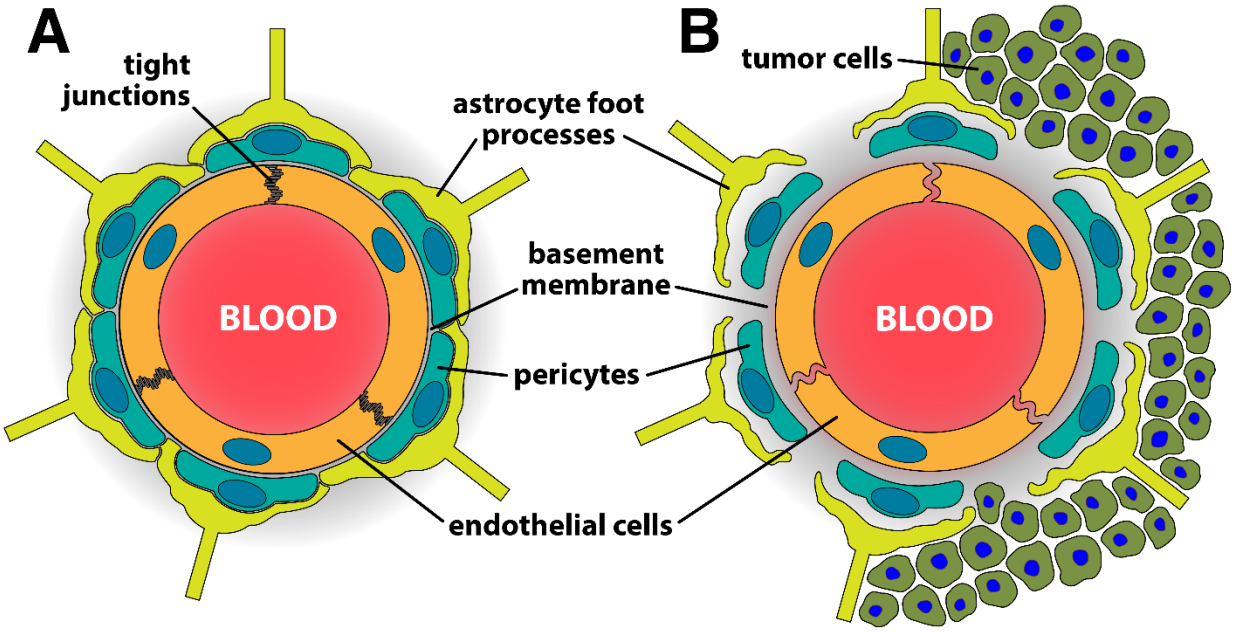

Figure 2.1. Differences between the BBB and BTB. Endothelial cells in a healthy brain are held together by tight junction proteins and prevent paracellular transport. The endothelial cells are surrounded by a basement membrane embedded with pericytes and astrocytic foot processes along the outside (A). The BTB is leakier than the BBB due to lack of tight junction proteins and decreased association of astrocytic end-foot processes and pericytes with the barrier (B).

Chemotherapeutic Agent	Cancer Type	Molecular Target	Clinical Status	Substrate		Brain-to-Plasma Ratio	Ref.
				P-GP	BCRP		
Vemurafenib	Melanoma	Mutant BRAF	Approved	Yes	Yes	1.00 ± 0.19	112, 113
Dabrafenib	Melanoma, Non-Small Cell Lung Cancer, and Thyroid Cancer	Mutant BRAF	Approved	Yes	Yes	0.25	114
Trametinib	Melanoma, Non-Small Cell Lung Cancer, and Thyroid Cancer	MEK	Approved	Yes	No	2.45 ± 1.3	115
Cobimetinib	Melanoma	MEK	Approved	Yes	No	1.1, 6.2	116
Palbociclib	Breast Cancer	CDK4/6	Approved	Yes	Yes	28 ± 6	117
Doxorubicin	Breast Cancer, Leukemia, Lymphoma, Ovarian Cancer, Neuroblastoma, Bone Cancer, and Thyroid Cancer	Topoisomer-ase II	Approved	Yes	Yes	0.0014	118
Paclitaxel	Breast Cancer, Lung Cancer, Ovarian Cancer, and Kaposi's Sarcoma	Tubulin beta-1 chain, Apoptosis regulator Bcl-2	Approved	Yes	No	<3%	17, 106

Table 2.1. Brain-to-plasma ratio of various P-gp and BCRP substrate chemotherapeutic agents for the treatment of brain metastases. Brain concentrations of most drugs are less than 10% of their plasma concentrations.

Chapter 3

Effects of whole-brain radiation therapy on the blood–brain barrier in immunocompetent and immunocompromised mouse models

3.1 Introduction

The blood–brain barrier (BBB) is a selectively permeable, tightly regulated physiochemical barrier between the blood and brain parenchyma [1]. Endothelial cells are locked together by tight junction proteins and sheathed by a basement membrane embedded with pericytes. Astrocyte foot processes encompass the outermost layer. These components work together to regulate molecule passage into the brain [2]. Lipophilic molecules may diffuse across the barrier, but efflux transporter pumps, including P-glycoprotein (P-gp) and breast cancer resistance protein (BCRP), actively shuttle molecules back into the systemic blood circulation [3]. During metastasis, cancer cells infiltrate the brain parenchyma and as they grow displace BBB components resulting in a “leaky” blood-tumor barrier (BTB). Although the BTB is more permeable than BBB, it does not allow drug accumulation in cytotoxic concentrations at the tumor bed [4, 5]. This is one reason for poor prognosis and treatment failure among patients with brain metastases [6].

Treatment for brain metastases includes a combination of radiation therapy, chemotherapy, and/or surgical resection. Depending on the size and number of metastases, patients receive stereotactic radiosurgery (SRS) and/or whole-brain radiation therapy (WBRT) [7]. In the case of multiple metastases, WBRT is most

commonly administered as 30 Gy in 10 fractions. While this improves overall survival, cognitive decline is often seen within six months of treatment.

The timing and magnitude of WBRT vascular permeability changes are not well defined. Unfortunately, most studies have used variable radiotherapy doses and timeframes, leading to results which cannot be easily compared [8–13]. Nevertheless, for the literature that is consistent it appears that BBB disruption occurs anywhere between 24 h and 4 weeks following radiotherapy [14–16].

Multiple studies have shown a synergistic effect of combining radiotherapy with immunotherapy [17–22]. A recent report evaluating immunotherapy efficacy after SRS demonstrated patients with melanoma brain metastases had better outcomes if the immunotherapy was delivered within 7 days of radiation [23]. Optimal timing of immunotherapy administration with radiation is unclear and varies between tumor type, but is important to elicit a robust immune response [24]. Furthermore, local radiotherapy to the primary tumor can benefit brain metastases via an abscopal effect, which is hypothesized to be associated with heightened anti-tumor immunity [25]. Whole-brain radiation therapy induces neuroinflammation with aggregation of immune cells along the BBB and increased proinflammatory mediators in the brain, such as TNF-α. Blocking TNF-α with a recombinant antibody reduces BBB permeability changes following WBRT in mice [10]. This provides evidence of the inflammatory response to radiation playing a role in the magnitude of BBB disruption. Majority of brain metastasis animal models are immunocompromised [26] and this may affect studies investigating BBB/BTB permeability following WBRT.

This study aims to determine the effect of the immune response in radiation-

mediated BBB disruption. Herein we evaluated BBB disruption and immune responses in immunocompetent and athymic nude immunocompromised mice with one dose of 15.5 Gy, which has a biological effective dose (BED) of 39.5 Gy. This is similar to the BED of the clinical treatment regimen (30 Gy in 10 fraction, BED = 39) [27, 28]. We hypothesized that WBRT in immunocompetent mice would result in a higher magnitude of BBB permeability in comparison to athymic immunocompromised mice. We utilized *in situ* brain perfusions and quantitative fluorescent and phosphorescent imaging to identify BBB permeability changes within 24 h following WBRT. A time- and size-dependent opening of the BBB following WBRT in immunocompetent mice was observed, without similar observations in immunocompromised mice. We evaluated presence of proinflammatory mediators in the brain and serum of immunocompetent and immunocompromised mice post-WBRT and observed increased TNF-α serum concentrations and CXCL1 brain concentrations in both strains. These data suggest the immune response may play a role in the magnitude and timing of BBB disruption following WBRT.

3.2 Methods

Animals

All animal experiments were approved by the Institutional Animal Care and Use Committee at West Virginia University. Female C57Bl/6 and C57Bl/6 athymic nude mice were purchased from Jackson Laboratory (Bar Harbor, ME). All animals were approximately 8–10 weeks of age and 25 g during experiments.

Animals were allowed to acclimate for at least one week prior to experimentation. Irradiation protocol The XenX irradiator (Xstrahl, Suwanee, GA) at West Virginia University was commissioned to deliver accurate, clinically-relevant doses of radiation as previously described [29]. C57Bl/6 and C57Bl/6 athymic nude mice were anesthetized with 1–3% isoflurane. All animals were treated with whole-brain irradiation except animals administered 3 kDa Texas Red dextran and ^{14}C-AIB tracers, which were treated with irradiation only on the right hemisphere. Sham control mice were anesthetized with 1–3% isoflurane and placed into the XenX irradiator for the same amount of time it takes to dose mice with 15.5 Gy (~ 5.5 min).

In-situ brain perfusion technique

The in-situ brain perfusion technique was modified from Takasato et al. [30, 31]. Physiological buffer (2.4 nM NaH_2PO_4, 4.2 mM KCl, 24 mM $NaHCO_3$, 128 mM NaCl, 1.5 mM $CaCl_2$, 0.9 mM $MgCl_2$ and 9 mM D-glucose) with ^{14}C-sucrose (Moravek Biochemicals, Brea, CA) and ^{3}H-ivermectin (Moravek Biochemicals, Brea, CA) was prepared, filtered, and heated to 37 °C. At various time points (3–24 h), mice were anesthetized with ketamine (75–100 mg/kg) and xylazine (6–8 mg/kg) followed by whole brain perfusion for two minutes. Brains were collected and sectioned into cortical tissue, subcortical tissue, cerebellum, and brain stem. Sections were weighed and digested with 3 mL Solvable (PerkinElmer, Waltham, MA) in scintillation vials overnight at 55 °C. UltimaGold LSC Cocktail (PerkinElmer, Waltham, MA) was added to samples, vortexed, and read on a Tri-Carb Liquid Scintillation Counter (PerkinElmer, Waltham, MA).

Integrity of the BBB is reported as increases in the vascular space (mL/g) while ivermectin uptake/efflux transporter activity is reported as unidirectional transfer constant, K_{in} (mL/s/g). The vascular volume and K_{in} were calculated as described previously with the equation below [30].

Tracer administration and brain processing

TxRd 3 kDa dextran (Invitrogen, Waltham, MA) and ^{14}C-α-aminoisobutyric acid (AIB) (American Radiolabeled Chemicals, Saint Louis, MO) were injected in concentrations of 6 mg/kg and 100 µCi/animal respectively via tail vein and circulated for 10 min. Brains were collected and snap-frozen in isopentane then stored at −20 °C until sliced. Frozen brains were sliced at 20 µm thickness using a Leica CM3050 cryostat (Leica Microsystems, Los Angeles, CA).

Fluorescent imaging, phosphorescent imaging, and analysis

Fluorescent analyses were performed using an Olympus MVX10 stereomicroscope (Olympus, Tokyo, Japan) (optical zoom range 0.63–12.6, NA = 0.5) with a Hamamatsu ORCA Flash4.0 v2 sCMOS and DAPI/FITC/RFP/Cy5/Cy7 filter set. Sections were imaged using RFP (588 nm) channel to detect 3 kDa Texas red (TxRd) dextran. CellSens image analysis software (Olympus, Tokyo, Japan) was used to quantitate 3 kDa TxRd dextran accumulation. The same slides were placed in quantitative autoradiography cassettes (GE Healthcare Life Sciences, Chicago, IL) with corresponding 14C standards (0.1–862 nCi/g). A 20 × 40 super-resolution phosphor screen (Fujifilm Life Sciences, Cambridge, MA) was placed over the slides and developed for 21

days. Screens were read on FUJI FLA-7000 (Fujifilm Life Sciences, Cambridge, MA) high-resolution phosphor imager. Quantification of ^{14}C-AIB was analyzed with MCID Analysis Software (Inter-Focus Imaging, Cambridge, England). Accumulation of ^{14}C-AIB is reported as nCi/g while 3 kDa TxRd accumulation is sum intensity/area.

Cytokine protein quantification

Sample preparation for V-PLEX Proinflammatory Panel 1 Mouse kit (Meso Scale Diagnostics, Rockville, MD) was described previously [32]. Brains were collected and snap-frozen in isopentane then stored at −20 °C until time of homogenization. Brains were homogenized in RIPA buffer (Thermo Fisher Scientific, Waltham, MA) with Halt Protease and Phosphatase Inhibitor Cocktail (Thermo Fisher Scientific, Waltham, MA). Samples were centrifuged at 13,300 RPM for 15 min at 4 °C. Supernatant was collected and stored at −20 °C. Pierce BCA Protein Assay was performed to determine total protein concentration. Samples were diluted and loaded on the MSD plate at the same total protein concentrations. Manufacturer's protocol for the V-PLEX Proinflammatory Panel 1 Mouse kit was followed as described. Plates were read with Meso Quickplex SQ 120 (Meso Scale Diagnostics, Rockville, MD) and data was analyzed via MSD Discovery Workbench software (Meso Scale Diagnostics, Rockville, MD). Concentrations of cytokines are presented as pg/mL.

Statistical analysis

Data were analyzed and plotted with GraphPad Prism 8 software (GraphPad

Software, San Diego, CA). Results are presented as mean ± SEM unless noted otherwise. Statistical differences between two groups were assessed using Student's t test. One-way ANOVA with a Tukey posttest was utilized for data with more than two groups. Differences were considered statistically significant at $p < 0.05$ (*).

3.2 Results

BBB disruption and dysfunctional efflux transporter activity following WBRT in immunocompetent mice

To evaluate BBB permeability and efflux transporter function after WBRT, we performed *in-situ* brain perfusions with trace amounts of radiolabeled ^{14}C-sucrose, an impermeable marker of BBB integrity, and ^{3}H-ivermectin, an efflux transporter substrate, in physiological buffer at various time points (3–24 h) post-radiation. We observed a significant increase in ^{14}C-sucrose and ^{3}H-ivermectin brain uptake 12 h post-WBRT in immunocompetent C57Bl/6 mice (**Fig. 3.1**). The ^{14}C-sucrose uptake of wild-type (WT) control mice was $1.4 \pm 0.2 \times 10^{-5}$ mL/g and 12 h post-WBRT it was significantly higher ($p < 0.05$) at $3.6 \pm 0.8 \times 10^{-5}$ mL/g. In a similar manner, the uptake of ^{3}H-ivermectin in WT control mice ($4.7 \pm 1.5 \times 10^{-4}$ mL/s/g) significantly increased ($p < 0.05$) to $1.7 \pm 0.6 \times 10^{-3}$ mL/s/g 12 h after being treated with WBRT. No significant differences in ^{14}C-sucrose or ^{3}H-ivermectin whole brain uptake were observed in athymic nude C57Bl/6 mice (**Fig. 3.2**). Athymic nude control mice had a ^{14}C-sucrose uptake of 1.4×10^{-5} mL/g and 12 h post-WBRT ^{14}C-sucrose uptake ($1.5 \pm 0.2 \times 10^{-5}$ mL/g) remained non-significantly altered. The uptake of ^{3}H-ivermectin did not significantly change between the athymic nude control and 12 h post-WBRT mice, 1.1 ± 0.1 × 10–3 mL/s/g and 3.7 ± 1.4 × 10–3 mL/s/g,

respectively. We did not observe significant differences in the two mouse strains baseline ^{14}C-sucrose uptake, however, there was a significant increase ($p < 0.05$) in the uptake of ^{3}H-ivermectin in the athymic nude C57Bl/6 mice (**Supp. Fig. 3.1**).

Time- and size-dependent opening of the BBB post-WBRT

To confirm the BBB permeability alterations observed above, we completed additional experiments where we injected ^{14}C-AIB (~ 103 Da) and TxRd dextran (3 kDa) at various time points (3–24 h) after half-brain irradiation (15.5 Gy). Uptake of ^{14}C-AIB and TxRd dextran in the irradiated side of the brain were compared to the contralateral side. A significant increase in ^{14}C-AIB and TxRd dextran uptake was noted 12 h post-radiation in the immunocompetent mice (**Fig. 3.3A**, **3.3C**). Brain accumulation of ^{14}C-AIB at 12 h significantly increased ($p < 0.05$) to 11.0 ± 1.3 nCi/g in the treated side compared to 7.2 ± 0.6 nCi/g in the contralateral side. For the larger tracer, TxRd 3 kDa dextran, accumulation in the contralateral side of the WT brains was 15.1 ± 0.6 SI/area while the irradiated side had a significant increase ($p < 0.05$) of 18.0 ± 0.8 SI/area. Uptake of ^{14}C-AIB was five-fold higher than TxRd 3 kDa dextran in WT brains 12 h post-irradiation. No differences were observed in ^{14}C-AIB brain uptake in the athymic nude mice (**Fig. 3.3B**). Accumulation of ^{14}C-AIB in nude mice on the untreated side was 18.2 ± 1.2 nCi/g and did not significantly increase with radiation (22.7 ± 1.8 nCi/g). We observed a decrease in 3 kDa TxRd dextran uptake in athymic nude C57Bl/6 mice 12H post-WBRT (**Fig. 3.3D**). The contralateral side of nude mice brains was 12.2 ± 0.2 SI/area and significantly decreased ($p < 0.05$) to 11.1 ± 0.3 SI/area 12 h post-WBRT.

Alterations in proinflammatory cytokines in the brain and serum after WBRT

Radiation induces changes in cytokine concentrations in the brain and serum [33]. To evaluate presence of proinflammatory mediators in immunocompetent and immunocompromised mice post-WBRT, we assessed cytokine concentrations in the serum and brain with a proinflammatory MSD kit, which measures concentrations of 10 proinflammatory cytokines. The TNF-α serum concentrations were significantly increased in immunocompetent and immunocompromised mice (**Fig. 3.4A–C**). Concentration of TNF-α in the serum of WT mice immediately after WBRT was significantly higher ($p < 0.05$) than the control serum (19.0 ± 4.8 pg/mL and 4.3 ± 0.1 pg/mL, respectively) (**Fig. 3.4A**). In the nude mice, we observed an increase in TNF-α serum concentration at 12 h following radiation; control mice had 4.6 ± 0.4 pg/mL and treated mice significantly increased ($p < 0.05$) to 8.4 ± 0.8 pg/mL (**Fig. 3.4B**). When comparing fold changes between strains, WT mice immediately following radiation had 3.4 ± 1.1-fold higher concentration of TNF-α in serum and nude mice 12 h post-WBRT was significantly lower ($p < 0.05$) at 0.8 ± 0.2-fold (**Fig. 3.4C**). There were no significant differences in the serum concentrations of IL-1β, IL-2, IL-5, IL-6, IL-10, or CXCL1 in the WT or athymic nude mice following WBRT (**Supp. Fig. 3.4**, **Supp. Fig. 3.5**). The chemokine CXCL1 was significantly increased ($p < 0.05$) in the brains of WT mice 6 and 12 h post-WBRT with concentrations of 16.8 ± 1.4 pg/mL and 17.0 ± 0.5 pg/mL, respectively, in comparison to control concentration of 4.9 ± 0.4 pg/mL (**Fig. 3.4D**). The concentration of CXCL1 also increased in the athymic nude C57Bl/6 mice 12 h post-WBRT (**Fig. 3.4E**). Control nude mice had a CXCL1 brain concentration of 8.2 ± 0.4 pg/mL and increased significantly ($p < 0.05$) 12 h post-WBRT to a

concentration of 20.9 ± 1.5 pg/mL. There was a significant difference ($p < 0.05$) in the fold changes between the 12 h time points of the WT and athymic nude mice, 2.5 ± 0.1-fold and 1.5 ± 0.2-fold, respectively (**Fig. 3.4F**). Other cytokines significantly increased ($p < 0.05$) in the brains of WT mice following WBRT were TNF-α, IL-2, and IL-12p70 (**Fig. 3.5**). There were no significant differences in brain concentrations of IL-1β, IL-4, IL-5, IL-6, or IFN-γ in the WT or nude mice post-WBRT (**Supp. Fig. 3.6**, **Supp. Fig. 3.7**). Additionally, no differences were observed in brain concentrations of IL-2, IL-10, IL-12p70, or TNF-α in nude mice 12 h following radiation (**Supp. Fig. 3.7**).

3.3 Discussion

Whole-brain radiation therapy promotes neuroinflammation and disrupts the BBB. This is demonstrated by increased expression of proinflammatory mediators and decreased expression of tight junction proteins [34]. The majority of work in the preclinical cancer research field is performed with athymic nude mice which lack functional T-cells [35]. It is important to determine the effects WBRT may have on the BBB in athymic mice and immunocompetent mice, considering patient immune profiles lie somewhere in between during cancer treatment [36, 37]. Understanding the immune response to WBRT and the downstream effects on BBB permeability may be useful when designing treatment plans with concurrent immunotherapy, targeted therapy, or chemotherapy. Herein, we investigate the relationship between the immune response to WBRT and the effects on BBB integrity in a time- and size-dependent manner.

We observed in immunocompetent and athymic immunocompromised mice

BBB integrity was intact prior to WBRT, however, we observed disruption in the WT mice 12 h post-WBRT. These findings suggest radiation-mediated BBB permeability may be impacted by the presence of functional T-cells. T-cell dependent neuroinflammation and BBB disruption have been reported in neurodegenerative diseases, ischemic stroke, and chronic stress [38–41]. Interestingly, one study observed that transfer of non-CNS-specific activated T-cells into mice results in similar levels of BBB disruption as transfer of CNS-specific activated T-cells, a model of multiple sclerosis [42].

In contrast to the BBB integrity, we observed a decrease in efflux transporter activity in the athymic nude mice at baseline. A significant decrease in efflux activity 12 h post-WBRT was observed only in the WT mice, which returned to baseline 24 h post-radiation. Numerous studies have demonstrated proinflammatory mediators alter expression and functional activity of efflux transporters *in vitro* and *in vivo* [43]. Dysfunctional efflux transport activity has also been observed in patients with Alzheimer's disease. One study reported patients have efflux transport activity levels similar to those with pharmacological inhibitors [44, 45]. Neuroinflammation and presence of amyloid-β plaques are hallmarks of Alzheimer's disease. It is hypothesized that the reduced efflux transporter activity contributes to poor clearance of amyloid-β from the brain, leading to plaque accumulation. Our data correspond with the current literature and indicate an immune response-dependent window of time during which efflux transporter function is decreased after WBRT.

We confirmed BBB disruption following irradiation with quantitative imaging of fluorescent and radiolabeled molecules of two different sizes. The small radiolabeled molecule, ^{14}C-AIB (~ 103 Da), was five-fold higher in irradiated sides of

WT mouse brains 12 h post-WBRT in comparison to the larger molecule, 3 kDa TxRd dextran. Increased accumulation of the molecules was not observed in the athymic nude mice treated with WBRT. We have previously characterized size-dependent BBB/BTB disruption in our brain tumor models and healthy mice treated with low intensity focused ultrasound [46, 47]. In both cases, molecules with lower molecular weights accumulate in the brain to a higher degree than high molecular weight molecules. These data add to our previous work and demonstrate the impact of the immune response to WBRT on BBB permeability is time and size-dependent.

The presence of proinflammatory mediators in the serum and brain following WBRT was measured in the two mouse strains. We observed a significant increase in TNF-α in the serum of WT mice immediately following radiation and athymic nude mice 12 h post-WBRT. The increased fold change of TNF-α in WT mice immediately following WBRT was significantly higher than the fold change in the athymic nude mice 12 h post-WBRT. In the brain, CXCL1 concentrations were significantly increased in WT and nude mice 12 h post-WBRT. When comparing the two strains in relation to their controls, WT mice had a 2.5-fold increase in their CXCL1 brain concentration while nude mice had a 1.5-fold increase. These data suggest the nude mice have a delayed, lower magnitude inflammatory response to WBRT. The relationship between TNF-α and CXCL1 is well documented in the literature [48–51]. In endothelial cells, TNF-α binds to its receptor and initiates the JNK and p38 MAPK signaling pathways to secrete CXCL1 [49]. Additionally, TNF-α increases expression of CXCR2, the receptor of CXCL1, on endothelial cells and enhances adherence of Th17 cells, a proinflammatory subtype of T-helper cells associated with neuroinflammation [50, 51]. Th17 cells then cross the BBB, cause

neuronal cell death, and maintain the proinflammatory environment through immune cell recruitment and production of IL-17. Production of IL-17 has been shown to decrease the expression of tight junction proteins in mouse models of multiple sclerosis [48]. We hypothesize this pathway is activated in response to WBRT, leading to BBB disruption in WT but not athymic nude mice, schematic shown in **Fig. 3.6**.

Our study expands on previous work in the field by highlighting the impact of the immune response to WBRT on BBB dysfunction, however, there are a few limitations to our work. First, our studies were completed using a single dose of radiation at 15.5 Gy. Although this is a similar BED to the clinical dosing of 30 Gy in 10 fractions, the clinical dosing schedule may have differential effects. To determine the extent of altered efflux transporter activity, competitive inhibition experiments are needed. More work is necessary to elucidate the underlying mechanism of BBB disruption following WBRT in immunocompetent mice. Our previous work demonstrates BTB disruption in athymic nude mice post-WBRT, therefore, more research is required to determine the differences in WBRT-mediated BTB and BBB disruption with immunocompetent and immunocompromised mouse modeling.

3.4 Conclusion

The BBB is disrupted following WBRT, but the extent and timing of disruption vary between studies. It is necessary to understand factors which may be contributing to altered BBB permeability following irradiation to develop more efficacious treatment strategies when combining radiation with systemic therapy. Our work demonstrates the impact of the immune response to WBRT on BBB permeability in a time- and size-dependent manner. This is relevant in

the preclinical cancer research field due to the more frequent use of immunocompromised mice with human cancer cell lines. Our work suggests this may not be an accurate model of BBB permeability. Furthermore, we identified a window of time post-WBRT where efflux transporter activity is significantly decreased. Numerous anticancer therapeutics are substrates for efflux transporters, such as doxorubicin, vinblastine, and taxanes [52, 53]. A transient decrease in efflux transporter activity and an increase in BBB permeability may enhance delivery of these therapeutics across the BBB. We also offer a potential mechanism and avenue for further exploration.

3.5 References

1. Daneman R, Prat A. The blood–brain barrier. Cold Spring Harb Perspect Biol. 2015;7(1):a020412.
2. Abbott NJ, Patabendige AA, Dolman DE, Yusof SR, Begley DJ. Structure and function of the blood–brain barrier. Neurobiol Dis. 2010;37(1):13–25.
3. Golden PL, Pollack GM. Blood–brain barrier efflux transport. J Pharm Sci. 2003;92(9):1739–53.
4. Lockman PR, Mittapalli RK, Taskar KS, Rudraraju V, Gril B, Bohn KA, et al. Heterogeneous blood-tumor barrier permeability determines drug efficacy in experimental brain metastases of breast cancer. Clin Cancer Res. 2010;16(23):5664–78.
5. Blethen KE, Arsiwala TA, Fladeland RA, Sprowls SA, Panchal DM, Adkins CE, et al. Modulation of the blood-tumor barrier to enhance drug delivery and efficacy for brain metastases. Neurooncol Adv. 2021;3(Suppl 5):v133–43.
6. Boire A, Brastianos PK, Garzia L, Valiente M. Brain metastasis. Nat Rev Cancer. 2020;20(1):4–11.
7. Kotecha R, Gondi V, Ahluwalia MS, Brastianos PK, Mehta MP. Recent advances in managing brain metastasis. F1000Res. 2018;7.
8. van Vulpen M, Kal HB, Taphoorn MJ, El-Sharouni SY. Changes in blood-brain barrier permeability induced by radiotherapy: implications for timing of chemotherapy? (Review). Oncol Rep. 2002;9(4):683–8.
9. Qin D, Mo H, Ou G. Therapeutic effect on glioblastoma of chemotherapy on the basis of brain irradiation. Zhonghua Zhong Liu Za Zhi. 2001;23(2):168–9.
10. Wilson CM, Gaber MW, Sabek OM, Zawaski JA, Merchant TE. Radiation induced

astrogliosis and blood–brain barrier damage can be abrogated using anti-TNF treatment. Int J Radiat Oncol Biol Phys. 2009;74(3):934–41.

11. Yuan H, Gaber MW, McColgan T, Naimark MD, Kiani MF, Merchant TE. Radiation-induced permeability and leukocyte adhesion in the rat blood-brain barrier: modulation with anti-ICAM-1 antibodies. Brain Res. 2003;969(1–2):59–69.
12. Crowe W, Wang L, Zhang Z, Varagic J, Bourland JD, Chan MD, et al. MRI evaluation of the effects of whole brain radiotherapy on breast cancer brain metastasis. Int J Radiat Biol. 2019;95(3):338–46.
13. Lim WH, Choi SH, Yoo RE, Kang KM, Yun TJ, Kim JH, et al. Does radiation therapy increase gadolinium accumulation in the brain?: Quantitative analysis of T1 shortening using R1 relaxometry in glioblastoma multiforme patients. PLoS ONE. 2018;13(2):e0192838.
14. Teng F, Tsien CI, Lawrence TS, Cao Y. Blood-tumor barrier opening changes in brain metastases from pre to one-month post radiation therapy. Radiother Oncol. 2017;125(1):89–93.
15. Millar BA, Purdie TG, Yeung I, Pond GR, Billingsley S, Wong R, et al. Assessing perfusion changes during whole brain irradiation for patients with cerebral metastases. J Neurooncol. 2005;71(3):281–6.
16. Lee MC, Cha S, Chang SM, Nelson SJ. Dynamic susceptibility contrast perfusion imaging of radiation effects in normal-appearing brain tissue: changes in the first-pass and recirculation phases. J Magn Reson Imaging. 2005;21(6):683–93.
17. Antonia SJ, Villegas A, Daniel D, Vicente D, Murakami S, Hui R, et al. Durvalumab after chemoradiotherapy in stage III non-small-cell lung cancer. N Engl J Med. 2017;377(20):1919–29.

18. Mattes MD, Eubank TD, Almubarak M, Wen S, Marano GD, Jacobson GM, et al. A prospective trial evaluating the safety and systemic response from the concurrent use of radiation therapy with checkpoint inhibitor immunotherapy in metastatic non-small cell lung cancer. Clin Lung Cancer. 2021;22(4):268–73.
19. Bestvina CM, Pointer KB, Karrison T, Al-Hallaq H, Hoffman PC, Jelinek MJ, et al. A phase 1 trial of concurrent or sequential ipilimumab, nivolumab, and stereotactic body radiotherapy in patients with stage IV NSCLC study. J Thorac Oncol. 2022;17(1):130–40.
20. Theelen W, Chen D, Verma V, Hobbs BP, Peulen HMU, Aerts J, et al. Pembrolizumab with or without radiotherapy for metastatic non-small-cell lung cancer: a pooled analysis of two randomised trials. Lancet Respir Med. 2021;9(5):467–75.
21. Anzellini D, De Sanctis V, Valeriani M, Reverberi C, Marinelli L, Massaro M, et al. Stereotactic and hypofractionated radiotherapy associated with immune checkpoint inhibitor drugs: analysis of local control, toxicity, and outcome in a single research centre case study. Anticancer Res. 2021;41(10):5107–16.
22. Hu ZI, Ho AY, McArthur HL. Combined radiation therapy and immune checkpoint blockade therapy for breast cancer. Int J Radiat Oncol Biol Phys. 2017;99(1):153–64.
23. Wegner RE, Abel S, D'Amico RS, Mehta GU, Sheehan J. Time from stereotactic radiosurgery to immunotherapy in patients with melanoma brain metastases and impact on outcome. J Neurooncol. 2021;152(1):79–87.
24. Samstein R, Rimner A, Barker CA, Yamada Y. Combined immune checkpoint blockade and radiation therapy: timing and dose fractionation associated with

greatest survival duration among over 750 treated patients. Int J Radiat Oncol. 2017;99(2):S129–30.

25. Pangal DJ, Yarovinsky B, Cardinal T, Cote DJ, Ruzevick J, Attenello FJ, et al. The abscopal effect: systematic review in patients with brain and spine metastases. Neurooncol Adv. 2022;4(1):vdac132.

26. Valiente M, Van Swearingen AED, Anders CK, Bairoch A, Boire A, Bos PD, et al. Brain metastasis cell lines panel: a public resource of organotropic cell lines. Cancer Res. 2020;80(20):4314–23.

27. Bentzen SM, Dorr W, Gahbauer R, Howell RW, Joiner MC, Jones B, et al. Bioeffect modeling and equieffective dose concepts in radiation oncology–terminology, quantities and units. Radiother Oncol. 2012;105(2):266–8.

28. Lin X, DeAngelis LM. Treatment of brain metastases. J Clin Oncol. 2015;33(30):3475–84.

29. Sprowls SA, Pizzuti VJ, Pentz W, Nwafor DC, Siochi RAC, Lockman PR. Irradiator commissioning and dosimetry for assessment of lq alpha and beta parameters, radiation dosing schema, and in vivo dose deposition. J Vis Exp. 2021(169).

30. Takasato Y, Rapoport SI, Smith QR. An *in situ* brain perfusion technique to study cerebrovascular transport in the rat. Am J Physiol. 1984;247(3 Pt 2):H484–93.

31. Mittapalli RK, Manda VK, Bohn KA, Adkins CE, Lockman PR. Quantitative fluorescence microscopy provides high resolution imaging of passive diffusion and P-gp mediated efflux at the in vivo blood-brain barrier. J Neurosci Methods. 2013;219(1):188–95.

32. Walker WH 2nd, Bumgarner JR, Nelson RJ, Courtney DA. Transcardial perfusion is not required to accurately measure cytokines within the brain. J Neurosci Methods.

2020;334:108601.

33. Kyrkanides S, Olschowka JA, Williams JP, Hansen JT, O'Banion MK. TNF alpha and IL-1beta mediate intercellular adhesion molecule-1 induction via microglia-astrocyte interaction in CNS radiation injury. J Neuroimmunol. 1999;95(1–2):95–106.

34. Hladik D, Tapio S. Effects of ionizing radiation on the mammalian brain. Mutat Res Rev Mutat Res. 2016;770(Pt B):219–30.

35. Zhang Z, Burnley P, Coder B, Su DM. Insights on FoxN1 biological significance and usages of the "nude" mouse in studies of T-lymphopoiesis. Int J Biol Sci. 2012;8(8):1156–67.

36. Grossman SA, Ye X, Lesser G, Sloan A, Carraway H, Desideri S, et al. Immunosuppression in patients with high-grade gliomas treated with radiation and temozolomide. Clin Cancer Res. 2011;17(16):5473–80.

37. Lv Y, Song M, Tian X, Yv X, Liang N, Zhang J. Impact of radiotherapy on circulating lymphocyte subsets in patients with esophageal cancer. Medicine (Baltimore). 2020;99(36):e20993.

38. Balasa R, Barcutean L, Balasa A, Motataianu A, Roman-Filip C, Manu D. The action of TH17 cells on blood brain barrier in multiple sclerosis and experimental autoimmune encephalomyelitis. Hum Immunol. 2020;81(5):237–43.

39. Tan S, Shan Y, Wang Y, Lin Y, Liao S, Deng Z, et al. Exacerbation of oxygen glucose deprivation-induced blood-brain barrier disruption: potential pathogenic role of interleukin-9 in ischemic stroke. Clin Sci (Lond). 2017;131(13):1499–513.

40. Peng Z, Peng S, Lin K, Zhao B, Wei L, Tuo Q, et al. Chronic stress-induced depression requires the recruitment of peripheral Th17 cells into the brain. J

Neuroinflammation. 2022;19(1):186.

41. Zamudio F, Loon AR, Smeltzer S, Benyamine K, Navalpur Shanmugam NK, Stewart NJF, et al. TDP-43 mediated blood-brain barrier permeability and leukocyte infiltration promote neurodegeneration in a low-grade systemic inflammation mouse model. J Neuroinflammation. 2020;17(1):283.

42. Smorodchenko A, Wuerfel J, Pohl EE, Vogt J, Tysiak E, Glumm R, et al. CNS irrelevant T-cells enter the brain, cause blood-brain barrier disruption but no glial pathology. Eur J Neurosci. 2007;26(6):1387–98.

43. Saib S, Delavenne X. Inflammation induces changes in the functional expression of P-gp, BCRP, and MRP2: an overview of different models and consequences for drug disposition. Pharmaceutics. 2021;13(10).

44. van Assema DM, Lubberink M, Bauer M, van der Flier WM, Schuit RC, Windhorst AD, et al. Blood-brain barrier P-glycoprotein function in Alzheimer's disease. Brain. 2012;135(Pt 1):181–9.

45. Deo AK, Borson S, Link JM, Domino K, Eary JF, Ke B, et al. Activity of P-glycoprotein, a beta-amyloid transporter at the blood-brain barrier, Is compromised in patients with Mild Alzheimer disease. J Nucl Med. 2014;55(7):1106–11.

46. Mittapalli RK, Adkins CE, Bohn KA, Mohammad AS, Lockman JA, Lockman PR. Quantitative fluorescence microscopy measures vascular pore size in primary and metastatic brain tumors. Cancer Res. 2017;77(2):238–46.

47. Arsiwala TA, Sprowls SA, Blethen KE, Fladeland RA, Wolford CP, Kielkowski BN, et al. Characterization of passive permeability after low intensity focused ultrasound mediated blood-brain barrier disruption in a preclinical model. Fluids Barriers CNS. 2022;19(1):72.

48. Kebir H, Kreymborg K, Ifergan I, Dodelet-Devillers A, Cayrol R, Bernard M, et al. Human TH17 lymphocytes promote blood-brain barrier disruption and central nervous system inflammation. Nat Med. 2007;13(10):1173–5.

49. Lo HM, Lai TH, Li CH, Wu WB. TNF-alpha induces CXCL1 chemokine expression and release in human vascular endothelial cells in vitro via two distinct signaling pathways. Acta Pharmacol Sin. 2014;35(3):339–50.

50. Wu F, Zhao Y, Jiao T, Shi D, Zhu X, Zhang M, et al. CXCR2 is essential for cerebral endothelial activation and leukocyte recruitment during neuroinflammation. J Neuroinflammation. 2015;12:98.

51. Wojkowska DW, Szpakowski P, Glabinski A. Interleukin 17A promotes lymphocytes adhesion and induces CCL2 and CXCL1 release from brain endothelial cells. Int J Mol Sci. 2017;18(5).

52. Schinkel AH, Smit JJ, van Tellingen O, Beijnen JH, Wagenaar E, van Deemter L, et al. Disruption of the mouse mdr1a P-glycoprotein gene leads to a deficiency in the blood-brain barrier and to increased sensitivity to drugs. Cell. 1994;77(4):491–502.

53. Tsuji A. P-glycoprotein-mediated efflux transport of anticancer drugs at the blood–brain barrier. Ther Drug Monit. 1998;20(5):588–90.

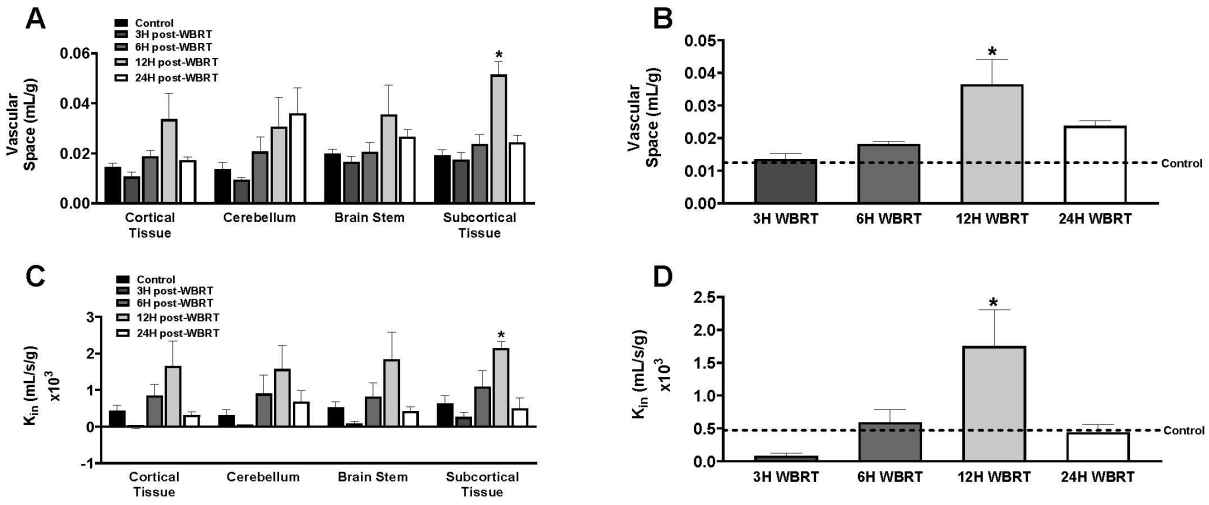

Figure 3.1. Disruption of BBB homeostasis following WBRT in immunocompetent mice. Significant increase in ^{14}C-sucrose (A, B) and ^{3}H-ivermectin (C, D) uptake observed regionally and in whole brains 12h following WBRT (15.5Gy) in wild-type C57Bl/6 mice. ($p<0.05$)

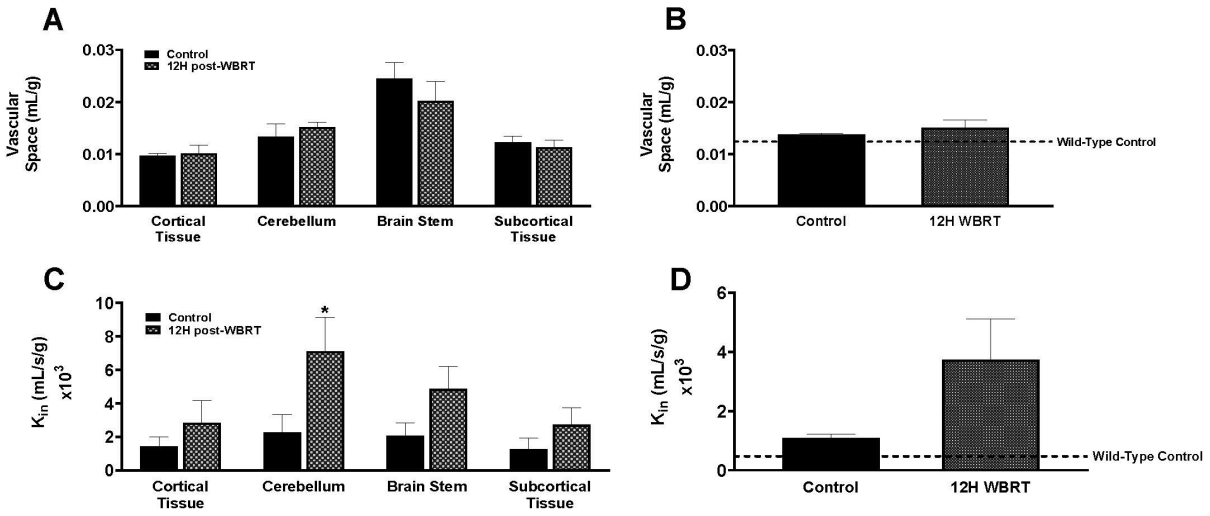

Figure 3.2. No significant changes in BBB homeostasis following WBRT in whole brains of immunocompromised mice. No significant differences in ^{14}C-sucrose uptake regionally (A) or in the whole brains (B) of nude mice 12 h following WBRT. Significant increase in ^{3}H-ivermectin uptake in the Cerebellum (C) of nude mice 12 h post-WBRT, but no significant changes in whole brain (D) uptake. ($p < 0.05$)

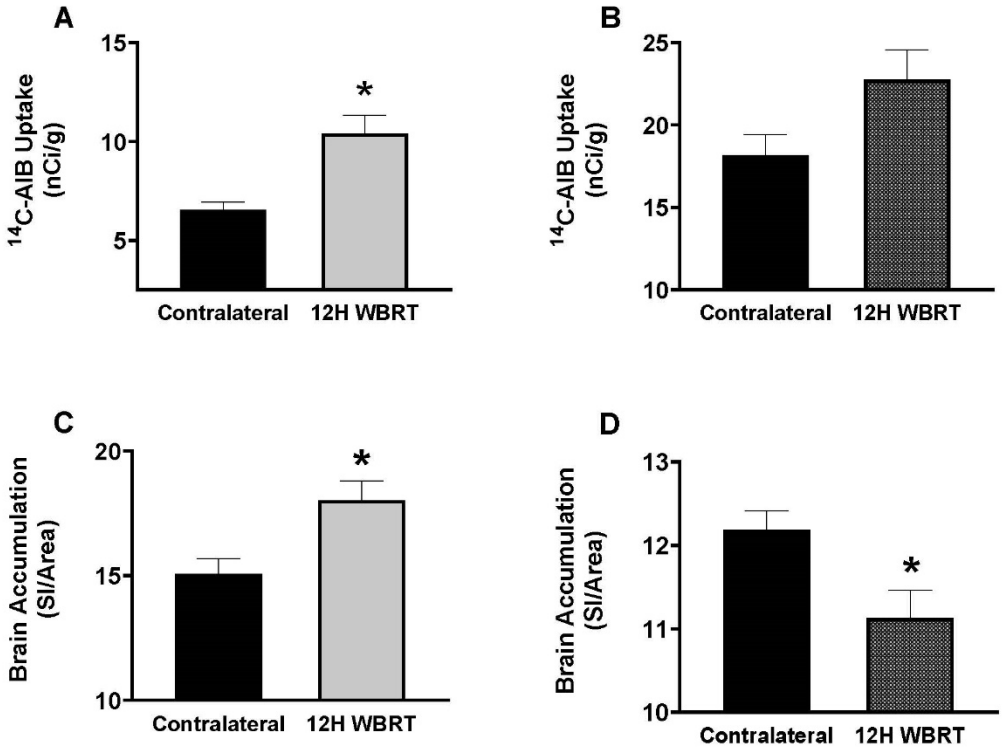

Figure 3.3. Increased BBB permeability following WBRT in immunocompetent mice is time and size-dependent. Significant ($p<0.05$) increase in 14C-AIB (A) and 3 kDa TxRd (C) uptake observed 12h following WBRT (15.5Gy) in wild-type C57Bl/6 mice, but not athymice nude C57Bl/6 mice (B, D).

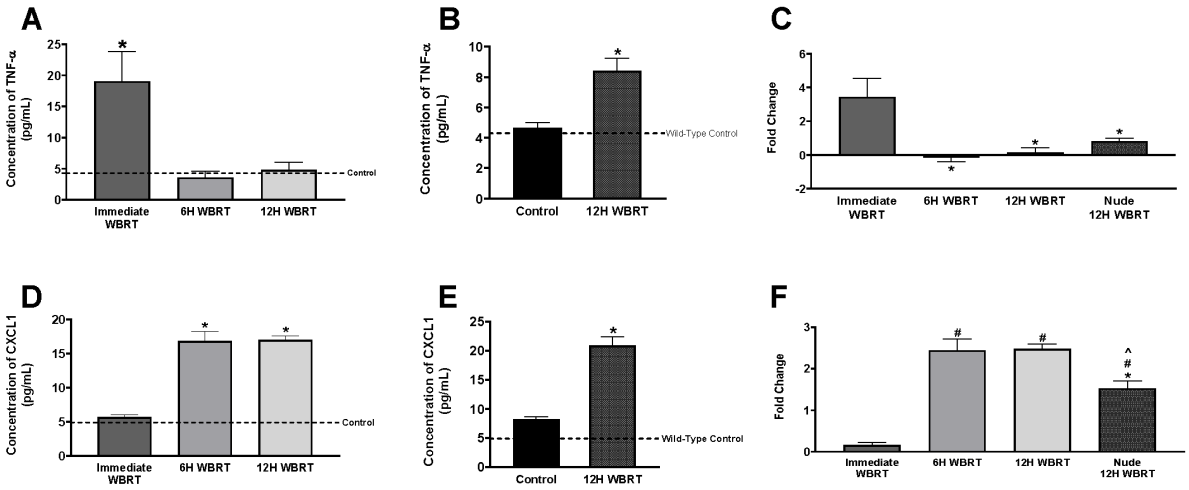

Figure 3.4. Increased proinflammatory mediators following WBRT in immunocompetent and immunocompromised mice. Significant increase of TNF-α in the serum of WT mice immediately after WBRT (15.5 Gy) (A). Significant increase of TNF-α in the serum of athymic nude mice 12h post-WBRT (B). The fold changes of TNF-α concentrations in the serum following WBRT are significantly decreased 6h and 12h in WT mice and 12h in nude mice in comparison to WT immediate concentrations (C). CXCL1 is significantly increased in the brains of WT mice 6h and 12h post-WBRT and in the brains of nude mice 12h post-WBRT (D, E). The fold changes of CXCL1 brain concentrations are significantly different between 12h timepoints of WT and nude strains (F). ($p < 0.05$)

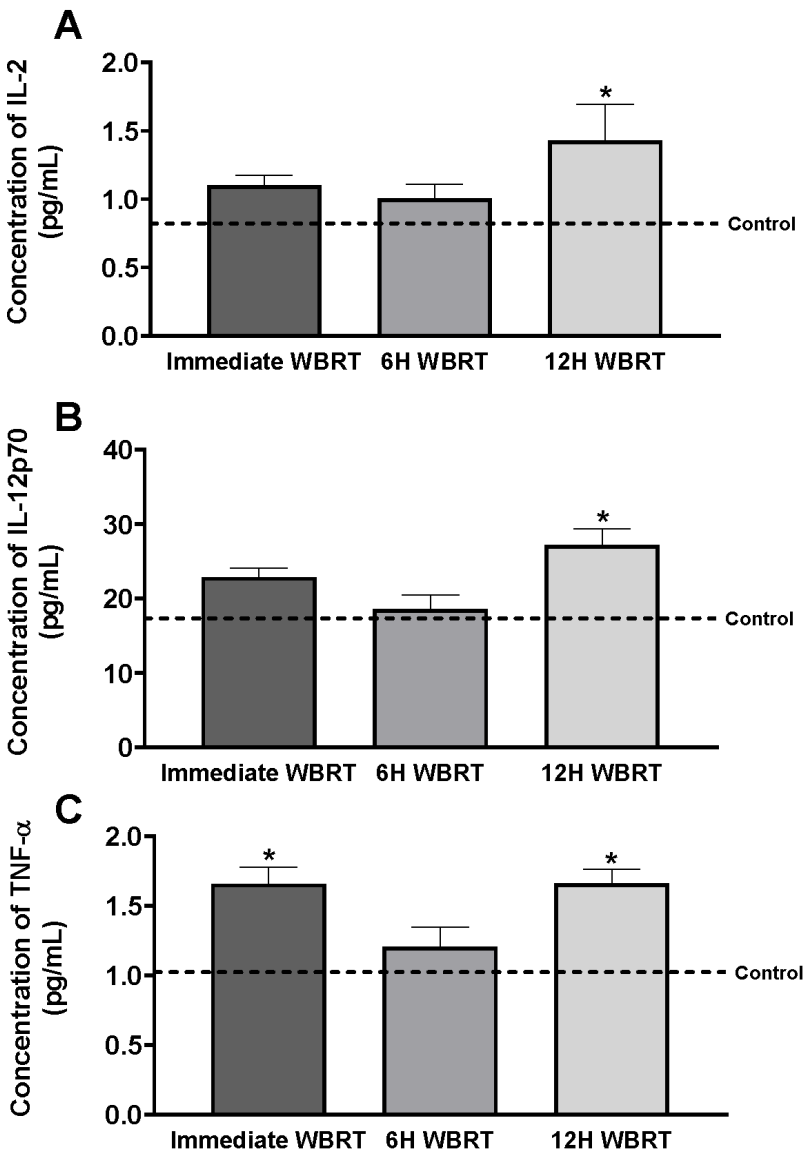

Figure 3.5. Proinflammatory cytokines significantly increased in brains of immunocompetent mice post-WBRT. IL-2 and IL-12p70 are significantly increased 12H post-WBRT in brains of wild-type mice (A, B). TNF-α is significantly increased immediately and 12H post-WBRT (15.5 Gy) in brains of wild-type mice (C). ($p < 0.05$)

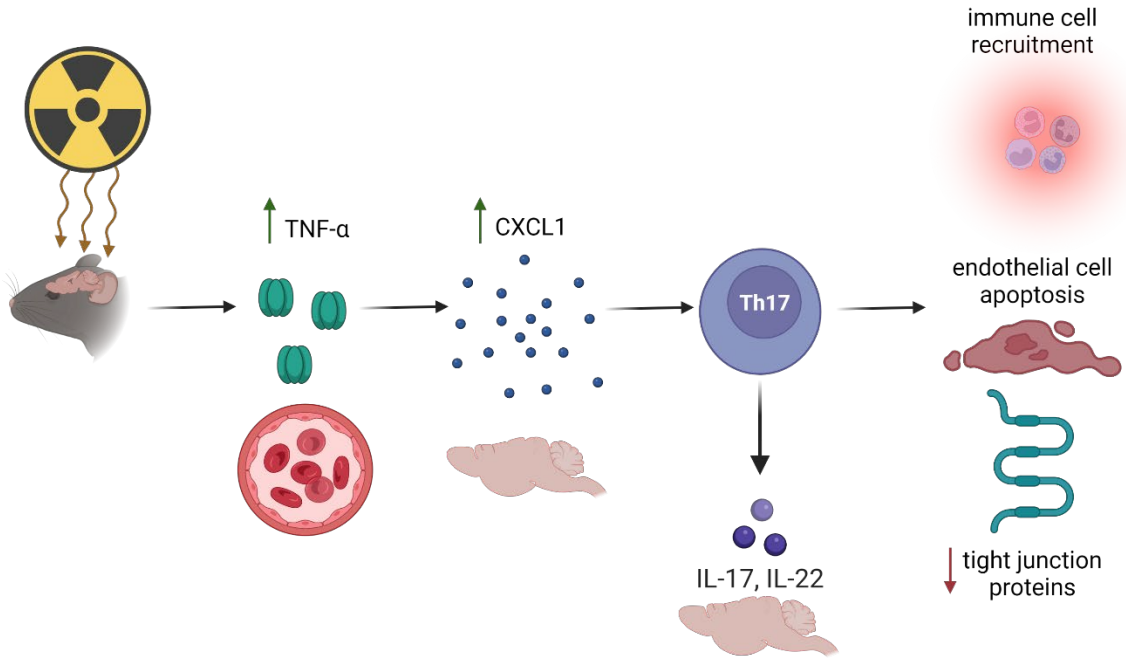

Figure 3.6. Proposed mechanism of T-cell dependent BBB disruption following WBRT. A schematic summarizing results and hypothesizing the mechanism of BBB disruption post-WBRT in the wild-type mice. Figure was created with BioRender.com.

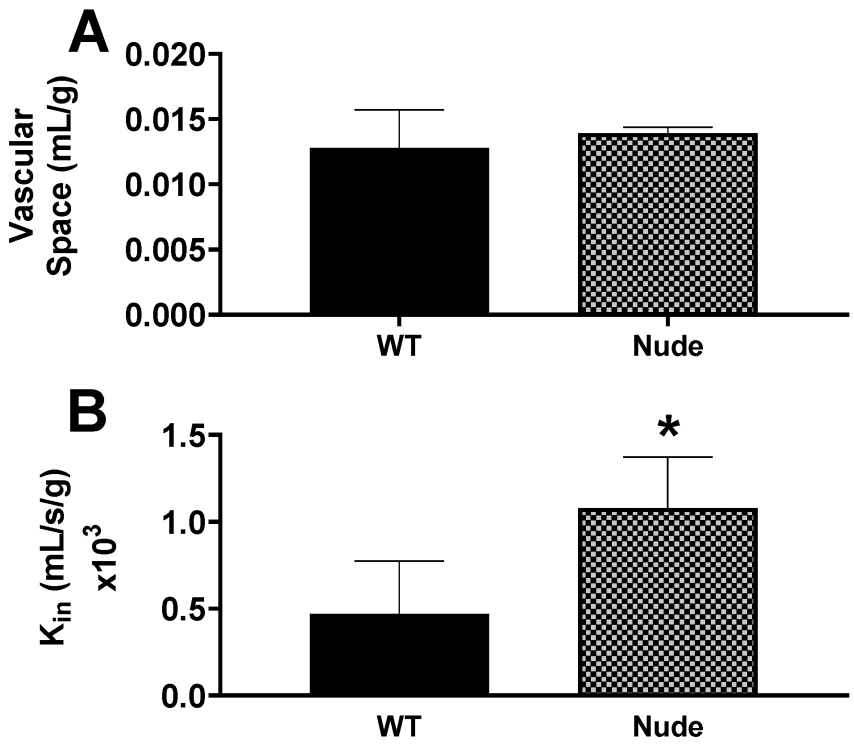

Supplemental Figure 3.1. Nude mice have significantly decreased efflux transporter function, but no difference in BBB integrity. No significant differences in ^{14}C-sucrose uptake between mouse strains at baseline (A). Nude mice had a significant increase in ^{3}H-ivermectin uptake at baseline. ($p < 0.05$)

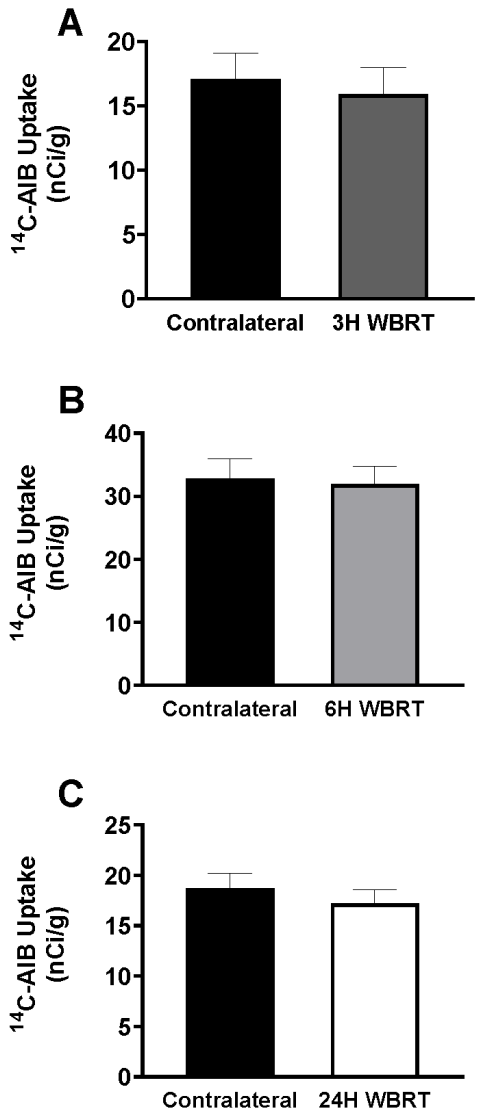

Supplemental Figure 3.2. No changes in BBB permeability following WBRT in immunocompetent mice 3, 6, or 24 hours post-WBRT. No significant differences in ^{14}C-AIB uptake observed 3, 6, or 24 hours following WBRT (15.5Gy) in wild-type C57Bl/6 mice. ($p>0.05$)

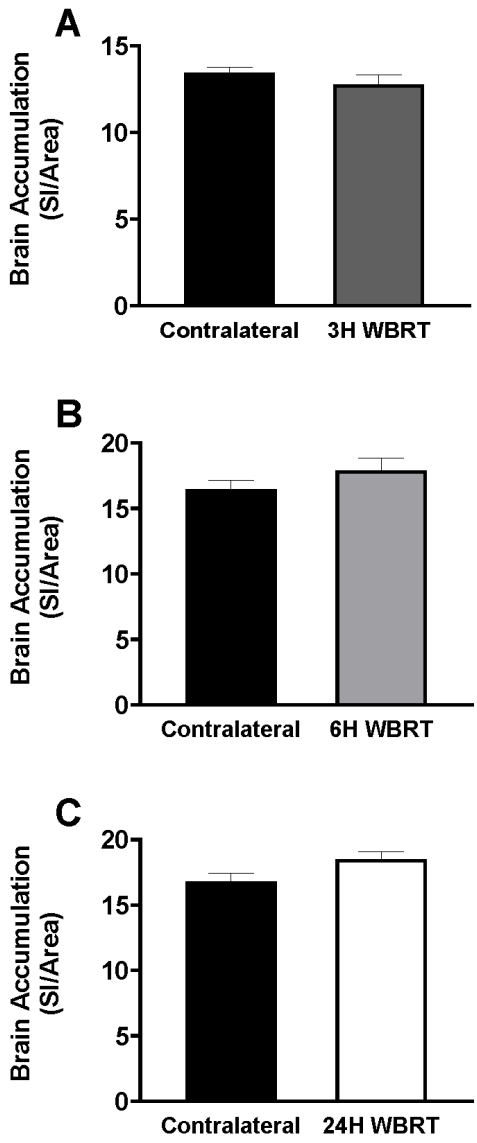

Supplemental Figure 3.3. No changes in BBB permeability following WBRT in immunocompetent mice 3, 6, or 24 hours post-WBRT. No significant differences in 3 kDa TxRd uptake observed 3, 6, or 24 hours following WBRT (15.5Gy) in wild-type C57Bl/6 mice. ($p>0.05$)

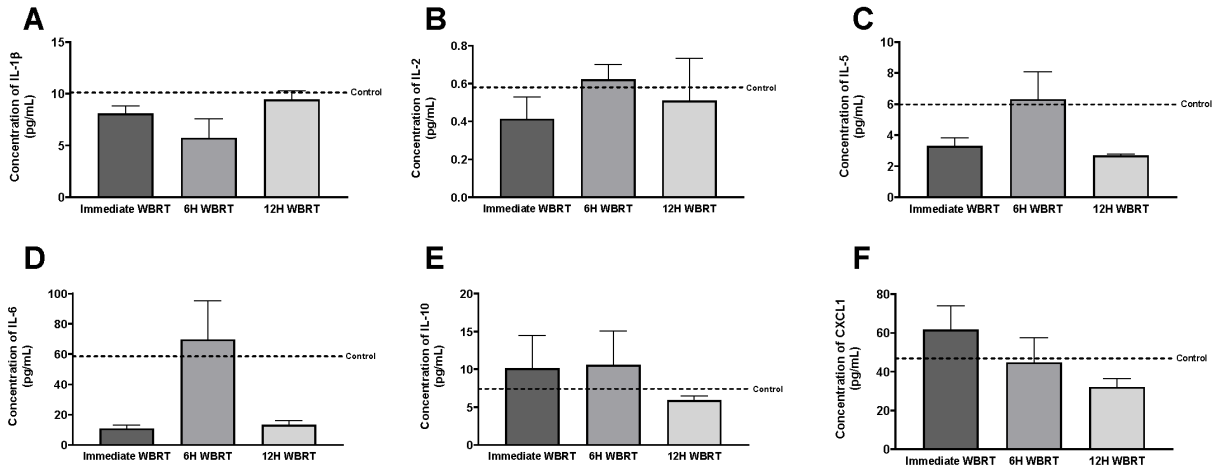

Supplemental Figure 3.4. No changes in proinflammatory cytokine concentrations in serum of immunocompetent mice post-WBRT. No significant differences in IL-1β (A), IL-2 (B), IL-5 (C), IL-6 (D), IL-10 (E), or CXCL1 (F) in WT mice serum immediately, 6h, or 12h following WBRT. ($p>0.05$)

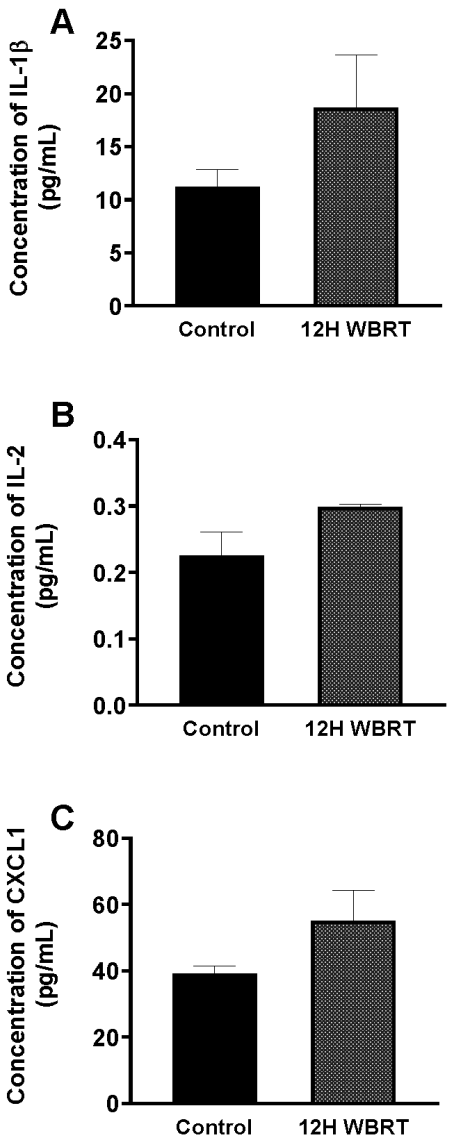

Supplemental Figure 3.5. No changes in proinflammatory cytokine concentrations in serum of immunocompromised mice post-WBRT. No significant differences in IL-1β (A), IL-2 (B), or CXCL1 (C) in nude mice serum 12h following WBRT. ($p>0.05$)

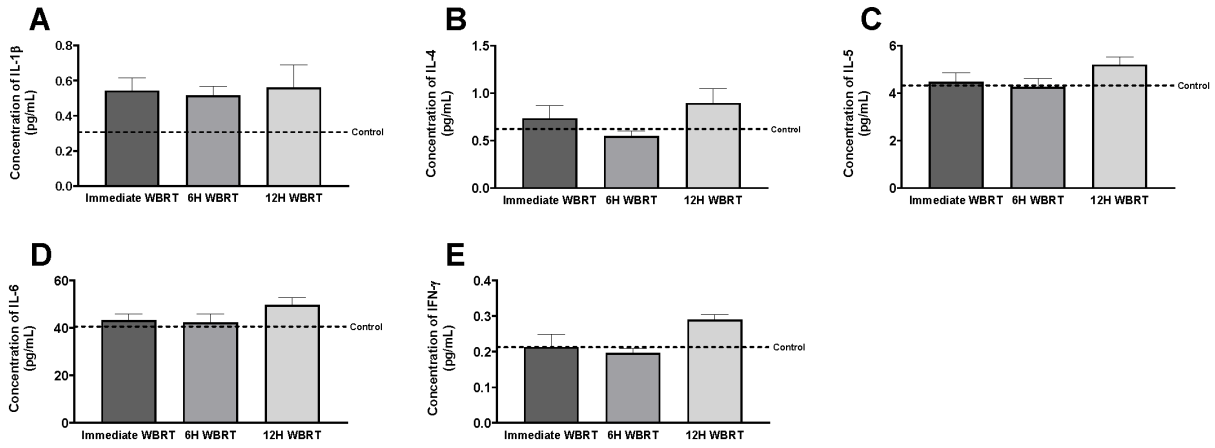

Supplemental Figure 3.6. No changes in proinflammatory cytokine concentrations in brain of immunocompetent mice post-WBRT. No significant differences in IL-1β (A), IL-4 (B), IL-5 (C), IL-6 (D), or IFN-γ (E) in WT mice brains immediately, 6h, or 12h following WBRT. ($p>0.05$)

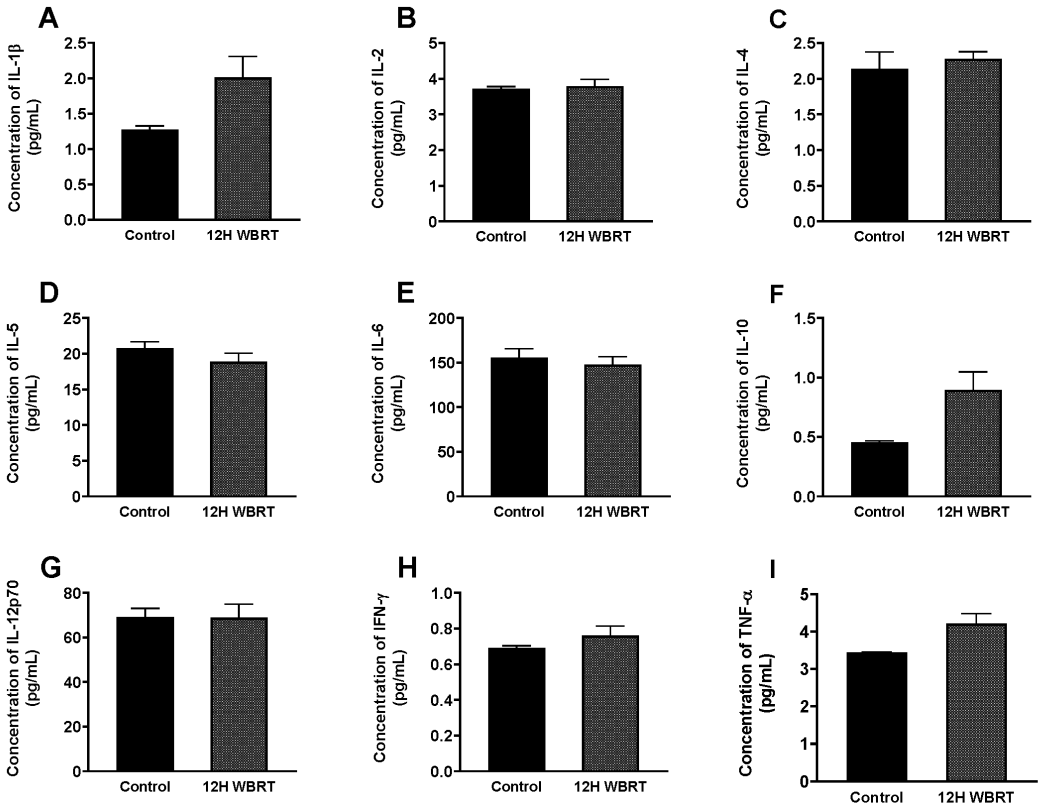

No changes in proinflammatory cytokine concentrations in brain of immunocompromised mice post-WBRT. No significant differences in IL-1β (A), IL-2 (B), IL-4 (C), IL-5 (D), IL-6 (E), IL-10 (F), IL-12p70 (G), IFN-γ (H), or TNF-α (I) in nude mice brains 12h following WBRT. ($p>0.05$)

Chapter 4

Coordination of anti-CTLA-4 with whole-brain radiation therapy decreases tumor burden during treatment in a novel syngeneic model of lung cancer brain metastasis.

4.1 Introduction

Lung cancer is the leading cause of cancer deaths globally and one of the most prominent cancer types to metastasize to the brain. Approximately 40% of patients develop brain metastases in their lifetime. Although advancements in treatment for lung cancer have been made within the past couple of decades, with five-year survival increasing from 14% to 24%, this does not stand true for the treatment of brain tumors [1]. Unfortunately, the five-year survival rate for lung cancer brain metastasis patients remains at only 4.7% [2]. Approved therapies for brain metastases include stereotactic radiosurgery (SRS), whole-brain radiation therapy (WBRT), surgical resection, chemotherapies and targeted therapies. Typically, patients will receive a combination of treatments to manage the primary tumor and metastases.

There is limited research on the efficacy of immunotherapy in brain metastasis patients due to exclusion from clinical trials and most research available is derived from retrospective clinical trial analyses [3-5]. From the minimal prospective clinical trial data available, immunotherapy results seem promising [6, 7]. A small phase II study in patients with previously untreated brain

metastases had an intracranial response rate of 29.7% with pembrolizumab [NCT02085070]. More prospective clinical trials are needed to validate the intracranial efficacy of immunotherapies.

An important research gap is the optimal administration sequencing of immunotherapy and radiotherapy. Peripheral tumor biology demonstrates the rationale for combining radiotherapy and immunotherapy to produce synergistic effects, presumably due to the abscopal response elicited by radiation [8, 9]. A recent phase I/II clinical trial evaluated the safety and efficacy of nivolumab and ipilimumab with concurrent SRS in patients with LCBM. The study concluded the combinatorial therapy had minimal toxicity and a 4-month progression-free survival rate of 70.7% [10]. However, it is still unclear which treatment should be administered first, and if the sequencing matters for patient outcomes. Additionally, sufficient lung cancer brain metastasis preclinical models to study immunotherapy efficacy are lacking, with most established models utilizing human cancer cells in immunocompromised animals [11].

Our previous data demonstrated an inflammatory response and breakdown of the blood-brain barrier 12 hours following whole-brain radiation therapy (WBRT) in wild-type C57Bl/6 mice [12]. Due to the aforementioned lack of syngeneic lung cancer brain metastasis models, we chose to generate a preclinical animal model to evaluate immunotherapy efficacy. We hypothesized that timed immunotherapy administration post-WBRT would decrease tumor burden and increase survival. The anti-CTLA-4 immunotherapy was selected because it mobilizes T-cells to “cold” tumors, elicits clonal diversity, recurrence following treatment is rare, and is shown to be efficacious in preclinical and clinical studies

when combined with radiotherapy [13-15]. Despite the fact that anti-PD-1 immunotherapy is more commonly administered in lung cancer patients [16, 17], it also has higher resistance and recurrence rates [18-20].

This study aimed to 1) develop a syngeneic lung cancer brain metastasis model and 2) evaluate if timed administration of immunotherapy with radiotherapy increases survival and decreases tumor burden. Herein we successfully generated a syngeneic lung cancer brain metastasis preclinical animal model to be utilized in immunocompetent and immunocompromised mice. The mice were treated with the clinical radiotherapy dosing schedule of 30Gy in 10 fractions delivered over 12 days. We hypothesized that immunotherapy would be more efficacious when delivered 12 hours post-WBRT than if it was delivered 24 hours prior to WBRT. We observed decreased tumor burden in the immunocompetent mice treated with immunotherapy 12 hours post-radiotherapy compared to mice treated with immunotherapy 24 hours prior to radiation. Unexpectedly, the effects of the immunotherapy and radiation were not long-lasting and treatment had no effect on survival. These data suggest the timeframe of immunotherapy delivery with radiotherapy plays a role in delaying tumor progression, treatment may need to be continued long-term, and immunotherapy for brain metastasis should be further characterized.

4.2 Methods and Materials

Cell culture

The parental LLC-Luc2 cell line was purchased from ATCC (Manassas, VA) and arrived transduced to express firefly luciferase which allowed for bioluminescence

imaging (BLI). Cells were cultured in DMEM (ATCC, Manassas, VA) supplemented with 10% fetal bovine serum (Global Life Sciences Solutions, Cranbury, NJ), 1% antibiotic-antimycotic (Thermo Fisher Scientific, Waltham, MA), and 2 µg/mL blasticidin (Thermo Fisher Scientific, Waltham, MA) to ensure selection of transduced cells. Cells were incubated at 37°C and 5% CO2. All cells used for *in vivo* and *in vitro* experiments were maintained between passages 1-8.

Scratch assay

A 24-well plate was coated with collagen (Sigma Aldrich, St. Louis, MO) at a concentration of 100 µg/mL and placed in a refrigerator at 4°C until cells were confluent in their respective T75 flasks. The parental and brain-tropic cell lines were plated at 5 x 10^5 cells/well and incubated overnight at 37°C and 5% CO2. The following day, a scratch was made in each well with a 200 µL pipette tip and imaged on the Olympus MVX stereomicroscope (Olympus, Tokyo, Japan) (optical zoom range 0.63-12.6, NA=0.5) immediately, 1, 2, 3, 6, 12, and 24 hours post-scratch. The wound healing application on ImageJ software was utilized to calculate scratch area of each image.

Animals and brain tumor model development

All animal experiments were approved by the Institutional Animal Care and Use Committee at West Virginia University. Female C57Bl/6 and athymic nude mice were purchased from Jackson Laboratory (Bar Harbor, ME). All animals were approximately 6-8 weeks of age and ~25g during tumor implantation. Animals were allowed to acclimate for at least one week prior to experimentation. Mice

were anesthetized with 2% isoflurane and placed into a stereotactic device (Stoelting, Wood Dale, IL). Animals were injected with 150,000 LLC cells suspended in 100 µL PBS in the left ventricle of the heart. Bi-weekly BLI was performed to confirm tumor presence in the brain. The protocol for development of the brain-seeking line was modified from Yoneda et al and previously described by our laboratory [18-19]. Animals were euthanized once we observed significant BLI signal and brains were collected then homogenized and digested with collagenase in DMEM. The homogenate was ejected from a 19G needle and strained with a 70 µm cell strainer. The solution was centrifuged and resuspended three times with DMEM and 50% FBS, PBS, and then 25% BSA in PBS to remove the myelin layer. The remaining cell pellet was resuspended in complete medium and cultured. Once the flask became confluent, cells were washed with PBS thrice and injected into mice. This process was repeated until the cells predominantly seeded into the brain, which was six times for the LLC cell line, referred to as LLC-Br.

Monitoring tumor progression, weight, and survival

Tumor progression and weight were monitored biweekly. Animals were injected intraperitoneally with 150 mg/kg D-luciferin potassium salt (PerkinElmer, Waltham, MA) and anesthetized with 2-3% isoflurane. Approximately 15 minutes post-injection, animals were imaged with the IVIS Spectrum CT (PerkinElmer, Waltham, MA) and bioluminescence (BLI) was captured at auto-exposure and one-minute time frames on Stage D with medium binning. BLI was quantified by drawing a region of interest (ROI) around the cranium or peripheral body of each mouse. The BLI is reported as radiance (photons/sec/cm2/steradian). The brain-to-body ratios

were calculated by dividing radiance of the brain ROI by the radiance of the peripheral body ROI. Fold change of brain BLI was normalized to radiance at day 3. Mice were euthanized when they displayed signs of neurological symptoms or had over 20% weight loss. Survival was monitored and plotted on a Kaplan-Meier curve.

Irradiation protocol

As described previously, the XenX irradiator (Xstrahl, Suwanee, GA) at West Virginia University was commissioned to deliver clinically-relevant doses of radiation [20]. On day 3, mice were randomized into five groups and began treatment. Mice receiving radiation therapy were anesthetized with 1-3% isoflurane and treated with whole-brain irradiation at a dose of 30Gy in 10 fractions delivered over 12 days, the clinical radiation treatment schedule. Solid water phantoms were used while treating cells to provide buildup and backscatter. Cells were treated with 3Gy and then returned to the incubator.

Immunotherapy preparation and administration

The anti-CTLA-4 antibody (Bio X Cell, Lebanon, NH) was diluted in Bio X Cell's recommended InVivoPure dilution buffer (pH 7.0) to deliver 100 µg of antibody/100 µL intraperitoneally. Immunotherapy treatment groups began treatment on day 3 and were treated twice more on days 6 and 9. The vehicle group received mouse IgG2b isotype control antibody (Bio X Cell, Lebanon, NH) diluted 100 µg/100 µL in the dilution buffer and delivered on the same days the immunotherapy groups received treatment.

Statistical analysis

Data were analyzed and plotted with GraphPad Prism 8 software (GraphPad Software, San Diego, CA). Results are presented as mean ± S.E.M. unless noted otherwise. Statistical differences between two groups were assessed using Student's t-test. One-way ANOVA with a Tukey posttest was utilized for data with more than two groups. Differences were considered statistically significant at $p < 0.05$ (*).

4.3 Results

Development of the brain tropic LLC-Br cell line

Wild-type C57Bl/6 mice were injected intracardially with LLC cells and allowed to develop brain tumors, which were then excised and cultured ex vivo. This process was repeated for six passages. The ratio of bioluminescent signal (radiance) in the brain versus the body increased with each passage, shown in **Figure 4.1A**. Passage 6 had significantly higher brain-to-body tumor burden at than the previous passages, with a ratio of 5.8 ± 2.4. This is the passage we continued our experiments with, referred to as LLC-Br. Brain tumor growth kinetics of LLC-Br and the parental, LLC-P, were monitored with bioluminescent imaging. Despite the fact the LLC-Br mice had greater brain-specific tumor burden, we did not observe any differences in the in vivo growth rates between the LLC-Br and LLC-P cell lines, as shown in Figure 1B. The presence of brain tumors with the LLC-Br model was confirmed with 3D bioluminescent CT imaging (**Figure 4.1C**).

In vitro characterization of LLC-Br compared to LLC-P

The in vitro cell growth rates of the parental and brain tropic cell lines, were similar to the in vivo data with no significant differences (**Figure 4.2A-B**). To evaluate the invasive capabilities of the LLC-Br and LLC-P, a scratch assay was performed. We observed a significant increase in percent wound closure over time in the LLC-Br cell line compared to the parental, as demonstrated by the area under the curve increasing from 1221 ± 44 to 1823 ± 115 (**Figure 4.2C-D**).

Similar tumor burden in wild-type and nude mice 22 days post-inoculation

The LLC-Br tumor progression with BLI in WT C57Bl/6 and nude mice was measured to confirm our model can be used in both mouse strains, as shown in **Figure 4.3**. At day 22, we observed no differences in total brain tumor burden between the nude mice (10202 ± 6989) and WT mice (27434 ± 12040), shown in **Figure 4.3B**. Additionally, similar median survivals were observed, with nude mice having a median survival of 21 days and 19 days for WT mice (**Figure 4.3C**).

Immunotherapy survival study results

We were interested in evaluating timed delivery of immunotherapy in combination with WBRT, so we injected nude and WT mice with LLC-Br and treated with radiation therapy 24h after or 12h before immunotherapy. The WT mice had a significant decrease in tumor burden in the α-CTLA-4 only (208 ± 50) and α-CTLA-4 administered 12h post-WBRT (204 ± 93) groups 14 days after treatment compared to the vehicle (622 ± 144) group (**Figure 4.4A-B**, **Figure 4.5A-B**, **Figure 4.6A-B**). At day 18, all treatment groups had significantly lower tumor burden compared to the control group (**Figure 4.4C**, **Figure 4.5C**, **Figure**

4.6C), however, by day 22 none of the treatment groups were different from the vehicle mice (**Figure 4.4D**, **Figure 4.5D**, **Figure 4.6D**). Additionally, there were no significant differences observed in survival or weight loss (**Figure 4.4E-F**, **Figure 4.5E-F**, **Figure 4.6E-F**). All treatment groups had median survival times of 22 days compared to 19 days for the vehicle group.

In the radiation groups, a significant increase in tumor burden was observed in WT mice treated with α-CTLA-4 24 hours prior to WBRT compared to the mice treated with immunotherapy 12 hours after radiation at days 14 (**Figure 4.5B**), 18 (**Figure 4.5C**), and 22 (**Figure 4.5D**). This group was also significantly increased compared to the radiation-only treated mice at days 18 (**Figure 4.5C**) and 22 (**Figure 4.5D**).

When comparing the immunotherapy groups, the WT mice treated with α-CTLA-4 24 hours prior to radiation had a higher tumor burden than mice treated with α-CTLA-4 only at day 14 (**Figure 4.6B**). The group treated with α-CTLA-4 12 hours after radiation had a significantly lower tumor burden at day 22 compared to the α-CTLA-4 only group (**Figure 4.6D**).

As anticipated, the only treatment group with decreased tumor burden in the nude mice was the radiation-only group at day 18 (**Supp. Fig. 4.1C**). Surprisingly, this effect was absent at day 22 (**Supp. Fig. 4.1D**). Similar to the WT mice, no significant differences in survival or weight loss were observed between groups (**Supp. Fig. 4.1E-F**, **Supp. Fig. 4.2E-F**, **Supp. Fig. 4.3E-F**).

Discussion

Lung cancer brain metastasis is a difficult disease to treat, partially due to the

existence of the blood-tumor barrier (BTB), which restricts the distribution of systemic therapeutic agents to tumors. A potential treatment option to overcome this barrier is immunotherapy because it triggers activated immune cells to cross the barrier and attack cancer cells within the brain. In order for the treatment to be most effective, priming of the immune response and timing of administration is critical. Without proper brain metastasis preclinical models, the sequencing of immunotherapy with other treatment modalities cannot be elucidated. Herein, we established a novel syngeneic lung cancer brain metastasis model to evaluate the efficacy of immunotherapy and whole-brain radiation therapy.

We observed a significant increase in brain tumor burden compared to body burden upon the sixth passage of the LLC cell line. This indicates a sufficient model to observe brain tumor-specific effects of treatment. The brain-specific tumor burden was confirmed with in vivo 3D bioluminescent imaging. As expected, the brain-tropic LLC-Br cell line exhibits increased motility compared to the parental, LLC-P, cell line as measured by in vitro scratch assay. Additionally, we observed no differences in the growth rates of LLC-P or LLC-Br cell lines in vitro or in vivo. Our model also has similar in vivo growth rates and survival times in WT and nude mice, suggesting it is an appropriate model to compare effects of the immune response on brain metastases and the blood-tumor barrier.

When comparing vehicle, radiation, and α-CTLA-4 groups, significant decreases in tumor burden were observed at days 14 and 18, but not at the conclusion of the study (day 22). Unexpectedly, these treatments did not have an effect on survival or weight loss. We hypothesize this could be occurring due to the rapid growth rate of the LLC-Br cells. The treatments may delay tumor

progression during and shortly following treatment, but the tumors recur and mice succumb to the disease. This also occurs clinically, with 73-76% of patients treated with stereotactic radiosurgery (SRS) experiencing recurrence. When combined with WBRT, this decreases to 27-46% of patients [24]. Recurrence with immunotherapy is typically observed with α-PD-1; approximately 20% of patients with non-small cell lung cancer (NSCLC) initially respond to α-PD-1 treatment, but the majority develop resistance [25, 26].

In the radiation treated groups, we observed a significant increase in tumor burden in mice treated with α-CTLA-4 24 hours before radiation. There were no differences between the radiation-only group and mice treated with anti-CTLA-4 12 hours post-WBRT. A similar non-significant trend was observed in the nude mice. Human-derived NSCLC cell lines express CTLA-4 and treatment with α-CTLA-4 antibody can induce PD-L1 expression. Additionally, the binding of α-CTLA-4 promotes cell proliferation through activation of the EGFR pathway [27]. Activation of EGFR is associated with increased radioresistance and metastatic capabilities in lung cancer [28-30]. It can also result in DNA synthesis, proliferation, and cell cycle arrest [31]. It is well documented that the phase of the cell cycle affects radiotherapy response, with cells in the late S phase being most radioresistant and cells in the M phase most radiosensitive [32, 33]. A study in 2020 demonstrated inhibition of EGFR/HER2 signaling in LLC cells results in decreased proliferation, reduced metastasis, and increased radiosensitivity [34]. We treated LLC-Br cells with α-CTLA-4 for 72 hours and noted a significant increase in percent survival based on an MTT assay (**Supp. Fig. 4.4**). Therefore, we hypothesize that the radioprotective effect we observed could be due to α-

CTLA-4 stimulating EGFR signaling, promoting proliferation, and potentially arresting cells in a more radioresistant phase of the cell cycle.

Between all of the immunotherapy groups, the mice treated with α-CTLA-4 12 hours post-radiation had the lowest tumor burden while the mice treated with α-CTLA-4 24 hours prior to radiation had the highest tumor burden. These data suggest the timing of immunotherapy administration with radiotherapy does play a role in the efficacy of treatment and needs further investigation. Treatment with α-CTLA-4 has varied effects depending on cell type and microenvironment [35], which could contribute to the varied responses observed in immunotherapy studies.

Although we generated a syngeneic lung cancer brain metastasis model and completed a study with immunotherapy and radiotherapy, our work has its limitations. First, this study only evaluated a single dose of α-CTLA-4 with radiotherapy. Future studies should evaluate if there is a dose effect of α-CTLA-4 when coordinated with WBRT. Additionally, we studied α-CTLA-4 as a single immunotherapy because we hypothesized it would mobilize T-cells to the brain tumors more effectively than α-PD-1 therapy. Studies to investigate coordination of α-CTLA-4 and αPD-1 administration in combination with radiation should be performed. We hypothesize combining α-PD-1 with α-CTLA-4 would enhance the synergistic effects we observed. Lastly, studies are needed to evaluate the mechanism of immunotherapy delaying progression with radiotherapy timed coordination.

Conclusions

Patients with lung cancer brain metastases have poor prognosis and usually succumb to the disease within a year after diagnosis. Immunotherapy is a promising treatment modality for brain tumors, but preclinical models are limited. Our study demonstrates we successfully created a syngeneic lung cancer brain metastasis model which can be used to evaluate immunotherapy efficacy. The model has a similar growth rate to its parental cell line, but higher motility. Additionally, we observed that combining α-CTLA-4 after radiation decreases brain tumor burden compared to α-CTLA-4 alone and administration of α-CTLA-4 prior to radiation. These data demonstrate the importance of optimizing the sequence of treatment modalities and potentially increasing immunotherapy treatment throughout the course of disease to ensure positive outcomes. Further research is needed in the field of brain metastasis immunotherapy and we aim to contribute with our novel lung cancer brain metastasis model.

References

1. Lofling, L., et al., Temporal trends in lung cancer survival: a population-based study. Acta Oncol, 2022. 61(5): p. 625-631.

2. Yuan, J., et al., Prognosis of lung cancer with simple brain metastasis patients and establishment of survival prediction models: a study based on real events. BMC Pulm Med, 2022. 22(1): p. 162.

3. Veccia, A., et al., Management of brain metastases from lung cancer in the era of immunotherapy: a review of the literature. Future Oncol, 2021. 17(5): p. 597-609.

4. Yang, G., L. Xing, and X. Sun, Navigate Towards the Immunotherapy Era: Value of Immune Checkpoint Inhibitors in Non-Small Cell Lung Cancer Patients With Brain Metastases. Front Immunol, 2022. 13: p. 852811.

5. Sun, L., et al., Outcomes in Patients With Non-small-cell Lung Cancer With Brain Metastases Treated With Pembrolizumab-based Therapy. Clin Lung Cancer, 2021. 22(1): p. 58-66 e3.

6. Ready, N.E., et al., First-line nivolumab plus ipilimumab for metastatic non-small cell lung cancer, including patients with ECOG performance status 2 and other special populations: CheckMate 817. J Immunother Cancer, 2023. 11(2).

7. Reck, M., et al., Systemic and Intracranial Outcomes With First-Line Nivolumab Plus Ipilimumab in Patients With Metastatic NSCLC and Baseline Brain Metastases From CheckMate 227 Part 1. J Thorac Oncol, 2023. 18(8): p. 1055-1069.

8. Theelen, W., et al., Pembrolizumab with or without radiotherapy for

metastatic non-small-cell lung cancer: a pooled analysis of two randomised trials. Lancet Respir Med, 2021. 9(5): p. 467-475.

9. Kong, Y., et al., PD-1 Inhibitor Combined With Radiotherapy and GM-CSF (PRaG) in Patients With Metastatic Solid Tumors: An Open-Label Phase II Study. Front Immunol, 2022. 13: p. 952066.

10. Altan, M., et al., Nivolumab and ipilimumab with concurrent stereotactic radiosurgery for intracranial metastases from non-small cell lung cancer: analysis of the safety cohort for non-randomized, open-label, phase I/II trial. J Immunother Cancer, 2023. 11(7).

11. Valiente, M., et al., Brain Metastasis Cell Lines Panel: A Public Resource of Organotropic Cell Lines. Cancer Res, 2020. 80(20): p. 4314-4323.

12. Blethen, K.E., et al., Effects of whole-brain radiation therapy on the blood-brain barrier in immunocompetent and immunocompromised mouse models. Radiat Oncol, 2023. 18(1): p. 22.

13. Formenti, S.C., et al., Radiotherapy induces responses of lung cancer to CTLA-4 blockade. Nat Med, 2018. 24(12): p. 1845-1851.

14. Twyman-Saint Victor, C., et al., Radiation and dual checkpoint blockade activate non-redundant immune mechanisms in cancer. Nature, 2015. 520(7547): p. 373-7.

15. Yoshimoto, Y., et al., Radiotherapy-induced anti-tumor immunity contributes to the therapeutic efficacy of irradiation and can be augmented by CTLA-4 blockade in a mouse model. PLoS One, 2014. 9(3): p. e92572.

16. Reck, M., J. Remon, and M.D. Hellmann, First-Line Immunotherapy for Non-Small-Cell Lung Cancer. J Clin Oncol, 2022. 40(6): p. 586-597.

17. Masuda, K., et al., Efficacy of anti-PD-1 antibodies in NSCLC patients with an EGFR mutation and high PD-L1 expression. J Cancer Res Clin Oncol, 2021. 147(1): p. 245-251.

18. Lahiri, A., et al., Lung cancer immunotherapy: progress, pitfalls, and promises. Mol Cancer, 2023. 22(1): p. 40.

19. Vesely, M.D., T. Zhang, and L. Chen, Resistance Mechanisms to Anti-PD Cancer Immunotherapy. Annu Rev Immunol, 2022. 40: p. 45-74.

20. Creelan, B.C., et al., Tumor-infiltrating lymphocyte treatment for anti-PD-1-resistant metastatic lung cancer: a phase 1 trial. Nat Med, 2021. 27(8): p. 1410-1418.

21. Yoneda, T., et al., A bone-seeking clone exhibits different biological properties from the MDA-MB-231 parental human breast cancer cells and a brain-seeking clone in vivo and in vitro. J Bone Miner Res, 2001. 16(8): p. 1486-95.

22. Shah, N., et al., Drug resistance occurred in a newly characterized preclinical model of lung cancer brain metastasis. BMC Cancer, 2020. 20(1): p. 292.

23. Sprowls, S.A., et al., Irradiator Commissioning and Dosimetry for Assessment of LQ alpha and beta Parameters, Radiation Dosing Schema, and in vivo Dose Deposition. J Vis Exp, 2021(169).

24. Stockham, A.L., et al., Management of recurrent brain metastasis after radiosurgery. Prog Neurol Surg, 2012. 25: p. 273-86.

25. Borghaei, H., et al., Nivolumab versus Docetaxel in Advanced Nonsquamous Non-Small-Cell Lung Cancer. N Engl J Med, 2015. 373(17): p.

1627-39.

26. Horn, L., et al., Nivolumab Versus Docetaxel in Previously Treated Patients With Advanced Non-Small-Cell Lung Cancer: Two-Year Outcomes From Two Randomized, Open-Label, Phase III Trials (CheckMate 017 and CheckMate 057). J Clin Oncol, 2017. 35(35): p. 3924-3933.

27. Zhang, H., et al., Tumour cell-intrinsic CTLA4 regulates PD-L1 expression in non-small cell lung cancer. J Cell Mol Med, 2019. 23(1): p. 535-542.

28. Kim, J.C., et al., Correlation of HER1/EGFR expression and degree of radiosensitizing effect of the HER1/EGFR-tyrosine kinase inhibitor erlotinib. Indian J Biochem Biophys, 2005. 42(6): p. 358-65.

29. Burdak-Rothkamm, S., et al., Radiosensitivity of tumor cell lines after pretreatment with the EGFR tyrosine kinase inhibitor ZD1839 (Iressa). Strahlenther Onkol, 2005. 181(3): p. 197-204.

30. Chen, G., et al., Golgi Phosphoprotein 3 Confers Radioresistance via Stabilizing EGFR in Lung Adenocarcinoma. Int J Radiat Oncol Biol Phys, 2022. 112(5): p. 1216-1228.

31. Lui, V.W. and J.R. Grandis, EGFR-mediated cell cycle regulation. Anticancer Res, 2002. 22(1A): p. 1-11.

32. Liu, C., et al., The Cell Cycle G2/M Block Is an Indicator of Cellular Radiosensitivity. Dose Response, 2019. 17(4): p. 1559325819891008.

33. Jung, S.Y., et al., Radiosensitizing Effect of Novel Phenylpyrimidine Derivatives on Human Lung Cancer Cells via Cell Cycle Perturbation. J Pharmacol Exp Ther, 2019. 370(3): p. 514-527.

34. Tien, Y., et al., Targeting human epidermal growth factor receptor 2 enhances radiosensitivity and reduces the metastatic potential of Lewis lung carcinoma cells. Radiat Oncol, 2020. 15(1): p. 58.

35. Oyewole-Said, D., et al., Beyond T-Cells: Functional Characterization of CTLA-4 Expression in Immune and Non-Immune Cell Types. Front Immunol, 2020. 11: p. 608024.

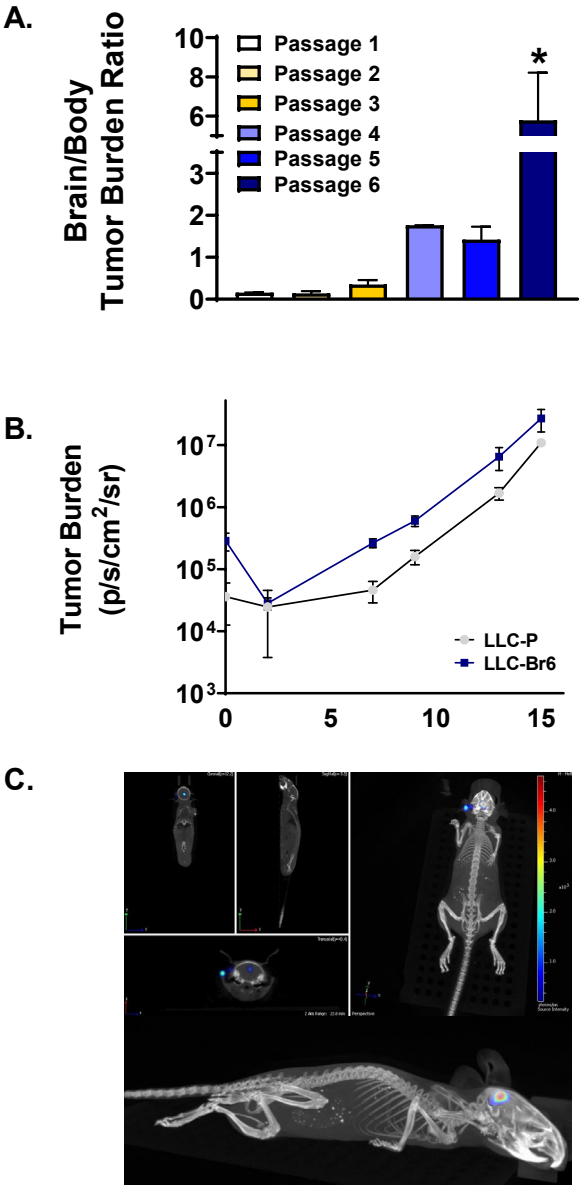

Figure 4.1: Tumor burden in the brain increases with passages of LLC brain explants. The ratio of bioluminescence (radiance) in the brain vs body of mice increases over passages of the LLC-Br cell line. Passage 6 has a significantly higher brain vs body ratio at D14 in comparison to all previous passages (A). Comparison of the growth kinetics of the parental LLC (LLC-P) to the brain tropic (LLC-Br) cell line in vivo (B). Localization of tumor cells in the brain was confirmed with 3D bioluminescent CT imaging (C). ($p<0.05$)

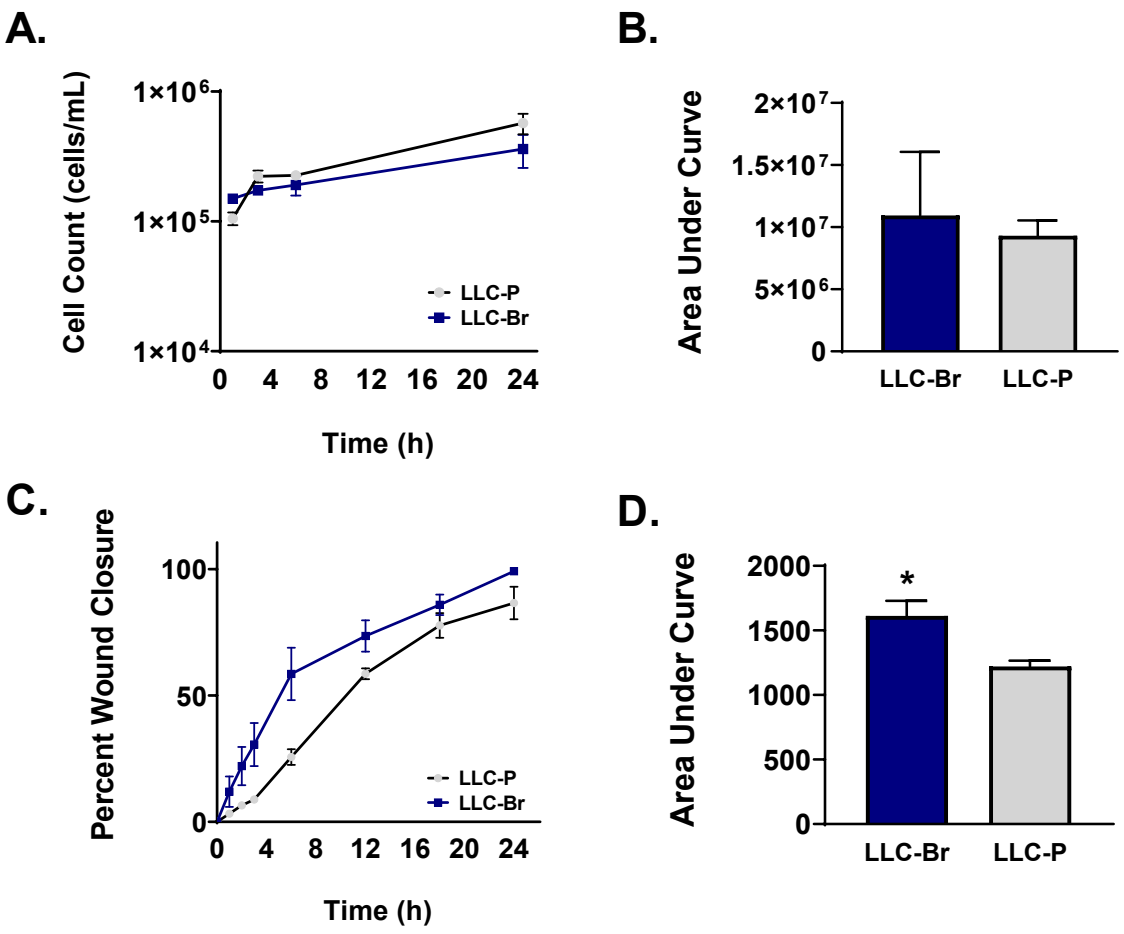

Figure 4.2: LLC-Br has a higher migration rate, but similar growth rate compared to LLC-P. Comparison of the growth kinetics of the parental LLC (LLC-P) to the brain tropic (LLC-Br) cell line in vitro (A-B). LLC-Br and LLC-P percent wound closure over time (n = 12) (C). LLC-Br has significantly increased cell migration compared to the parental LLC (D). ($p<0.05$)

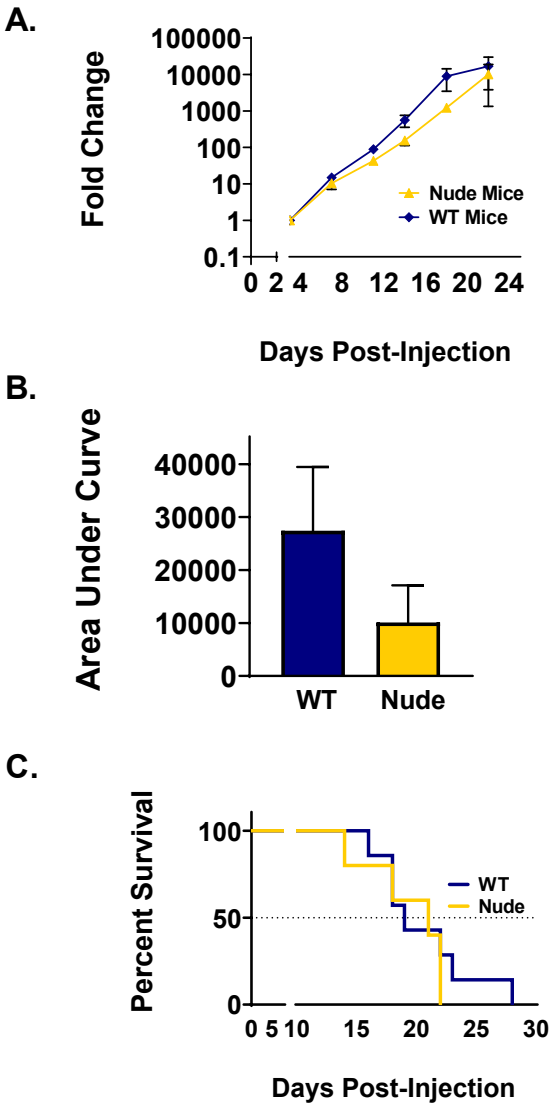

Figure 4.3: Similar tumor burden and survival in WT and nude mice. Tumor progression of LLC-Br in wild-type and athymic nude mice as measured by bioluminescence imaging normalized to day 3 (A). No significant differences in tumor burden between wild-type and nude mice as measured by area under the curve at day 22 (B). Kaplan-Meier plot of survival of WT and nude mice with LLC-Br tumors (C).($p>0.05$)

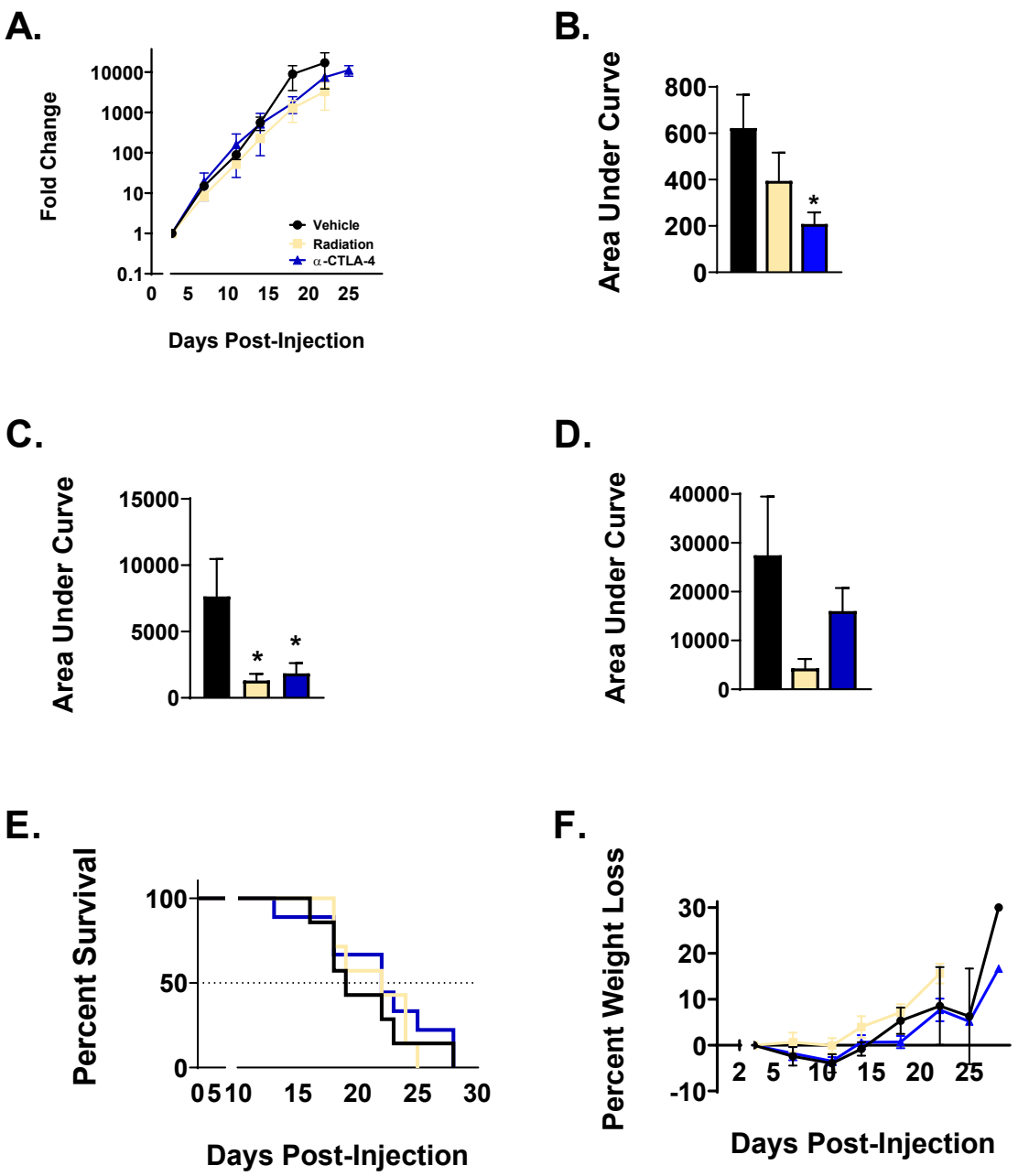

Figure 4.4: Delay in tumor progression until the conclusion of treatment in control groups. (A) Tumor progression of LLC-Br in wild-type mice treated with vehicle, radiation, or α-CTLA-4 as measured by bioluminescent imaging normalized to day 3. (B) Significant decrease in tumor burden of mice treated with α-CTLA-4 compared to vehicle at day 14. (C) Significant decrease in tumor burden of mice treated with radiation or α-CTLA-4 only at day 18. (D) No significant differences in tumor burden between vehicle, radiation, and α-CTLA-4 groups as measured by area under the curve at day 22. (E) Kaplan-Meier plot of survival of WT mice with LLC-Br tumors treated with vehicle, radiation, or α-CTLA-4. (F) No significant differences in percent weight loss were observed. N = 7-9 mice/group, $p < 0.05$ (*)

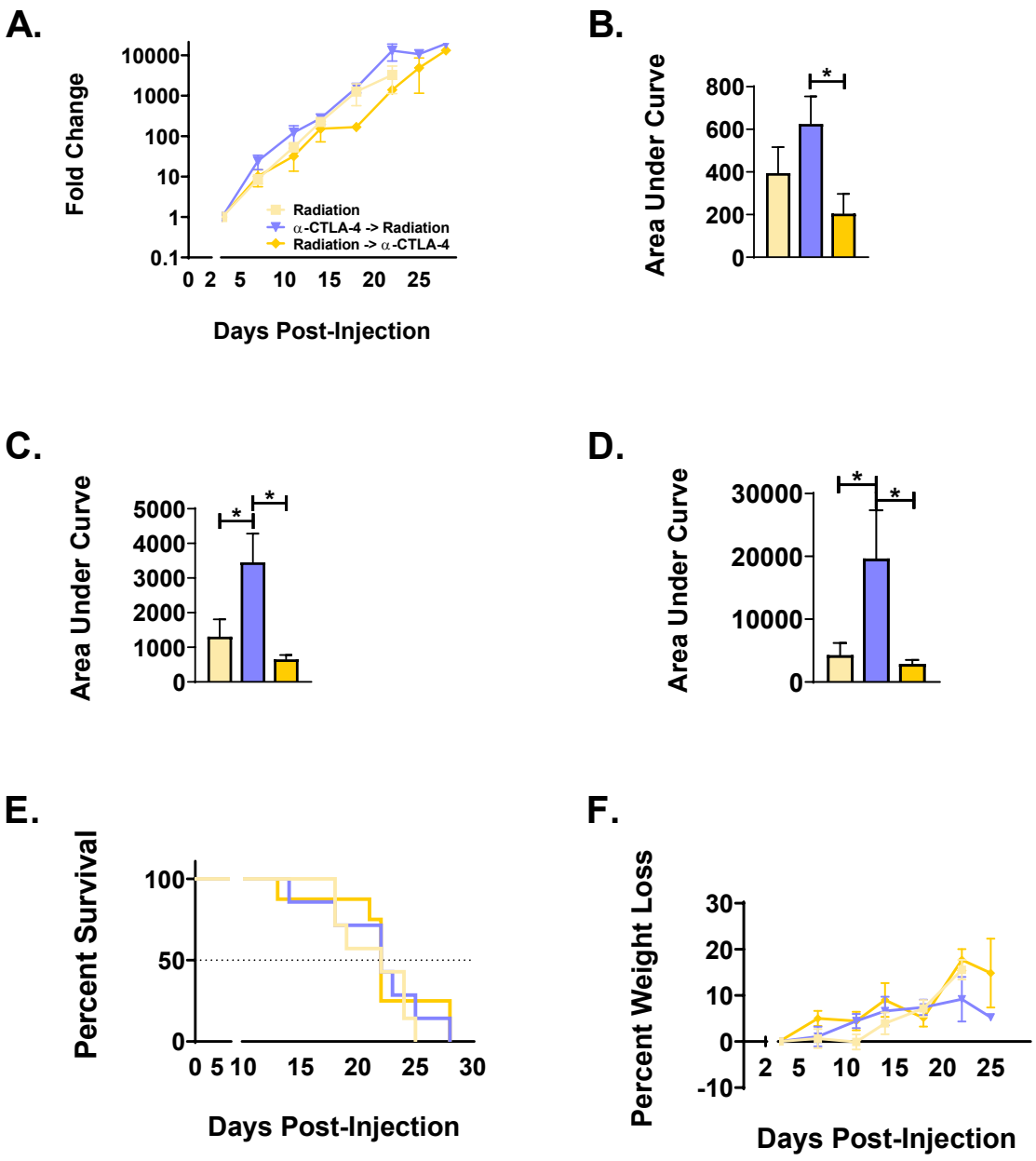

Figure 4.5: Potential tumor protective role of administering α-CTLA-4 24 hours prior to whole-brain radiation therapy. (A) Tumor progression of LLC-Br in wild-type mice treated with radiation, α-CTLA-4 24 hours before radiation, or anti-CTLA-4 12 hours after radiation as measured by bioluminescent imaging normalized to day 3. (B) Significant increase in tumor burden of mice treated with α-CTLA-4 24 hours prior to radiation compared to 12 hours after at day 14. (C) Significant increase in tumor

burden of mice treated with α-CTLA-4 24 hours prior to radiation at day 18. (D) Wild-type mice treated with α-CTLA-4 24 hours before radiation had significantly higher tumor burden compared to radiation and α-CTLA-4 12 hours after radiation groups as measured by area under the curve at day 22. (E) Kaplan-Meier plot of WT mice survival with LLC-Br tumors treated with radiation +/- α-CTLA-4. (F) No significant differences in percent weight loss were observed in radiation groups. N = 7-9 mice/group, $p < 0.05$ (*)

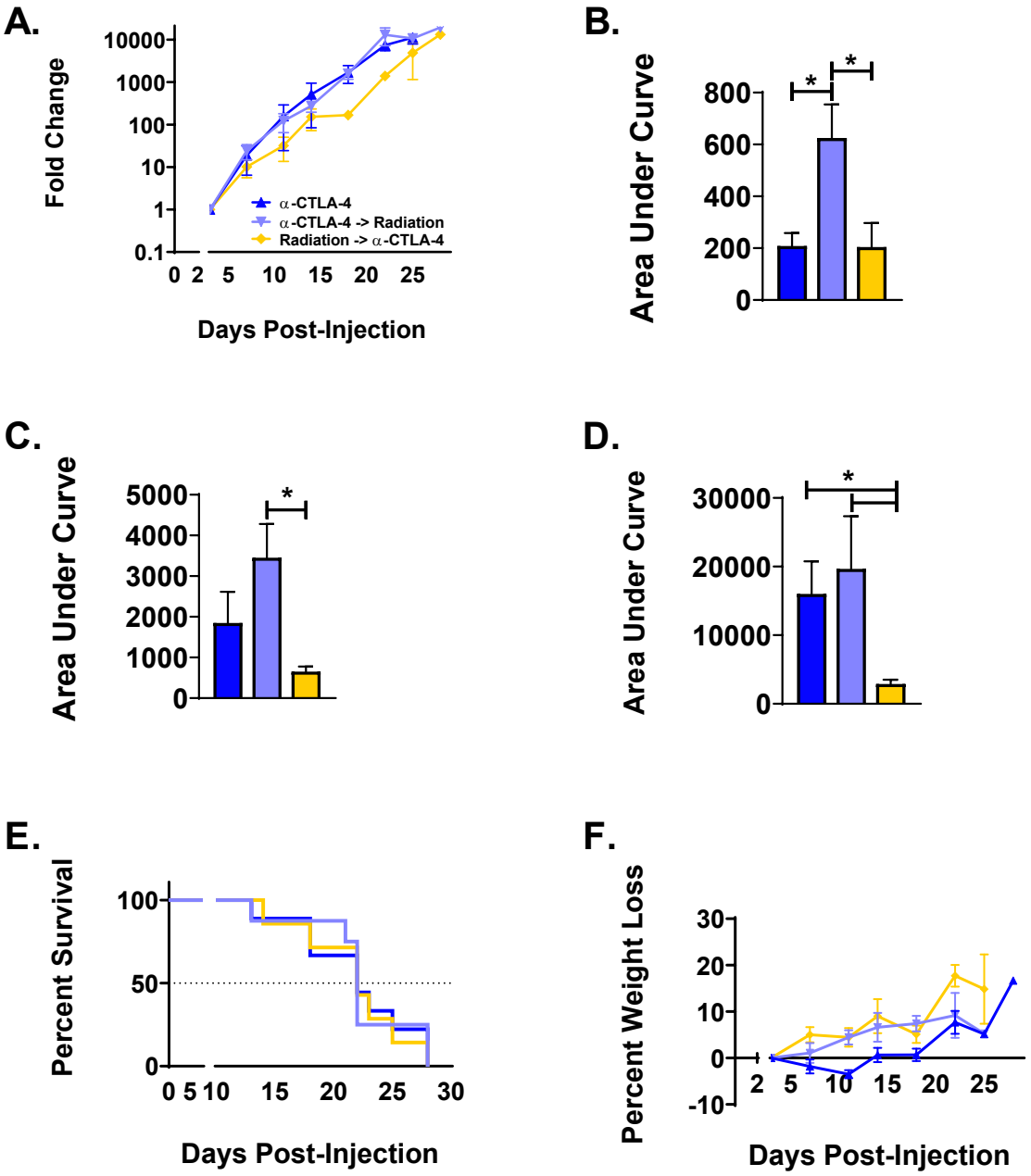

Figure 4.6: Administering α-CTLA-4 12 hours post-radiation decreases tumor burden. (A) Tumor progression of LLC-Br in wild-type mice treated with α-CTLA-4 only, α-CTLA-4 24 hours before radiation, or α-CTLA-4 12 hours after radiation as measured by bioluminescent imaging normalized to day 3. (B) Mice treated with α-CTLA-4 24 hours prior to radiation had significantly higher brain tumor burden at day 14 compared to immunotherapy only or immunotherapy delivered 12 hours post-WBRT. (C) Mice treated with α-CTLA-4 12 hours post-WBRT had significantly lower brain tumor burden at day 18 than mice administered immunotherapy 24 hours prior to radiation. (D) Wild-type mice treated with α-CTLA-4 12 hours after radiation had significantly lower tumor burden compared to α-CTLA-4 only and α-CTLA-4 24 hours before radiation groups as measured by area under the curve at day 22. (E) Kaplan-

Meier plot of WT mice survival with LLC-Br tumors treated with α-CTLA-4 +/- radiation. (F) No significant differences in percent weight loss were observed in the immunotherapy groups. N = 7-9 mice/group, $p < 0.05$ (*)

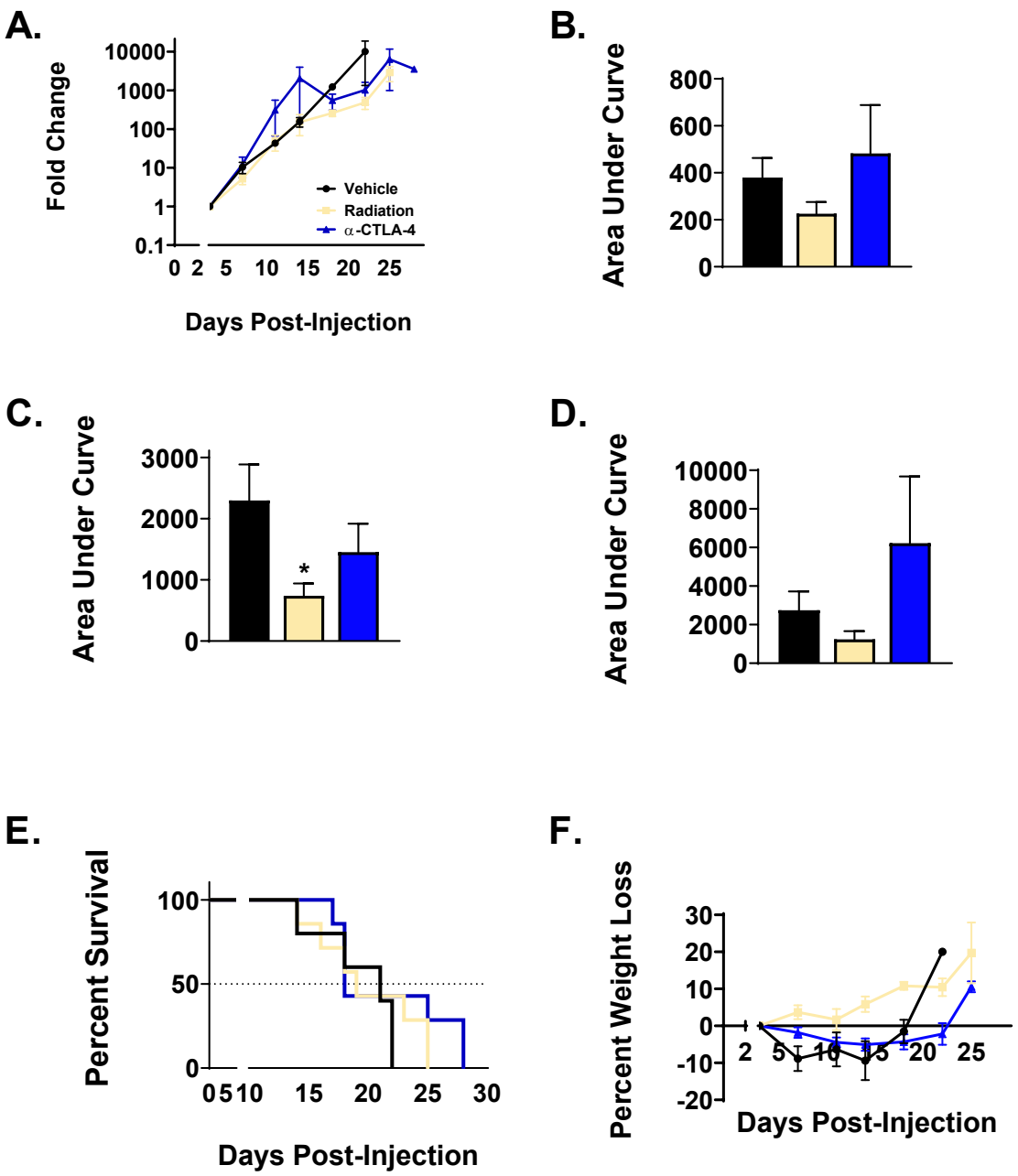

Supplemental Figure 4.1: No significant differences in tumor burden or survival in control immunocompromised groups. (A) Tumor progression of LLC-Br in nude mice treated with vehicle, radiation, or anti-CTLA-4 measured by bioluminescent imaging normalized to day 3. No differences were observed in tumor burden at day 14 (B) or 22 (D), survival (E), or percent weight loss (F). (C) The only decrease in tumor burden was observed at day 18 in the radiation group. ($p>0.05$)

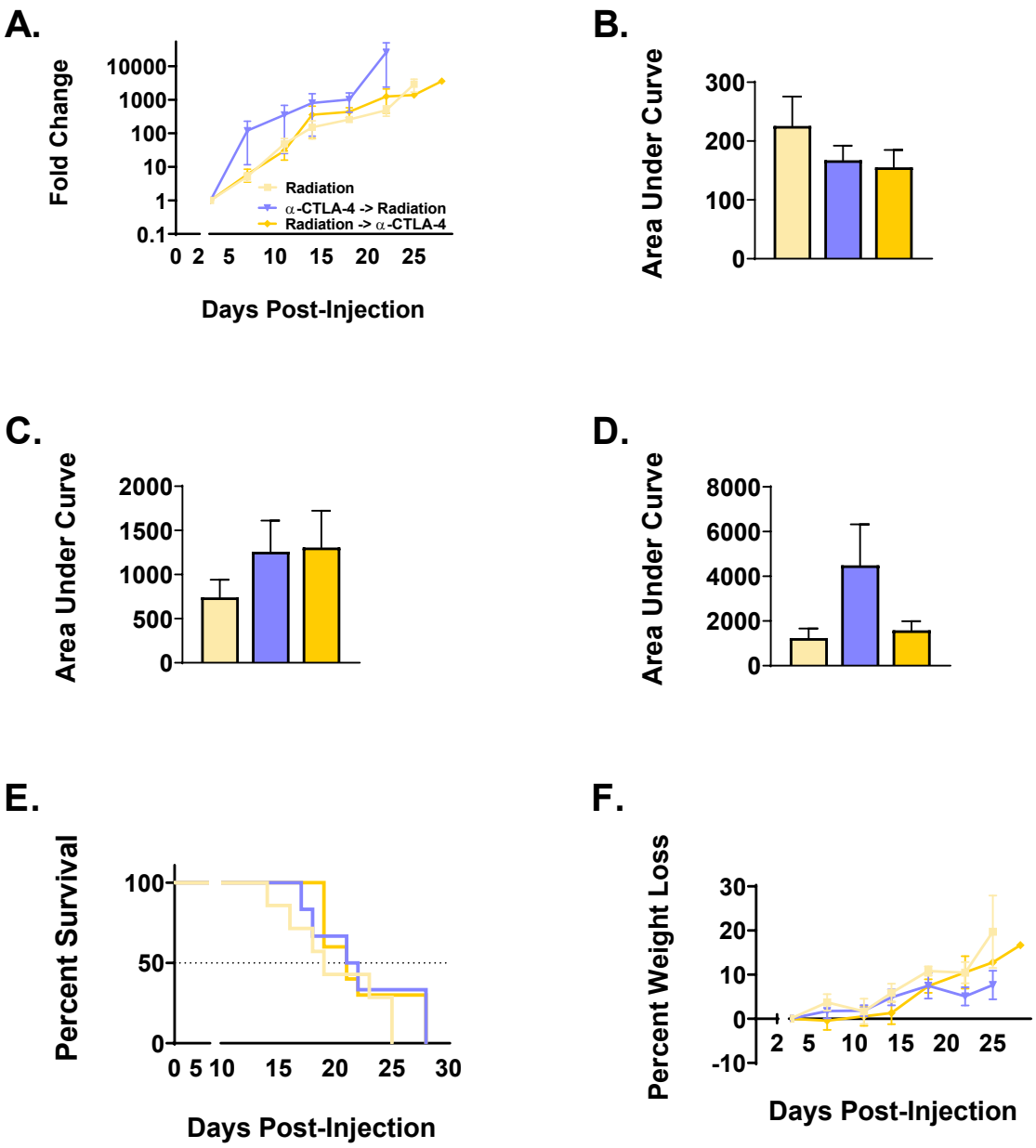

Supplemental Figure 4.2: No changes in tumor burden or survival in irradiated immunocompromised groups. Tumor progression of LLC-Br in nude mice treated with radiation +/- anti-CTLA-4 measured by bioluminescent imaging normalized to day 3 (A). No differences were observed in tumor burden at days 14(B), 18 (C) 22 (D), survival (E), or percent weight loss (F). ($p>0.05$)

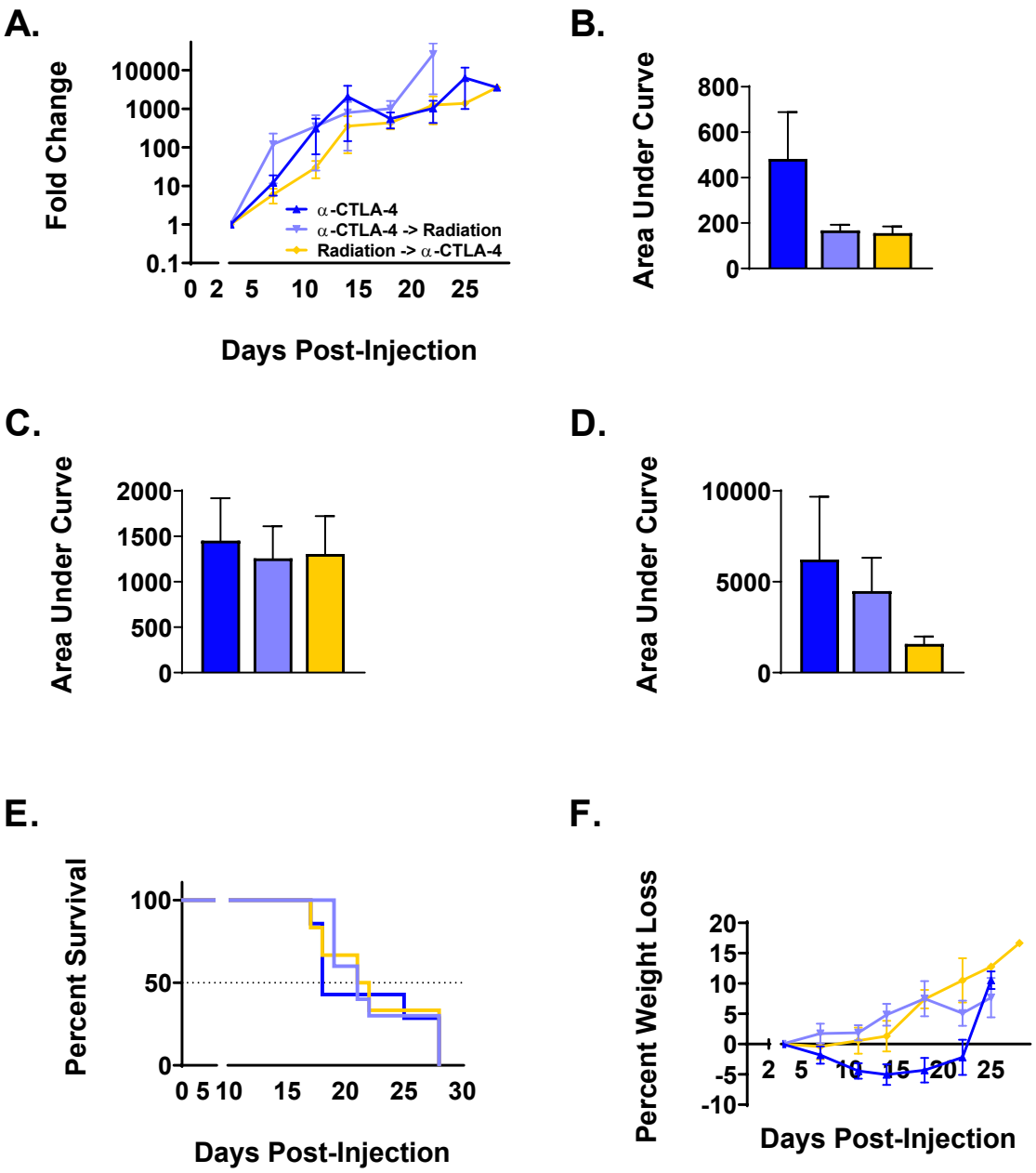

Supplemental Figure 4.3: No significant differences in tumor burden or survival in immunotherapy groups of immunocompromised mice. (A)Tumor progression of LLC-Br in nude mice treated with anti-CTLA-4 +/- radiation measured by bioluminescent imaging normalized to day 3. No differences were observed in tumor burden at days 14 (B), 18 (C), 22 (D), survival (E), or percent weight loss (F). ($p>0.05$)

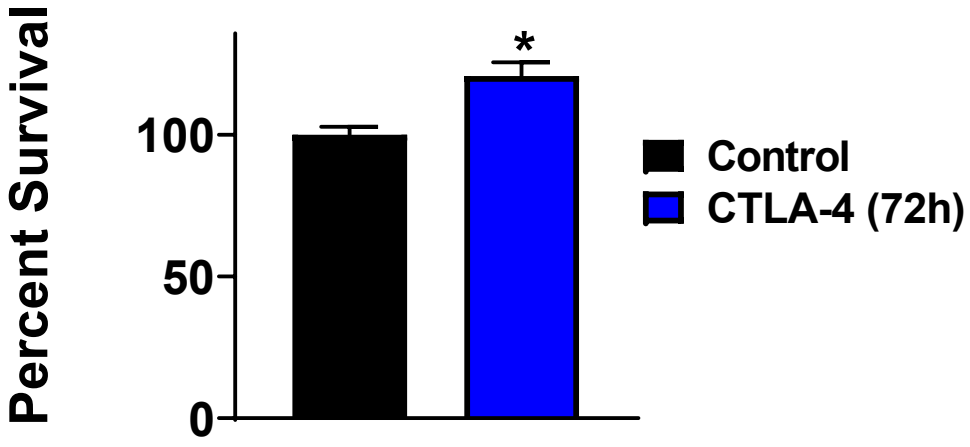

Supplemental Figure 4.4: Significant increase in percent survival of LLC-Br cells when treated with immunotherapy for 72 hours. LLC-Br cells had significantly higher percent survival after treatment with α-CTLA-4 for 72 hours compared to LLC-Br cells treated with the isotype control antibody. ($p<0.05$)

Chapter 5

Conclusions and Future Directions

5.1 Conclusions

In conclusion, this dissertation provided a detailed review on the blood-brain and blood-tumor barriers, brain metastases, and modalities to overcome brain barriers to treat metastatic brain tumors. Herein, we also evaluated the magnitude of blood-tumor barrier disruption following whole-brain radiation therapy in mice with and without functional immune systems. Additionally, we developed a preclinical syngeneic lung cancer brain metastasis model. The model was utilized to observe the efficacy of timed administration of immunotherapy in combination with radiation therapy.

Whole-brain radiation therapy is a common treatment modality for patients with multiple brain metastases. Although treatment with radiotherapy alone does not provide modest increase in survival, clinical studies have shown it can increase efficacy of systemic therapeutics. We found that WBRT (15.5Gy) increases BBB permeability 12 hours after treatment in immunocompetent mice, but not immunocompromised mice. Interestingly, efflux transporter activity is also decreased at this timepoint. In the serum of WT mice, TNF-α is significantly increased immediately following WBRT. The concentration of the chemokine CXCL-1 was also increased in the brains of WT and nude mice 12 hours post-radiation. Together, these data provide an optimal window of time following irradiation which may allow increased drug penetration into the brain.

Immunotherapy is a hopeful option for treatment of brain metastases, but there is limited data in this patient subset and preclinical models are not easily

available. It is unknown if there is an optimal time of administration post-radiotherapy that would result in robust immune responses and tumor kill. We generated a LCBM preclinical mouse model which can be used to evaluate immunotherapy efficacy. We found a significant increase in brain tumor burden upon the sixth passage of the LLC cell line. The LLC-Br cell line has increased motility, but no alteration in cell growth rate *in vitro* compared to the parental. We observed a significant decrease in tumor burden when α-CTLA-4 immunotherapy was administered 12 hours post-WBRT instead of 24 hours prior. These data suggest the timing of immunotherapy administration may affect patient outcomes.

In summary, the research from this dissertation details the difficulty in developing efficacious treatments for brain metastasis of lung cancer. However, the goal is that this work will push the field forward and provide a useful model for future immunotherapy studies for lung cancer brain metastasis.

5.1 Future Directions

Future studies that are resultant of this work will include the following:

WBRT has been shown to increase permeability and decrease efflux transporter activity 12 hours after treatment in immunocompetent mice. The majority of chemotherapeutics are subject to efflux transporters. **Future studies evaluating timed administration of known chemotherapeutic substrates of efflux transporters in immunocompetent brain metastasis models should be performed. The unidirectional transfer constant (K_{in}) of efflux transporter substrates will be evaluated in tumor bearing mice post-radiation to determine if the effect observed in naïve mice still applies. Furthermore, an efficacy study with timed administration of these therapeutics will be performed to observe any potential tumor kill or survival benefits.**

Immunotherapy has changed the way we research cancer and emphasizes the importance of the tumor microenvironment. The data herein indicate that immunotherapy delivery at specific time points following radiation can drastically alter the efficacy. However, in our efficacy study none of the treatments resulted in an increase in survival. **Future studies will include addition of PD-1 inhibitors with and without radiotherapy. We will evaluate if the sequence of immunotherapies (ie. CTLA-4 before/after PD-1) effects the tumor burden or survival outcomes. Additionally, we will investigate the use of low-intensity focused ultrasound to 1) prime the immune response before**

immunotherapy administration and 2) increase immune cell infiltration into brain metastases.

Research has improved the management of lung cancer within the past decade. As the success in managing peripheral disease increases, the incidence of brain metastases increases as well. Treating CNS tumors is much more complex than peripheral tumors due to the unique microenvironment and tightly regulated blood-brain barrier. Immunotherapy, novel drug formulations, and blood-brain barrier disruption techniques provide hope for the treatment of brain metastases.

In terms of reframing my dissertation work to my aims during my postdoctoral position, I will be focusing on primary brain tumors. Under the guidance of Dr. Grant, I will be applying the techniques learned at WVU to evaluate the effects of low-intensity focused ultrasound (LIFU) on primary brain tumors, the blood-tumor barrier, and immune response. We aim to develop a therapeutic strategy incorporating LIFU and immunotherapeutics.